

**“STUDY AND ANALYSIS OF SPOT WELDING OF DISSIMILAR MATERIAL 1008
LOW CARBON STEEL -5052 ALUMINUM ALLOY”**

A Thesis Submitted
In Partial Fulfillment of the Requirements
for the Degree of

MATER OF TECHNOLOGY

In
PRODUCTION AND INDUSTRIAL ENGINEERING

By

MD KHALID MUMTAZ

Enrollment No: 1500101753

Under the Supervision of

Dr. Mohd. Shahnawaz Alam



DEPARTMENT OF MECHANICAL ENGINEERING,
INTEGRAL UNIVERSITY, LUCKNOW

JULY 2020

INTEGRAL UNIVERSITY



LUCKNOW Certificate

Certified that **MD KHALID MUMTAZ** , Enrollment No. (1500101753) has carried out the research work presented in this thesis entitled “ **Study and Analysis of spot welding of Dissimilar Material 1008 Low Carbon – 5052 Aluminum Alloy**” for the award of **Master of Technology** from Integral University, Lucknow under my supervision. The project / thesis embodies results of original work, and studies are carried out by the student himself and the contents of the thesis do not form the basis for the award of any other degree to the candidate or to anybody else from this or any other University/Institution.

Date:

(Dr. MOHD. SHAHNAWAZ ALAM)

(Professor)

(Integral University, Lucknow)

ABSTRACT

Resistance spot welding is one of the oldest of the electric welding processes in use by industries today. The weld is made by a combination of heat, pressure, and time. As the name resistance welding implies, it is the resistance of the material to be welded to current flow that causes a localized heating in the part. Resistance spot welding is mostly used to weld various sheet metal products. Typically the sheets are in the 0.5-3.0 mm thickness range. The resistance spot welding of dissimilar materials is generally more challenging than that of similar materials due to differences in the physical, chemical and mechanical properties of the base metals. The influence of the primary welding parameters affects the heat input such as, peak current on the morphology, micro hardness and tensile shear load bearing capacity of weldment. Database regarding dissimilar materials resistance spot welding is very limited hence much research work is going on this field by various researchers, but most of work is on low thickness material typically 1mm to 2 mm. This work is an attempt to reveals aspects of the resistance spot welding of dissimilar materials of higher thickness typically 3mm. In this work resistance spot welding is performed on two different metal steels named low carbon steel, high strength low alloy steel with variation in current rating keeping of the parameters as constant. Although the bearing force of joint shows a linear relation with current rating but at higher current rating poor joint appearance is obtained also cavities are formed in joint.

ACKNOWLEDGEMENTS

I would like to articulate my deep gratitude to my project guide **Dr MOHD. SHAHNAWAZ ALAM** (Professor) who has always been my motivation for carrying out the project. An assemblage of this nature could never have been attempted without reference to and inspiration from the works of others whose details are mentioned in reference section. I acknowledge my indebtedness to all of them. Last but not the least to all of my friends who were patiently extended all sorts of help for accomplishing this undertaking. I have a gratification in expressing my sincere thanks to **Dr. P. K. Bharti**, Prof. and Head of the Department of Mechanical Engineering, Integral University, Lucknow, for providing their necessary departmental facilities during the course of this work. I have a pleasure in expressing my sincere thanks to **MOHD. ANAS**, Assistance Professor and M.Tech coordinator, Department of Mechanical Engineering, Integral University, Lucknow, for their kind support and permission to perform various work in workshop and also thankful to all workshop members for their support and help in dissertation work. Also I am very thankful Mechanical Engineering department Head and all other members of Mechanical Engineering department for their help and support during my dissertation work, and I would also thank to all department faculties for their kind support during my dissertation work. And in last I would fail in my duty if I do not thank my parents who were a great source of encouragement.

MD KHALID MUMTAZ

TABLE OF CONTENTS

CHAPTER NO.	TITLE	PAGE NO.
	ABSTRACT	iii
	LIST OF TABLES	xvii
	LIST OF FIGURES	xix
	LIST OF SYMBOLS AND ABBREVIATIONS	xxv
1.	INTRODUCTION	1
	CLASSIFICATION OF WELDING PROCESSES	3
	SOLID STATE WELDING	5
	PRINCIPLE OF ERSW PROCESS	12
	Heat Generation	14
	Pressure	15
	Electrode Tips	16
	Electrode Tip Size	17
	Pressure or Welding Force	17
	Heat Balance	18
	Surface Conditions	18
	MATERIALS DATA FOR RESISTANCE	
	SPOT WELDING	18
	Mild Steel	19
	Stainless Steel	20
	Aluminium Alloy	21
	WELDING OF VARIOUS COMBINATIONS	23
	Welding of SS Alloys:	23

CHAPTER NO.	TITLE	PAGE NO.
	Welding of AISI1020 Alloys	24
	Welding of AL Alloys	25
	TYPES OF AIS5052-AISI1020, AISI1020-AI, AIS5052-AI ALLOYS SELECTED FOR THIS INVESTIGATION	26
	MOTIVATION OF THIS RESEARCH	26
	ORGANISATION OF THIS RESEARCH WORK	27
	SUMMARY	29
2.	LITERATURE REVIEW	31
	REVIEWS ON SIGNIFICANCES OF RSW WELDING PROCESS	32
	REVIEW ON THE VARIOUS PROCESS PARAMETERS OF RSW PROCESS	38
	REVIEW ON OPTIMIZATION & PREDICTION OF RSW PROCESS PARAMETERS	42
	REVIEW ON MECHANICAL AND METALLURGICAL PROPERTIES OF RSW WELD JOINTS	47
	REVIEW ON ANALYSING THE RSW PROCESS USING VARIOUS SOFTWARES	54
	REVIEW ON VARIOUS TYPE OF CORROSION TESTS ON RSW JOINTS	57
	INFERENCE FROM LITERATURE SURVEY AND PROBLEM IDENTIFICATION	59
	SUMMARY	60

CHAPTER NO.	TITLE	PAGE NO.
3.	OBJECTIVES AND METHODOLOGIES	61
	OBJECTIVES	64
	METHODOLOGY	70
	SUMMARY	72
4.	EXPERIMENTAL METHODS AND MATERIALS	73
	MATERIALS SELECTION	73
	ERSW WELDING MACHINE	74
	WELDING PROCESS PARAMETERS	75
	Selected ERSW Process Parameters for Trail Experiments	75
	ERSW Process Parameters for Optimization and Prediction Techniques	76
	MECHANICAL TESTING	76
	TSFL Test	76
	Micro Hardness test	77
	METALLURGICAL TESTING	79
	POTENTIODYNAMIC POLARISATION TEST	80
	SUMMARY	82
5.	SELECTED WELDING PROCESS PARAMETERS	83
	TRIAL EXPERIMENTS FOR SIMILAR JOINTS	83
	Trial Experimental Study for AIS5052-AIS5052 Similar Joints	83
	Trial Experimental study for AISI1020-AISI1020 Similar Joints	85

CHAPTER NO.	TITLE	PAGE NO.
	TRIAL EXPERIMENTAL STUDY FOR DISSIMILAR JOINTS	87
	Trial Experimental study for AIS5052-AISI1020 joints	87
	Trial Experimental study for AISI1020-AA1008 joints	89
	Trial Experimental study for AIS5052-AA1008 joints	91
	SUMMARY	93
6.	OPTIMIZATION AND PREDICTION MODEL FOR ERSW PROCESS USING RSM AND ANOVA TECHNIQUES	94
	OPTIMIZATION OF ERSW INPUT PROCESS PARAMETERS FOR WELDING OF AIS5052-AISI1020, AISI1020-AA1008 AND AIS5052- AA1008 DISSIMILAR JOINTS	94
	An overview of Design of Experiments (DOE)	95
	Response surface methodology (RSM)	95
	Analysis of variance (ANOVA)	96
	DEVELOPMENT OF RSM MODEL FOR OPTIMIZATION OF ERSW PROCESS PARAMETERS	98
	DEVELOPMENT OF ANOVA MODEL FOR PREDICTION OF MECHANICAL AND NUGGET DIAMETER FOR ERSW JOINTS	99
	SUMMARY	99

CHAPTER NO.	TITLE	PAGE NO.
7.	RESULTS AND DISCUSSION	101
	EXPERIMENTAL INVESTIGATION ON THE EFFECT OF WELD PRESSURE ON MECHANICAL AND METALLURGICAL PROPERTIES OF ERSW WELDED AIS5052– AIS5052, AISI1020-AISI1020 SIMILAR JOINTS	101
	Mechanical and Metallurgical Investigation of AIS5052 – AIS5052 Joints	102
	Analysis of TSFL and hardness results	102
	Analysis of metallurgical results	105
	Mechanical and Metallurgical Investigation of AISI1020 – AISI1020 Joints	111
	Analysis of TSFL and hardness results	111
	Analysis of Metallurgical results	115
	OPTIMIZATION OF ERSW WELD PROCESS PARAMETERS' USING RSM METHOD FOR AIS5052-AISI1020, AISI1020- AA1008 AND AIS5052-AA1008 DISSIMILAR JOINTS USING RSM	120
	RSM Results for AIS5052-AISI1020 Dissimilar Joints	120
	Optimizing weld input process parameters for TSFL strength	126
	Optimizing weld input process parameters for Microhardness	128
	Optimizing weld input process parameters for nugget diameter	131

CHAPTER NO.	TITLE	PAGE NO.
	RSM Results for AISI1020-AA1008	
	Dissimilar Joints	133
	Optimizing weld input process parameters for TSFL strength	
	139	
	Optimizing weld input process parameters for microhardness	
	141	
	Optimizing weld input process parameters for nugget diameter	
	144	
	RSM Results for AIS5052-AA1008	
	Dissimilar Joints	147
	Optimizing weld input process parameters for TSFL strength	
	152	
	Optimizing weld input process parameters for microhardness	
	154	
	Optimizing weld input process parameters for nugget diameter	
	157	
	Confirmation Test Results for Optimized	
	The condition of Dissimilar Joints	159
	PREDICTION OF ERSW PROCESS	
	PARAMETER FOR WELDING OF AIS5052-	
	AISI1020, AISI1020-AA1008,	
	AIS5052-AA1008 DISSIMILAR JOINTS	161
	Prediction of Process Parameters ERSW Welded	
	AIS5052-AISI1020, Dissimilar	
	Joints Using ANOVA	161
	ANOVA results for TSFL	
	Analysis	161
	ANOVA results for hardness	
	analysis	164

CHAPTER NO.	TITLE	PAGE NO.
	ANOVA results for nugget diameter analysis	167
	Prediction of Process Parameters ERSW Welded AISI1020-AA1008 Dissimilar Joints using ANOVA	171
	ANOVA results for TSFL analysis	171
	ANOVA results for hardness Analysis	173
	ANOVA results for nugget diameter analysis	177
	Prediction of Process Parameters ERSW Welded AIA5052-AA1008 Dissimilar Joints Using ANOVA	180
	ANOVA results for TSFL analysis	180
	ANOVA results for microhardness analysis	184
	ANOVA results for nugget diameter analysis	187
	RESULT OF CORROSION STUDY	189
	Corrosion Rate Analysis on AIS5052-AISI1020 Dissimilar ERSW Welded Joints at Optimum Condition	190
	Corrosion Rate Analysis on AISI1020-AA1008 Dissimilar ERSW Welded Joints at Optimum Condition	191
	Corrosion Rate Analysis on AIS5052-AA1008 Dissimilar ERSW Welded Joints at Optimum Condition	192

CHAPTER NO.	TITLE	PAGE NO.
	Comparison of Corrosion Rate of AIS5052- AISI1020, AISI1020-AA1008 and AIS5052-AA1008 Joints	193
	SUMMARY	194
8.	CONCLUSION AND SCOPE OF FUTURE WORK	195
	WELDING OF AIS5052 SIMILAR JOINTS USING ERSW WELDING PROCESS AT DIFFERENT WELD PRESSURE	195
	WELDING OF AISI1020 SIMILAR JOINTS USING ERSW WELDING PROCESS AT DIFFERENT WELD PRESSURE	196
	OPTIMIZATION OF WELD INPUT PARAMETER ON MECHANICAL PROPERTIES AND NUGGET DIAMETER OF ERSW WELDED AIS5052-AISI1020, AISI1020-AA1008 AND AIS5052-AA1008 DISSIMILAR JOINTS USING RSM TECHNIQUE	198
	Optimization using RSM for AIS5052-AISI1020 Joints	198
	Optimization using RSM for AISI1020-AA1008 Joints	200
	Optimization using RSM for AIS5052-AA1008 Joints	201

CHAPTER NO.	TITLE	PAGE NO.
	PREDICTION OF TSFL, MICROHARDNESS AND NUGGET DIAMETER ON ERSW WELDED AIS5052- AISI1020, AISI1020-AA1008, AND AIS5052-AA1008 DISSIMILAR JOINTS	
	USING ANOVA	203
	Prediction of TSFL, Micro Hardness and Nugget Diameter on ERSW Welded AIS5052-AISI1020 Dissimilar Joint	
	using ANOVA	203
	Prediction of TSFL, Micro Hardness and Nugget Diameter on ERSW Welded AISI1020-AA1008 Dissimilar Joint	
	Using ANOVA	204
	Prediction of TSFL, Micro Hardness and Nugget Diameter on ERSW Welded AIS5052-AA1008 Dissimilar Joint	
	Using ANOVA	205
	FUTURE WORK	205
	REFERENCES	207
	LIST OF PUBLICATIONS	218

LIST OF TABLES

TABLE NO.	TITLE	PAGE NO.
1.1	The composition of Mild Steel (Low Carbon Steel)	20
1.2	Composition Of stainless steel	21
1.3	Composition of Aluminium	22
1.4	Comparative Physical Properties of Stainless Steel and Carbon	24
4.1	Chemical Compositions of Selected Base Materials	74
4.2	Mechanical Properties of Selected Base Materials	74
5.1	The weld process parameters AIS5052-AIS5052	85
5.2	The weld process parameters of AISI1020-AISI1020	87
7.1	Results obtained from TSFL and microhardness tests for AIS5052 similar joints	104
7.2	Weight percentage of elements on the sample welded at 3.7kgf	108
7.3	TAFEL Data Model Data for AIS5052 similar joint welded at the weld pressure 3.7kgf	110
7.4	Results obtained from TSFL and microhardness tests for AISI1020 similar joints	113
7.5	Weight percentage of elements on the sample welded at 3.7kgf	117
7.6	TAFEL Data Model Data for AISI1020 similar joint welded at the weld pressure 3.7kgf	119

TABLE NO.	TITLE	PAGE NO.
	Process Parameters and their levels for AIS5052(SS)-AISI1020(MS) dissimilar joints	120
	Result of confirmation and predicted values by RSM	160
	Results of ANOVA for TSFL	162
	Results of ANOVA for hardness	166
	Results of ANOVA for Nugget diameter	168
	Results of ANOVA for TSFL	172
	Results of ANOVA for Hardness	174
	Results of ANOVA for Nugget diameter	179
	Results of ANOVA for TSFL	181
	Results of ANOVA for Hardness	185
	Results of ANOVA for Nugget diameter	187
	Optimized Corrosion rate analysis	191
	Optimized Corrosion rate analysis	192
	Optimized Corrosion rate analysis	193

LIST OF FIGURES

FIGURE NO.	TITLE	PAGE NO.
1.1	Classification of Solid State Welding	6
1.2	Schematic diagram of Electrical Resistance Spot Welding process	13
3.1(a)	Schematic workflow chart phase-I	66
3.1(b)	Schematic workflow chart phase-II	67
3.1(c)	Schematic workflow chart phase-III	68
3.1(d)	Schematic workflow chart	69
4.1	Photographic View of the ERSW machine deployed in this study	75
4.2	Specimen Dimensions (all dimensions are in mm)	76
4.3	TSFL machine	77
4.4	Hardness sample	78
4.5	Micro Vickers Hardness Tester Machine	78
4.6	Photographic image of Optical Microscope	79
4.7	Photographic image of Scanning Electron Microscope (SEM)	80
4.8	Experimental setup for potentiodynamic polarization test	81
4.9	Samples of Corrosion Test	81
5.1	Photographic view of the AIS5052-AIS5052 samples before the weld	84
5.2	Photographic view of the AIS5052-AIS5052 samples after the weld	84

FIGURE NO.	TITLE	PAGE NO.
	Photographic view of the AISI1020-AISI1020 samples before the weld	86
	Photographic view of the AISI1020-AISI1020 samples after the weld	86
	Photographic view of the AIS5052-AISI1020 samples before the weld	88
	Photographic view of the AIS5052-AISI1020 samples after the weld	88
	Photographic view of the AIS5052-AISI1020 samples before TSFL Test	89
	Top view of AIS5052-AISI1020 samples after TSFL Test	89
	Photographic view of the AISI1020-AA1008 samples before the weld	90
	Photographic view of the AISI1020-AA1008 samples after the weld	90
5.8.1	Photographic view of the AISI1020-AA1008 samples after TSFL test	91
	Photographic view of the AIS5052-AA1008 samples before the weld	92
	Photographic view of the AIS5052-AA1008 samples after the weld	92
5.10.1	Photographic view of the AIS5052-AA1008 samples after TSFL Test	93
7.1	Photographic view of TSFL test samples of AIS5052-AIS5052 Similar joints before testing	102

FIGURE NO.	TITLE	PAGE NO.
7.2	Photographic image of TSFL tested samples of AIS5052 – AIS5052 similar welded joints after testing.	103
7.3	TSFL test results for the samples welded at three different weld pressure conditions for AIS5052 Similar joints.	103
7.4(a)	Photographic view of microhardness samples of AIS5052 similar joints	104
7.4(b)	Microhardness test result for the samples welded at various weld pressures	105
7.5	(a) to (f) shows the Macro-micro image and Nugget diameter of the AIS5052 similar joints welded at various weld pressure	106
7.6	(a) SEM image of the sample welded at the weld pressure of 3.7kgf (b) EDS plot of the sample welded at weld pressure 3.7kgf	108
7.7	Factography images of TSFL tested sample welded at the weld pressure 3.7kgf.	109
7.8	TAFEL plot for AISI 304 similar joints welded at 3.7Kgf weld pressure	110
7.9	Photographic view of TSFL test samples of AISI1020-AISI1020 Similar joints before testing.	111
7.10	Photographic image of TSFL tested samples of AISI1020 – AISI1020 similar welded joints after testing.	112
7.11	TSFL test results for the samples welded at three different weld pressure conditions for AISI1020 Similar joints.	112

FIGURE NO.	TITLE	PAGE NO.
7.12(a)	Photographic view of microhardness samples of AISI1020 similar joints	114
7.12(b)	Microhardness test result for the samples welded at various weld pressures	114
7.13	(a) to (f) shows the Macro-micro image and Nugget diameter of the AISI1020 similar joints welded at various weld pressure	115
7.14	(a) SEM image of the sample welded at the weld pressure of 3.7kgf (b) EDS plot of the sample welded at weld pressure 3.7kgf	117
7.15	Factography images of the TSFL tested sample welded at weld pressure 3.7kgf.	118
7.16	TAFEL plot for AISI1020 for welded at 3.7Kgf weld pressure	119
7.16.1	(a) and (b) TSFL specimen of AIS5052-AISI1020 and Hardness test sample of AIS5052-AISI1020	121
7.17(a to o)	Cross-Sectional Macrostructure and Nugget images of the TSFL samples	122
7.17.1	The TSFL, microhardness and nugget diameter values of AIS5052 and AISI1020	125
7.18(a to f)	Various interaction plots 3D (a,c e) and 2D (bdf) plots for TSFL.	126
7.19(a to f)	Various interaction plots for hardness, figure (a,c,e) shows 3D plots and figures (b,d,f) shows the 2D plots.	129

FIGURE NO.	TITLE	PAGE NO.
7.20(a to f)	Various interaction plots for nugget diameter. figure (a,c,e) shows 3D plots and figures (b,d,f) shows the 2D plots.	131
7.20.1	(a) and (b) TSFL specimen of AISI1020-AA1008 and Hardness test sample of AISI1020-AA1008	134
7.20.2	Cross-Sectional Macrostructure and Nugget images of the TSFL samples	135
7.20.3	The TSFL, microhardness and nugget diameter values of AISI1020-AA1008	138
7.21(a to f)	Various interaction 3D (a,c,e) and 2D (bdf) plots for TSFL.	139
7.22(a to f)	Various interaction plots for hardness, figure (a,c,e) shows 3D plots and figures (b,d,f) shows the 2D plots.	142
7.23(a to f)	Various interaction plots for nugget diameter. figure (a,c,e) shows 3D plots and figures (b,d,f) shows the 2D plots.	145
7.23.1	(a) and (b) TSFL specimen of AIS5052-AA1008 and Hardness test sample of AIS5052- AA1008	147
7.23.1.1	Welded TSFL sample, hardness sample, and nugget images	148
7.23.2	The TSFL, microhardness and nugget diameter values of AIS5052 and AA1008	151
7.24	Various interaction plots for TSFL figure (a,c,e) shows 3D plots and figures (b,d,f) shows the 2D plots.	152

FIGURE NO.	TITLE	PAGE NO.
7.25(a to f)	Various interaction plots for TSFL figure (a,c,e) shows 3D plots and figures (b,d,f) shows the 2D plots	155
7.26(a to f)	Various interaction plots for TSFL figure (a,c,e) shows 3D plots and figures (b,d,f) shows the 2D plots.	157
7.27	Corrosion Tested Sample Image of AIS5052-AISI1020	190
7.28	Corrosion rate analysis(optimized)	191
7.29	Corrosion Tested Sample Image of AISI1020-AA1008	191
7.30	Corrosion rate analysis(optimized)	192
7.31	Corrosion Tested Sample Image of AIS5052-AA1008	192
7.32	Corrosion rate analysis(optimized)	103
7.33	Corrosion rate of AIS5052-AISI1020, AISI1020-AA1008 and AIS5052-AA1008 joints	103

CHAPTER 1

INTRODUCTION

The current world is so busy that, it needs things to get over or get completed at a very early and short duration of time. The world is in the stage of pushing things hard and fast to get the best and efficient methods to hold things together and bind the necessary things together at the right the place. In the field of engineering, things are getting changed on a regular day to day at a much greater pace. Every day we come up with new things new methods evolve and revolve in the field of mechanical engineering and the few of them will stay and will be focused till the very end of mankind and one of them is welding.

In the current scenario, there has been so many researches done and still going on in the field of welding technology. Countless works are been carried on in the recent times in the different streams of welding with consideration of so many factors from each and every bit of materials and tools used during the process by changing the properties and values and usages etc. Let's start with the basic introduction along from the history to the various types of the current research work importance will be discussed in this introduction section.

It is always essential for joining separate pieces of metal together through an electrochemical reaction that renders them homogeneous and physically one piece. It's very important if you want to build something that demands material continuity, as in where joints and the fasteners would be

insufficient or inappropriate for reasons of strength, pressure, corrosion or any other environmental concerns. Welding isn't meant for the weak people around in this demanding world. As someone who personally gave it a try our self, we can tell you it's not as easy as it may seem as we are getting evolved with new and new challenges. This is a hot, difficult and physically tasking job as we all know but absolutely necessary for a variety of products and infrastructures. Most people don't realize the importance of welding as it plays in day to day life from the consumers to the general public to the company leaders.

Welding is a process of joining the metal pieces by the application of heat on them. Welding is one of the least expensive process and widely used now a day in manufacturing sectors. Welding joints different metals by means of a number of processes in which heat is supplied either electrically or by mean of a gas torch over the materials. Different welding processes are used in the manufacturing of the Automobiles bodies, structural works, tanks, and general mechanical repair work. In the production and manufacturing industries, welding is used in refineries and pipeline fabrication. Now through all these thoughts, it may be called as the secondary manufacturing process.

The different form of defining welding is that it is a fabrication or sculptural process that joins materials generally usually metals or thermoplastics by causing fusion, which is distinct from lower temperature metal-joining techniques such as brazing and soldering, which do not melt the base metal.

The History of Welding

For a common man asking 'What is welding?' we are generally not aware of the fact that most of the work and technological advancement has made welding what it is as of today. The previous examples of welding have

been discovered which dates back to thousands of years ago. It was known as forge welding which simply involved the heating of two metal surfaces and hammering them together through force or pressure. This was only during the 19th Century that welding as a process gained its importance and has become what we know it as currently. While asking ‘What is welding?’ very few people can understand that it’s forge welding that was done without the use of electricity. Through the years when this welding was very labor intensive, the industrial revolution gave rise to the getting different and better, improved methods of welding that we know at present.

Why welding is so important

When questioned about ‘What is the importance of welding?’ we seldom always realize that without this style of metal work, many structures would cease to exist. A best-experienced welder will be able to join metal in such a way that it is not able to be part are separated so easily unless it is split. Welding is an absolutely essential component of industries such as the automotive industry, the construction industry and even the aviation industry all through till date and in future too. It’s also used even in oil rigs out in the sea which makes use of various forms of welding in order to withstand the extreme harsh oceanic style weather conditions.

CLASSIFICATION OF WELDING PROCESSES

They are different types of welding identifications are made and they have been as many as around 35 different welding and brazing process and several soldering methods, in use by the industry each day. There are so many various ways of classifying the welding based on different assets and they may be classified on the basis of source of heat (process, uses, flames, arc etc.)

In general, various welding processes are classified as follows.

1. Gas Welding

- (a) Air Acetylene
- (b) Oxy-Acetylene
- (c) Oxy-Hydrogen Welding

2 ARC Welding

- (a) Carbon Arc welding
- (b) Plasma Arc welding
- (c) Shield Metal Arc Welding
- (d) T.I.G. (Tungsten Inert Gas Welding)
- (e) M.I.G. (Metal Inert Gas Welding)

3 Resistance Welding

- (a) Spot welding
- (b) Seam welding
- (c) Projection welding
- (d) Resistance Butt welding
- (e) Flash Butt welding

4 Solid State Welding

- (a) Cold welding
- (b) Diffusion welding
- (c) Forge welding
- (d) Fabrication welding
- (e) Hot pressure welding
- (f) Roll welding

5 Thermo Chemical Welding

- (a) Thermit welding
- (b) Atomic welding

6 Radiant Energy Welding

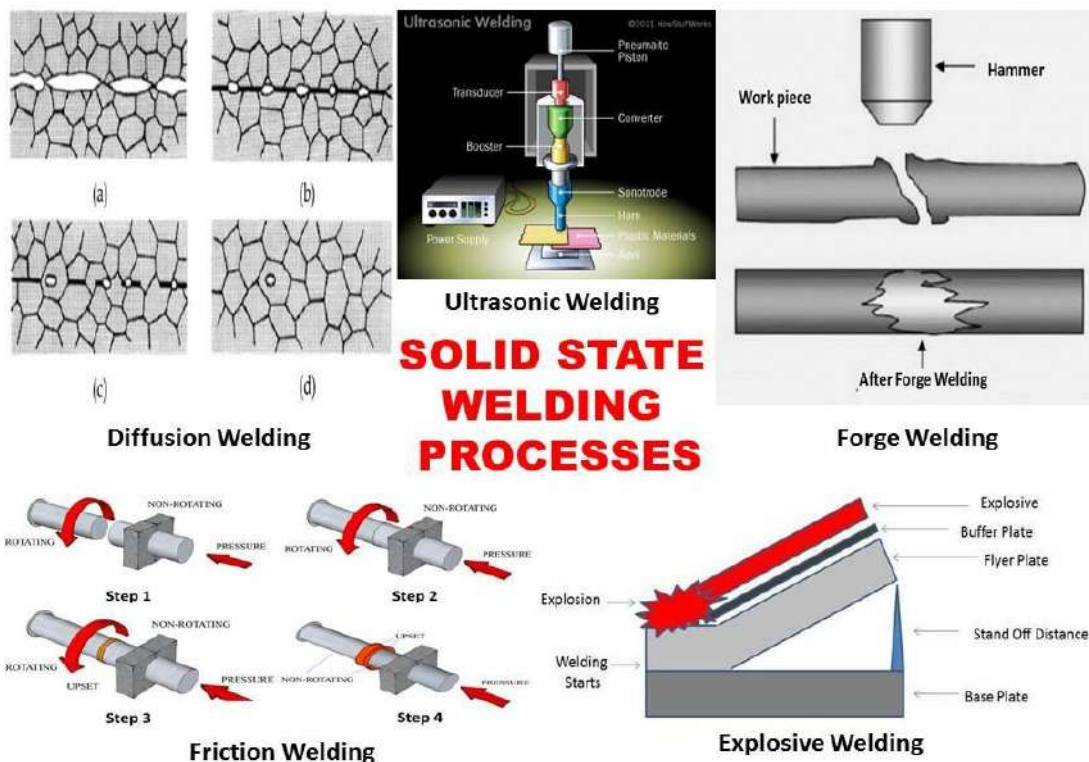
- (a) Electric Beam Welding
- (b) Laser Beam Welding

In this research work, the prime focus is on the Solid state welding and that to Electrical Resistance Spot welding. So to start about let's begin with the various types as follows

SOLID STATE WELDING

Why it's been that solid-state welding is selected for this research work:

- This Welding is free from microstructure defects as like the pores, the non-metallic inclusions, the segregation of alloying elements.
- The Mechanical properties of the weld are similar to those of the parent metals which is being used in the SSW process.
- In SSW there are no consumable materials used.
- IN SSW the dissimilar metals can be easily joined (carbon alloy, steel - aluminum alloy steel - copper alloy).



(Source: Dawi 2013)

Figure 1.1 Classification of Solid State Welding

There are few problems to be considered as in this which is been looked upon in this,

- There is an always a necessity in this for a thorough surface preparation needed like degreasing, oxides removal, brushing/sanding.
- The experimental set up is very expensive.

The following processes are related to Solid State welding:

- Forge Welding (FOW)
- Cold Welding (CW)
- Friction Welding (FRW)
- Explosive Welding (EXW)
- Diffusion Welding (DFW)
- Ultrasonic Welding (USW)

Forge Welding (FOW)

The Forge Welding is a style of Solid State Welding process, in which the low carbon steel parts are heated to about 1800°F (1000°C) and then forged to obtain the output. Prior to Forge Welding, all the parts are scarfed in order to prevent the entrapment of oxides in the joint. The Forge Welding is used in general in most of the blacksmith shops and for the manufacturing metal art pieces and welded tubes.

Cold Welding (CW)

In Cold Welding is a Solid State Welding process, in which the two workpieces are joined together at the room temperature and under the pressure, which causes a substantial deformation of the welded parts and providing an intimate contact between the welded surfaces with ease.

As an outcome of the deformation, the oxide film covering the welded parts breaks open and the clean metal surfaces get revealed. The necessary intimate contact between these pure surfaces provides a strong binding and defect-less bonding. The Aluminum alloys, Copper alloys, low carbon steels, Nickel alloys, and other ductile metals may be comfortably welded by Cold Welding. The Cold Welding is widely used in for the manufacturing of bi-metal steel - aluminum alloy strips, and for cladding of aluminum alloy strips by other aluminum alloys or pure aluminum. The bi-metallic strips are produced by the rolling technology. Different styles of presses are also used for Cold Welding. Mostly Cold Welding can also be easily automated.

Friction Welding (FRW)

In the Friction Welding, in this, the two cylindrical parts are brought into contact due to a friction pressure when one of them rotates. Here the friction between the joining parts results in heating their respective ends. The forge pressure is applied to the pieces that are been providing the formation of the joint.

Through this the Carbon steels, Alloy steels, Tool and die steels, Stainless steels, Aluminum alloys, Copper alloys, Magnesium alloys, Nickel alloys, Titanium alloys may be conveniently joined by Friction Welding.

Explosive Welding (EXW)

In Explosive, the welded parts (plates) are metallurgically bonded through the result of oblique impact pressure exerted on them by a controlled detonation of an explosive charge implied during the process.

One among the welded parts (i.e.) the base plate is rested on an anvil and the second part (i.e.) the flyer plate is located above the base plate with an angled or constant interface clearance between them

The explosive charge is placed on the required flyer plate. The required detonation starts at on the edge of the plate and propagates at a high velocity all along the plate. The maximum detonation velocity is around 120% of the material sonic velocity. The slags are then expelled by the jet created just ahead of the bonding front formed Almost all the commercial metals and alloys may be bonded or welded by the Explosive Welding process.

The dissimilar metals may be joined by means of the Explosive Welding:

- Copper to steel;
- Nickel to steel;
- Aluminum to steel;
- Tungsten to steel;
- Titanium to steel;
- Copper to aluminum.

Explosive Welding is used for manufacturing of clad tubes and pipes, in pressure vessels, in building aerospace structures, the heat exchangers, in bi-metal sliding bearings, in the ship structures, weld transitions, corrosion resistant chemical process tanks.

Diffusion Welding (DFW)

The diffusion welding process, the pressure applied to two workpieces with carefully cleaned surfaces and at an elevated temperature below the melting point of the metals. Bonding of the materials is a result of mutual diffusion of their interface atoms.

In order to keep the bonded surfaces clean and clear from oxides and other air contaminations, the process is essentially conducted in a vacuum. There is no appreciable deformation of the workpieces will occur in Diffusion Welding. Diffusion Welding is most seldom referred to as Solid State Welding (SSW).

Diffusion Welding is able to bind the dissimilar metals, which are difficult to be welded by most other welding processes:

- Steel to tungsten;
- Steel to niobium;
- Stainless steel to titanium;
- Gold to copper alloys.

This style of the welding process is widely used in aerospace and rocketry, electronics, nuclear applications, and manufacturing composite materials.

Ultrasonic Welding (USW)

In this type of welding process, both the workpieces are bonded as a result of a pressure exerted on the welded parts combined with the application of high-frequency acoustic vibration through the ultrasonic. The Ultrasonic vibration causes friction between the parts, which results in a much closer contact between the two surfaces with the necessary simultaneous local heating of the contact area surfaces. Interatomic bond is formed under these conditions, providing the much needed strong joint. The ultrasonic cycle takes about just 1 sec. The frequency of acoustic vibrations falls in the range 20 to 70 KHz

The thickness of the welded parts is limited by the power of the ultrasonic generator. Ultrasonic Welding is used mainly for bonding small workpieces in electronics, for manufacturing communication devices, medical tools, watches, in the automotive industry.

Electric Resistance Welded (ERW) pipe is manufactured by the various cold-forming processes done on a sheet of steel into a cylindrical shape. The necessary current is then passed between the two edges of the steel to be joined to heat the steel to a point at which the edges are forced together to form a bond without the use of required welding filler material. Initially stage this manufacturing process used very low-frequency A.C. current to heat the edges from the 1920s until 1970. In 1970, the low-frequency process was superseded by the high-frequency ERW process which produced a higher and better quality weld.

As the time progressed, the welds of low-frequency ERW pipe was found to be limited to selective seam corrosion all over and the hook cracks and inadequate bonding of the seams have so very low-frequency resistant welding and is no longer used in the manufacturing of pipes. The

high-frequency process is still being used in the manufacture of pipes for the uses in pipeline construction.

The ERSW involves totally three stages; the first one involves the electrodes being brought on to the surface of the metal and applying the necessary slightest amount of pressure over them for a period of time. Then the current from the electrodes is relatively then applied briefly for some time and after which the applied current is removed and the electrodes it stays in the place for the material to cool down systematically. The required weld times range from 0.01 sec to 0.63 sec depending on the thickness of the material used and the electrode force applied and the electrodes diameter.

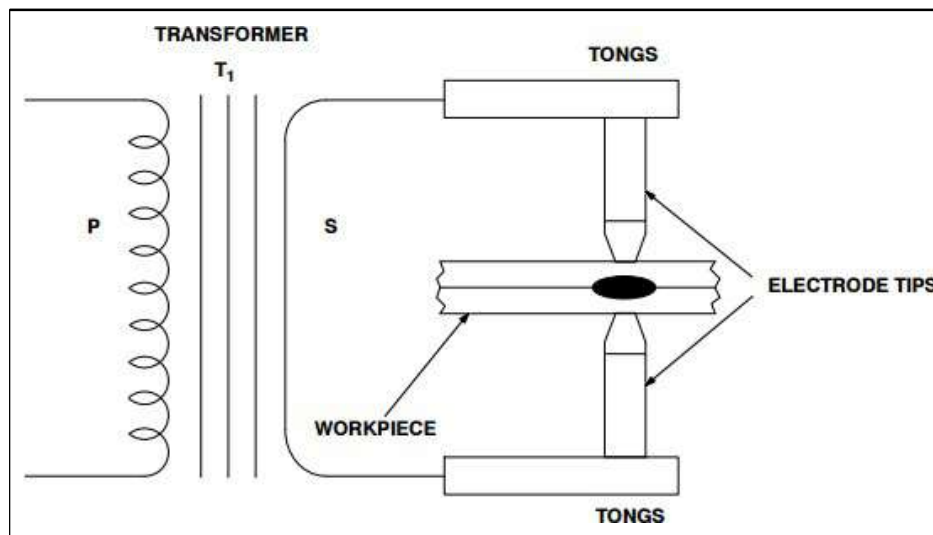
PRINCIPLE OF ERSW

This is attained when current flow through electrode tips and the pieces of metal to be joined necessarily. The resistance of the base metal to electrical current flow causes localized heating in the required joints and the necessary weld is formed. Resistance welding processes are the fast and reliable means of joining thin sheets of metal together. Required weld is created by first applying the necessary pressure on the two parts to be joined. After attaining the correct amount of pressure is applied, current is passed between the two (or more) overlapped necessary sheets. The resistive heating results in the melting and formation of a “weld nugget” or a “weld seam”.

Resistance spot welding is the most common of the resistance welding processes widely used presently. It is used extensively in the automotive, appliance, furniture, and aircraft industries to join sheet materials for the various requirements. In this style of the welding process, water-cooled, copper electrodes are used to clamp the sheets to be welded together into the place. The force applied to the electrodes ensures intimate contact between all the parts in the weld configuration mentioned as the requirement.

The appropriate current is then passed across the electrodes through the sheets. The resistance of the metal to the localized flow of current produces heat

- Process variables
 - Current
 - Time
 - Force
 - Spot and seam welding



(Source: Aravithan dragam 2015)

Figure 1.2 Schematic diagram of Electrical Resistance Spot Welding process

The Resistance spot welding machines are constructed with so minimum resistance which will be apparent in the transformer, flexible cables, tongs, and electrode tips etc. The resistance spot welding machines are destined to bring the welding current to the weldment in the most appropriate and efficient manner. The greatest relative resistance required is at the weldment. Here the term “relative” means with relation to the rest of the

actual welding circuit used. There are maximum six major points of resistance in the work area and they are mentioned below:

1. The point of contact between the electrode and the top workpiece.
2. The top workpiece.
3. The interface between the top and bottom workpieces.
4. The bottom workpiece.
5. The point of contact between the electrode and the bottom workpiece.
6. The resistance of electrode tips.

The resistances are always in series, and each point of the resistance will retard the flow of current. The necessary amount of resistance at the point are three and they are at the interface of the workpieces then it depends on the heat-transfer capabilities of the material, the material's electrical resistance, and finally the combined thickness of the materials at the welded joint. It is exactly at this part of the circuit that the nugget of the weld is formed preferably.

Heat Generation

A modification required for the Ohm's Law may be made when watts and heat are considered synonymous with each other. When the current is passed through a conductor the electrical resistance of the conductor to current flow will cause heat to be generated through them. The basic formula for heat generation may be stated:

$$H = I^2R$$

where,

H = Heat

I^2 = Welding Current Squared

R = Resistance.

The subsequent portion of a resistance spot welding circuit also includes the actual parts to be welded in a series of resistances. The complete additive value of this electrical resistance not only affects the current output of the resistance spot welding machine but also the heat generation in the circuit. The predominant fact is that although current value is the same in entire parts of the electrical circuit setup, the values of the resistance may vary considerably at different portions and positions in the circuit. The heat thus generated is always directly proportional to the resistance at any point in the electrical circuit.

Pressure

The effective pressure on the resistance spot weld should be carefully considered based on the necessity. The main purpose of pressure is to keep the parts intact to be welded in the joint interface. This gives the assured consistent for the electrical resistance and conductivity at the point where it has to be weld. It is essential that before the pressure is applied, the parts to be welded should be in intimate contact. Various investigations have revealed that high pressures exerted on the weld joint decrease with a decrease in the resistance at the point of contact between the workpiece surface and the electrode tip and. The greater the pressure lower would be the resistance factor. The necessary pressures, with intimate contact between the electrode tip and the base metal, tend to conduct the heat away from the

welding area. For greater pressures, higher currents are necessary, adversely lower pressures require the least amperage from the RSWM.

Electrode Tips

Through the various researches, Copper is the base metal normally used for resistance spot welding tips and tongs. The main purpose of the electrode tips is to conduct the regular flow of welding current to the workpiece, to be the prime focus point of the pressure applied to the necessary weld joint, and then to conduct heat from the work surface. The prime requisite of the tips is to maintain their integrity of shape and thermal and electrical conductivity under all working conditions. Electrode tips are generally made of copper alloys and other materials. The Resistance Welders Manufacturing Association have classified electrode tips into two major groups:

Group A – Copper based alloys

Group B – Refractory metal tips

The groups are further subclassed by number. Group A, Class I, II, III, IV, and V are made of copper alloys. Group B, Class 10, 11, 12, 13, and 14 are the refractory alloys.

Group A, these are class I style electrode tips and are the closest in composition to pure copper. As the number increases, the hardness and annealing temperature values also increase; whereas the thermal and electrical conductivity relatively decreases.

Group B consists of a composite mixture of copper and tungsten, etc., which are designed for wear resistance and compressive strength at high working temperatures. In the Group B, category, the Class 10 alloys have

around 40 percent of the conductivity of copper and with conductivity decreasing as the number value systematically increases. Generally, the Group B electrode tips are not normally used for applications in resistance spot welding machines.

Electrode Tip Size

It is through the electrode in which the welding current is permitted to flow into the used workpiece, which logically proves that the size of the electrode tip point controls the size of the resistance in the spot weld. So the diameter of the electrode tip point should be slightly less than the weld nugget diameter. In case if the electrodes tip diameter is too small for the application, the weld nugget will be small and weak as well. But if the electrode tip diameter is too large, then there a possible danger of overheating the base metal and developing voids and gas pockets in them. Also in either instance, the appearance and quality of the finished weld would not be an acceptable range.

$$\text{Electrode tip diameter} = 0.100 \text{ in.} + 2t$$

where “t” is the thickness in inches of one thickness of the metal to be welded.

The above-mentioned formula is applicable to the welding of metals of dissimilar thicknesses. The formula is applied to each thickness individually, and the proper electrode tip diameter should be selected for each size of the joint separately.

Pressure or Welding Force

There is a great effect on the amount of weld current that flows through the joint by the pressure exerted by the tongs and the electrode tips on the workpiece. The greater the pressure, Higher would be the welding current value if the pressure is greater within the capacity of the RSWM. Generally,

the samples of material to be welded are placed between the electrode tips and checked for adequate pressure to make the weld to happen. The tong and electrode tip travel should be adjusted to the minimum required an amount in order to prevent the “hammering” of the electrode tips and tip holders used.

Heat Balance

The heat balance is defined as the conditions of welding in which the fusion zone of the pieces to be joined are then subjected to an equal amount of heat and pressure. The poor weld may result for several reasons as the weldment has parts of unequal thermal characteristics, such as copper and steel materials. A greater amount of localized heating can be obtained in the steel than compared in copper and the reason behind would be because of copper having low electrical resistance and high thermal transfer characteristics whereas steel has high electrical resistance and low thermal transfer characteristics.

Surface Conditions

All most all metals develop oxides which can be detrimental to resistance spot welding mechanism. Few oxides, those which are precisely refractive in nature, are more troublesome than others metals. In addition, the mill scale found on hot-rolled steels will act as an effective insulator and also prevent good-quality resistance spot welding. The necessary material surfaces to be joined by this process should be clean, and free of oxides and other chemical compounds and should have a smooth surface.

MATERIALS DATA FOR RESISTANCE SPOT WELDING:

This section of the text will give a detailed account of the various materials used for resistance spot welding used in fabrication work. It is not

essential that all the possible problems that could arise will be answered through all possible methods. The purpose of this part of the text is to provide generalized operational data for use with resistance spot welding machines.

Materials Used

Similar metals:

- Low Carbon Steel or Mild Steel (AISI1020)
- Stainless Steel (AIS5052)
- Aluminium

Mild Steel

Carbon steel is sometimes referred to as 'mild steel' or 'plain carbon steel'. The American Iron and Steel Institute defines a carbon steel as having no more than 2 % carbon and no other appreciable alloying element. Carbon steel makes up the largest part of steel production and is used in a vast range of applications.

Typically carbon steels are stiff and strong. They also exhibit ferromagnetism (i.e. they are magnetic). This means they are extensively used in motors and electrical appliances. Welding carbon steels with a carbon content greater than 0.3 % require that special precautions be taken. However, welding carbon steel presents far fewer problems than welding stainless steels. The corrosion resistance of carbon steels is poor (i.e. they rust) and so they should not be used in a corrosive environment unless some form of protective coating is used.

Table 1.1 Composition of Mild Steel (Low Carbon Steel) (source: Alizadu-sh 2013)

Carbon	0.16-0.18%
Silicon	0.40% max
Manganese	0.70-0.90%
Sulphur	0.040% Max
Phosphorus	0.040% Max

Mild steel has a relatively low tensile strength, but it is cheap and easy to form; surface hardness can be increased through carburizing. It is often used when large quantities of steel are needed, for example as structural steel. The density of mild steel is approximately 7.85 g/cm^3 (7850 kg/m^3 or 0.284 lb/in^3) and Young's modulus is 200 GPa (29,000,000 psi).

Low-carbon steels suffer from yield-point run out where the material has two yield points. The first yield point (or upper yield point) is higher than the second and the yield drops dramatically after the upper yield point. If low-carbon steel is only stressed to some point between the upper and lower yield point and the surface develop Lüder bands. Low-carbon steels contain less carbon than other steels and are easier to cold-form, making them easier to handle.

Stainless Steel

Stainless steel is notable for its corrosion resistance, and it is widely used for food handling and cutlery among many other applications. Stainless steel does not readily corrode, rust or stain with water as ordinary steel does. However, it is not fully stain-proof in low-oxygen, high-salinity, or poor air-circulation environments. There are various grades and surface finishes of stainless steel to suit the environment the alloy must endure.

Stainless steel is used where both the properties of steel and corrosion resistance are required. Stainless steel differs from carbon steel by the amount of chromium present. Unprotected carbon steel rusts readily when exposed to air and moisture. This iron oxide film (the rust) is active and accelerates corrosion by making it easier for more iron oxide to form. Since iron oxide has a lower density than steel, the film expands and tends to flake and fall away. In comparison, stainless steels contain sufficient chromium to undergo passivation, forming an inert film of chromium oxide on the surface.

This layer prevents further corrosion by blocking oxygen diffusion to the steel surface and stops corrosion from spreading into the bulk of the metal. Passivation occurs only if the proportion of chromium is high enough and oxygen is present. Stainless steels resistance to corrosion and staining, low maintenance, and familiar lust remake it an ideal material for many applications.

Table 1.2 Composition of stainless steel (Source: Dursun 2007)

Carbon	0.055%
Chromium	18.2%
Nickel	8.10%
Manganese	8.10%
Silicon	8.35%
Sulfur	0.001%

Aluminium

Aluminium is the world's most abundant metal and is the third most common element, comprising 8% of the earth's crust. The versatility of

aluminium makes it the most widely used metal after steel. Although aluminium compounds have been used for thousands of years, aluminium metal was first produced around 170 years ago.

In the 100 years since the first industrial quantities of aluminium were produced, worldwide demand for aluminium has grown to around 29 million tons per year. About 22 million tons is new aluminium and 7 million tons is recycled aluminium scrap. The use of recycled aluminium is economically and environmentally compelling. It takes 14,000 kWh to produce 1 tonne of new aluminium. Conversely it takes only 5% of this to remelt and recycle one tonne of aluminium. There is no difference in quality between virgin and recycled aluminium alloys.

Table 1.3 Composition of Aluminium(Source: Hoe 1996)

Silicon	0.25 max
Iron	0.4 max
Copper	0,1
Manganese	0.1 max
Magnesium	0.1 max
Chromium	0.05-0.25 max
Zinc	0.10 max
Other	0.15 total max

Pure aluminium is soft, ductile, and corrosion resistant and has a high electrical conductivity. It is widely used for foil and conductor cables, but alloying with other elements is necessary to provide the higher strengths needed for other applications. Aluminium is one of the lightest engineering metals, having the strength to weight ratio superior to steel. By utilizing

various combinations of its advantageous properties such as strength, lightness, corrosion resistance, recyclability and formability, aluminium is being employed in an ever-increasing number of applications. This array of products ranges from structural materials through to thin packaging foils.

These are some of the benefits of the SPOT welding process

- Repeatability
- Increase return on investment
- Consistent quality welds
- Reduction of costs
- More movement flexibility

WELDING OF VARIOUS COMBINATIONS

In the field of engineering, many different types of manufacturing process have been evolving from the age-old days. Each and every day new and different style and types of manufacturing methods originate and among them many welding processes and a countless number of researches goes on in various parameters evolved. Each and everyday life in the present world is some way or the other related to many welding processes evolved. These divisions deal various combinations of welding alloys which can be researched upon.

Welding of AIS5052 Alloys

Most of the stainless steels are considered to have good Weldability and may be welded by several welding processes including the arc welding processes, resistance welding, friction welding and brazing. For any of these processes, joint surfaces and any filler metal must be clean. The thermal and

Electrical Conductivity of stainless steel is much less than carbon steel and coefficient of expansion is also higher. Low thermal conductivity tends to higher temperature rise in the vicinity of the weld and that coupled with a high coefficient of expansion leads to warpage and a higher incidence of weld cracking under restrained condition.

Table 1.4 Comparative Physical Properties of Stainless Steel and Carbon (Source: Dursun 2007)

Property	Martensitic	Ferritic	Austenitic	Carbon Steel
Thermal Conductivity Cal/Sec*cm ² °C/cm	0.059	0.049	0.033	0.104
Coefficient of Expansion µm/m/°C	11.2	11.2	18.2	13.2
Steel Electrical resistivity µΩ /cm	58	60	70	15
Melting range °C	1483-1532	1427-1510	1398-1454	1538

Welding of AISI1020 Alloys

Carbon steels contain trace amounts of alloying elements and account for 90% of total steel production. Carbon steels can be further categorized into three groups depending on their carbon content:

- Low Carbon Steels/Mild Steels contain up to 0.3% carbon
- Medium Carbon Steels contain 0.3 – 0.6% carbon
- High Carbon Steels contain more than 0.6% carbon

Alloy steels contain alloying elements (e.g. manganese, silicon, nickel, titanium, copper, chromium, and aluminum) in varying proportions in order to manipulate the steel's properties, such as its hardenability, corrosion resistance, strength, formability, weldability or ductility.

Applications for alloys steel include pipelines, auto parts, transformers, power generators and electric motors.

Welding of AL Alloys

There are various types of welding process used for joining aluminium alloys like Tungsten Inert Gas Welding (TIG), Metal Inert Gas Welding (MIG), Electron Beam Welding, Laser Beam Welding etc. To get the best of welding aluminium alloys the heat input plays a predominant role in joining. So it is very essential to take proper care in the selection of suitable welding process parameters to get highest and best quality welded joints. If there is not a proper weld process parameter selection then it may lead to major problems in the welding of aluminium alloys as mentioned below,

- There is solidification of cracking
- There might be low strength in HAZ in the nonheat treatable alloys employed.
- It leads to the possibility of hot cracking appearance.
- There is the issue of porous formation
- Vaporization of relatively more volatile alloying elements does occur.

TYPES OF AIS5052-AISI1020, AISI1020-AL, AIS5052-AL ALLOYS SELECTED FOR THE INVESTIGATION

In this work AISI 304(SS), AISI 1020(MS) and AA 1008(AA) are selected as base materials because they are widely used in commercial applications. The weldability of the above alloys using RSW process is difficult, because of the selection of unsuitable weld process parameters, which may result in various weld defects. Therefore, it is very important to analyze the influence of the various weld process parameters such as power, pressure and time on the mechanical properties, metallurgical characteristics and nugget dimensions of the welded joints.

To satisfy the above goal, the weld trials were conducted initially by varying the pressure for 3.3 to 3.8kgf and by keeping the power and time as constant in order to identify the effect of these parameters on mechanical and metallurgical properties of the weldments. Based on the above conditions the various similar and dissimilar joints such as AIS5052-AIS5052, AISI1020- AISI1020, AIS5052-AISI1020, AIS5052-AL, and AISI1020-AL are prepared.

MOTIVATION OF THIS RESEARCH

The prime motive of this investigation is to ensure the feasibility in welding of AIS5052-AIS5052, AISI1020-AISI1020, AIS5052-AISI1020, AISI1020-AL similar and dissimilar joints by RSW process. Similarly, this research work also concentrates on identifying suitable RSW weld process parameters for obtaining better mechanical and nugget dimensions using RSM and ANOVA tools. The individual investigation include

- An experimental investigation has been carried out on welding of AIS5052, AISI1020 and AA1008 similar and dissimilar joints with the help of RSW process by varying the weld pressure and keeping weld time and current as constant.

- To ensure the quality of welded joints, both mechanical and metallurgical tests were carried out.
- To predict and optimize the RSW weld input process parameters was carried out using RSM and ANOVA tools are used for all the similar and dissimilar joints by varying the weld process parameters such as power time and pressure on mechanical properties and nugget dimensions.
- To validate the optimized process parameters, the confirmation test was conducted and the experimentally obtained results were validated with the RSM and ANOVA results. Similarly, corrosion test was also conducted on the sample welded at the optimum condition and the obtained results were compared with the results obtained from the un-optimized weld samples.

ORGANISATION OF THIS RESEARCH WORK

The thesis is classified into 8 chapters. **Chapter 1** gives a brief introduction to the various types of welding processes, their classifications, materials, and their applications. It also gives us an account of ESRW Process and its components in detail. The introduction of various types of AIS5052, AISI1020, AL alloys, their classification and the properties are also discussed. The material is chosen for this investigation and the problems encountered in the welding of various combinations of AIS5052, AISI1020, and AL alloys are briefly discussed. The motivation of the research work and outline of the thesis are also presented in the final stages of this chapter

Chapter 2 gives a complete literature review about various material and process parameters employed in ESR welding which pays the way for this present investigation. A must illustriously survey is carried out

on the welding of different and dissimilar materials using ESR Welding Process and the importance of the welding process in the welding of different alloys. It also discusses literature related to optimization and prediction techniques applied in ERS Welding Process parameter for the welding of similar and dissimilar materials related to the varying mechanical property have also been reviewed and presented. The various testing and optimization and analysis work related to simulation of weld bead geometry are also reviewed. The outcome of the literature survey is also presented in this work.

Chapter 3 briefs about the objectives of the present investigation and the methodology followed for achieving the result on this present investigation. In this chapter the entire work is split up in the form of a flowchart is presented along with the various tests made use off.

Chapter 4 explores the experimental methods and materials adopted for this research work. It deals with the various composition and description about the chemical and mechanical properties of the base material. A complete description of the welding machine, weld procedure necessary for the trail experiments and optimization & prediction techniques are presented. It also briefs us about the various mechanical and metallurgical testing specifications selected and deployed in this work.

Chapter 5 details about the weld process parameters for conducting the feasibility study of selected materials of AISI 304(SS), AISI 1020(MS) and AA 1008(AA) dissimilar joints.

Chapter 6 puts forth the various optimization techniques employed to find out and identify the optimized weld input process parameters during the ERS welding process. It also gives an account of the models developed to predict the various mechanical properties of ERS welded joints for various materials by varying the input process parameters.

Chapter 7 reveals the results sums in the complete identification of mechanical properties and metallurgical characterization about the feasibility studies carried out in AISI 304(SS), AISI 1020(MS) and AA 1008(AA) dissimilar joints by varying the different process parameters. It essentially gives the results obtained from the simulation of weld bead geometry for dissimilar joints. To validate and to optimize process parameters, the confirmation test was conducted and the experimentally obtained results were validated with the RSM and ANOVA results. The optimized input weld process parameter obtained from various optimization techniques such as Taguchi and RSM are discussed and compared in detail in this section. Finally, the results obtained by various methods to predict the mechanical properties of the welded joints by varying the different weld input process parameter are also discussed in detail.

Chapter 8 concludes the results obtained for achieving the objectives of the present research and investigation are drawn as important inferences from various experimental investigations conducted, and their application of optimization and methods to predict and analysis using different simulation techniques. This chapter also provides valuable suggestions and forecasts about the scope, the limitations and next possible futuristic scope of the present investigations.

SUMMARY

This Chapter gives a detailed account of the introduction to the various types of welding processes, their classifications, materials and their applications of them. It gives a detailed insight into the ERSW Process and its all essential components in detail. The introduction to various types of AIS5052, AISI1020, AL alloys, their classification and the designations are been also discussed right through this chapter. The correct material chosen for this investigation and details of the problems encountered in the welding of

various dissimilar alloys are briefly discussed. The motivation about this research work and complete outline of the thesis are also presented in this chapter. The subsequent next chapters incorporate and discusses the various literature already available and the references related to welding of dissimilar weldments using ERSW process and various the optimization, then prediction and final simulation methods employed.

CHAPTER 2

LITERATURE REVIEW

This chapter elaborates and discusses in detail about the various literature available on welding of dissimilar metals and alloys of different materials using different welding processes and the importance of Electrical Resistance Spot Welding process in the welding of dissimilar weldments. In this aspects, there are the various parameter optimization methods and prediction techniques employed for optimization and presentation of Electrical Resistance Spot welding process as discussed in the existing research are also presented.

Over the years a lot of research has been done in the area of dissimilar welding and many interesting results have been brought up with regards to the problems encountered in dissimilar welding. The dissimilar welding findings are used in nuclear, petrochemical, electronics and several other industrial domains, this section also brings into account the work of the predecessors in this field.

At the end of the literature review, the limitations of the existing research and research gap are identified. Therefore, the objective of this chapter is to provide an overview of the past and present research investigations related to of Electrical Resistance Spot welding of various materials with different welding process parameters and the use different metal combination weldments

REVIEWS ON SIGNIFICANCES OF RSW WELDING PROCESS

In the current world, the industrial manufacturing of technical goods namely all the investment goods is hardly achievable without the use of technology. Among them such as Welding, brazing and adhesive bonding are used for the manufacture of automobiles of all kinds, shipbuilding, household appliances and electrical and electronic devices are most predominantly used for the construction of building structures in the private and industrial sectors. Presently, combined usage of technology accounts for the entire substantial proportion of all the industrial and manufacturing firms and their products. Therefore, the selection of suitable and apt welding process and proper weld process parameters are required to attain better quality joints in this study on dissimilar weldments.

Today it's always a tremendous importance of welding in engineering all over the globe, welding holds the majority of structures together - dams, bridges, cars, tractors, cranes, buildings, etc. The engineer who doesn't have a better understanding of this upcoming popular joining process then there lies a major problem which are exists, like the failures in designing a joint which is un-weldable. Welding gets very precise and specialized with more technical metals and applications.

Resistance Spot Welding (RSW) is a welding process in which two or more similar or dissimilar overlapping metal sheets are placed between two water-cooled copper alloy electrodes and large electrical current is passed through them for a controlled period of time under controlled pressure. The electrodes compress the base metals together and the electrical resistance at the metals interface causes a localized heating. When the flow of current increases, the electrode force is maintained while the weld metal rapidly cools and solidifies. The cooling is achieved by heat conduction via the two

water-cooled electrodes, which serve as efficient heat sinks, and also radially outwards through the sheets. The weld is normally formed in a fraction of a second and the electrodes are retracted after each weld is formed.

RSW is the dominant metal sheet joining process in the automotive industry because of minimum skill requirements, inexpensive equipment, ease of control, its versatility, high operating speeds, repeatability, suitability for automation or robotization and inclusion in high-production assembly lines. Moreover, the process can be used to join most metals provided suitable welding conditions are applied.

Khan *et al.* (2009) conducted experiments on welding of dissimilar material combinations of HSLA350/DP600 using RSW process. The optical and scanning electron microscopy tests were carried out. The obtained results show that welding current ranges widely and results in good weldability, the hardness in the fusion zone was higher than that of the base metal. The tensile shear load bearing capacity of dissimilar material welds increased with increasing peak weld, cross tension load bearing capacity of the dissimilar material. The weld nuggets were higher than that similar material and the fatigue performance of the dissimilar materials spot welds was similar to similar welds.

Jae Hyung Kim *et al.* (2013) used single-sided spot welding technique is for investigating the weldability by numerical analysis using a commercial CAE. The several factors are analyzed to find the optimal conditions. The resulting Lobe curve with respect time and the current was obtained, tensile strength test results support the reliability of the single-sided RSW joints.

Marashi *et al.* (2007) evaluated the magnetic properties were evaluated using a tensile shear test which was described by peak load, failure

energy, and failure mode. The increase in fusion size is accompanied by an increase in load carrying capacity and energy absorption capacity. Their conclusion is that the critical weld nugget diameter recommended is not sufficient to guarantee the pull out failure mode. The metallurgical properties should be considered to predict and to analyses, the spot weld failure modes precisely, and energy absorptions of spot welds are reduced significantly due to high electrode indentation depth.

Marashi *et al.* (2007) founded that the spot weld strength in the pull out failure mode is controlled by the strength and fusion zone size of galvanized steel side. Their results stated that the fusion zone size and failure mode are the most critical factors in the weld quality in terms of peak load and energy absorption governed by various parameters. The spot weld strength in the pullout failure mode is controlled by the strength and fusion zone size of the galvanized steel side. Higher hardness leads to pullout failure mode during the tensile shear test.

Hayriye Ertek Emre & Ramazan Kacar (2016) worked on the RSW of zinc galvanize coated and uncoated TRIP800 steel. The coating of the TRIP steel surface causes a decrease in the weld nugget size and tensile shear strength of the weldments. Their results show that the nugget size increased with an increase in current greater than 6kA. Increasing the heat input provides the extended nugget size and desired PF mode for both weldments, also hardness increases in the fusion zone and the HAZ of both weldments.

Hatsuhiko OIKAWA *et al.* (2007) had an investigation made in order to get high reliability in the welded joints of automobile components using suitable welding current ranges. For RSW process the outcome new welding techniques like Laser welding is been focused as a new trend with various problems, so RSW is better in this perspective, because of the higher strength level of steel sheets are going to be used for which RSW would be the better choice.

Patel *et al.* (2011) focused on dissimilar spot welds of magnesium-aluminum alloy using spot welding process. They observed that the layer of the intermetallic compound consists of $Al_{12}M_{17}$ formed at the weld center where the hardness becomes higher. The output was that the hardness of IMC's is significantly higher than that of base metal as confirmation made by three different methods such as EDS, XRD and micro-hardness test. Due to the intermetallic layer thickness, there were predominant cracks in the reaction layers.

Ranfeng Qiu *et al.* (2010) studied the interfacial characteristic of RSW steel-aluminum alloy joint. They conducted that the width of the discontinuous reaction layer formed in the weld increases with weld current and the thickness increases as approaching the center of the weld.

Qiu *et al.* (2008) observed reaction blocks in aluminum near the welding interface as estimated in hexagonal $AlFeCr$ having $a=2.451\text{nm}$ and $c=0.758\text{nm}$ based on HRTEM and SADP. The inference obtained is a two layers of reaction structures were found, a mixed layer of Fe_2Al_5 and $FeAl_3$, besides the A5052 and the approximate 35nm thick $FeAl_2$ and unusual structures of reaction blocks in Al near the welding interface were observed by them.

Vural *et al.* (2006) analyses the fatigue strength of RSW galvanized steel sheets and austenitic stainless steel AIS5052 sheets joined using a lap joint. They selected material combinations and nugget diameter as parameters. Either observation was their endurance limit of similar steel sheet combinations is higher than that of different steel sheets combinations as a result of unbalance between sheets occurs during the spot welding operations of steel sheets having different material properties especially welded using electrical resistance.

Cho & Rhee (2003) studied the nugget formation mechanism and its effects on the RSW welding process parameters which observed using a digital high-speed camera. The formation and growth were observed at 1000frames/sec and the shape of the heat generation during the initial stages was observed, as it progressed. The yellow-red heat zone directly related to the nugget was generated at the center of the weld. The dynamic resistance was affected by the change in length and area for the current flow rather than the temperature after saturation.

Alenius *et al.* (2006) explored the mechanical properties of spot welded dissimilar joints for stainless steel and galvanized steels. The failure load of the specimen's was around 72-78% of that of the lap shear specimen. Their conclusive evidence were that the failure types were plug failure in both the cases. The lap shear strength of dissimilar metal joints depends on the strength and thickness of non-stainless steel. They observed that dissimilar metals susceptible to hydrogen embrittlement in chlorine solution at room temperature and same in stainless steel joints when it was galvanically coupled to zinc.

Penner *et al.* (2014) made a study on dissimilar RSW of aluminum to magnesium with zinc coated steel interlayer's. The mechanical properties and microstructure of the welds were analyzed. Their conclusive evidence were that the Zn coated steel interlayer was utilized to prevent mixing odd Al and Mg alloys resulting in the much higher strength of the welds, and the joining mechanism took place at Al/steel and Mg/steel interfaces.

Sun *et al.* (2004) deal about the RSW of Aluminum alloy to Steel with transition material, from process to performance in which a cold rolled clad material was introduced as a transition to aid the resistance welding process. Their experimental results obtained shows that the nugget formation process was examined using consecutive metrological cross-sectioning and

two distinct fusions zones formed during spot welding. The static, dynamic and fatigue performance of these welds were examined and compared.

Weihua Zhang *et al.* (2013) conducted the interfacial microstructures and mechanical property examination on RSW joint of high strength steel and an aluminum alloy of 4047 AlSi12 interlayer and the effect of interlayers were studied. The results obtained from the study shows that the increasing thickness of interlayer the nugget diameter has shown a decreasing tendency and the thickness of the intermetallic compound layer decreased under optimized welding parameters. The tensile shear load of the welded joint experienced an increased tendency first and then it shows a decreased tendency with increasing inner layer thickness.

Xu *et al.* (2012) aimed to study and to evaluate the microstructures, tensile and fatigue properties of Weld Bonded (WB) magnesium to magnesium (Mg/Mg) similar joints and Mg/steel dissimilar joints in comparison of RSW of Mg/steel dissimilar joints. Their results obtained were the added adhesive layer diminished stress concentration around the nugget weld, and both WB Mg/Mg and Mg/Steel joints were significantly stronger than RSW Mg/steel joints in terms of the maximum tensile shear load and energy absorption, which would also increase with an increase in strain rate.

Subrammanian & Jabaraj (2013) made a research work on the RSW of stainless steel. Their study revealed that the hardness of the spot weld is greater than the hardness of the unwelded zone. Increasing the welding current increases the nugget size, welding current was found to be the most influential one to determine the tensile strength. The tensile forces have a proportional relationship with current and weld time increments until the expulsion limit occurs. The estimated cooling rate from the nugget edge to nugget center decreased from 10^5 to 10^4 Kelvin/sec.

REVIEW ON THE VARIOUS PROCESS PARAMETERS OF ERSW PROCESS

Efekt bochnikowania *et al.* (2016) made a study on the shunting effects in RSW which occurs when the electrical current is passed through the preceded spot welds in the case of multi-spot welding. Their conclusion focused on the reduction of shunting effects by determines the minimum spacing between spots for the given material thickness and welding schedule. The various numerical methods like FEA have been devoted to shunting, simplification in electrode shape, therefore, the configurations appear significant.

Makwana Brijesh *et al.* (2017) discussed the effects of process parameters for RSW process using the Taguchi Method. ANOVA analysis was carried out on the Macro examination for 2,0mm sheet thickness. The optimum results were the level of importance of the welding process parameters during the tensile test which was determined by the ANOVA method. There is a significant parameter power such as weld time increase and weld current.

Pereira *et al.* (2009) studied about the effect of process parameters on the strength of RSW in the 6082-T6 aluminum alloy, welded at different welding parameters. The outcome of their study was the increase in the weld current and time current increased the nugget diameter results in coarsened microstructure. The significant increase in failure load in static lap tests was observed in welds done with increasing current and time. The prediction of critical nugget size is to obtain pull-out failures in under matched welds.

Chetan R Patel & Dhaval A Patel (2012) worked on the effects of process parameters on the strength of Aluminum alloy A5052 sheets joints on 1 mm thickness sheet welded by RSW with cover plates. The welded where

subjected to tensile shear and hardness tests to determine the influence of welding parameters on quality effects. The results achieved by them shows that increase in time and current as made a significant impact on tensile load and hardness value also decreased by minor values.

Zoha Nasir & Khan (2016) made a critical review of Spot welding carried out by different investigators including optimization of process parameters. Their results briefs' about the information on the process parameters used to optimize the spot welding to obtain the highest quality welds.

Prasad S Salke & Kailash C Bhosale (2016) studied the optimization of a process parameter in RSW for unequal thickness sheets using the Grey Relational Analysis and Genetic Algorithm. The feasibility of tensile strength in RSW of the unequal thickness of CRC D2 sheet was successful. The ANOVA of the grey relational grade for multi-performance characteristics reveals that the electrode force is the most significant parameter.

Shende & Kadam (2017) aims to optimize the RSW process parameters by applying Taguchi methods. The result's shows that the T.S and N.D are proportional to current, pressure and weld time, also the high T.S was due to an increase in the width of N.D. The best combination of parameters for T.S and N.D is 10 kA, pressure 4 bars, and weld time 10 cycles. They concluded that time is the least effective on T.S and N.D, and the welding current is a most significant factor for the joints.

Shashi Dwivedi & Satpal Sharma (2014) studied the SAE 1010 steel sheets welded using RSW by changing the current, welding cycle, electrode force as the principal variables controlled in order to provide the necessary to form a better weld. Their conclusive evidence's are RSW was successful on welding of SAE 1010 sheets, and it shows proper fusion and

very less amount of cracks. The welding current, weld cycle and electrode force are the prominent factors. The shear T.S of SAE 1010 decreases and increases with the increase of welding currents increase in welding time and electrode force respectively.

Nizamettin Kahraman (2005) worked on Commercially Pure (C.P) titanium sheets (ASTM Grade 2) which were welded using RSW at different parameters and environmental conditions. Their results showed that increase in current time and electrode force increased the tensile shearing strength and the joints obtained under the argon atmosphere. The better tensile shearing strength and the welding nugget gave the highest hardness.

Feramuz Karci *et al.* (2008) dealt the characterization and understanding the effects of weld time and the influence of different weld atmosphere in the resistance spot welding of AISI 304 grade stainless steel. The deformation in tension lies between 5%, 10%, and 20%. The results produced that the final mechanical properties of weldment are directly related to the parameters of the process used, knowing the weld time and rate of deformation prior to welding.

Jeevan A Karande & Inamdar (2017) reviews about the effect of process parameters on RSW. The resistance welding process highly depends upon the process parameters, where current plays a major role and time, electrode force place the least role. Increase in welding current increases the T.S weld ANOVA and Taguchi have been effective tool for parametric optimization.

Heli Junno *et al.* (2015) discussed the identification of different spot-welding processes and the process optimization parameters leading to high-quality welding joints. In this self-organizing maps are used and optimal features for the training parameters were sought.

Pradeep *et al.* (2014) presented about the welding process design and parameters optimization of RSW used in joining of low carbon steel sheet of thickness 0.8mm and metal strips of cross section 10x5mm for electrical motor applications. The weld quality was at the acceptable range interval and numerical simulation of RSW process was also carried out with selected weld parameters.

Aravinthan Arumugan & Md. Amizi Nor (2015) concentrates on the parameters optimization when spot welding steel with dissimilar thickness and may use Grey Based Taguchi method using an L9 orthogonal array with three factors with each factors having three level. The results showed the welding currents showed the most significant contribution in the optimum welding schedule and it showed a distinct improvement in the increase of weld diameter and weld strength well as a decrease in the electrode indentation.

Quanfeng Song *et al.* (2005) made an experimental study to determine the electrical contact resistance in resistance welding of mild steel, stainless steel and aluminum to themselves. Their parametric study showed the influence of pressure is quite consistent and contact resistance decreases with pressure increases, while the temperature influence was more complex.

Dursun Ozyurek (2007) analyzed the influence of primary welding parameters affecting the heat input such as weld peak current on the weld quality such as surface appearance, weld nugget size, weld penetration, weld interval discontinuities, strength, and ductility was determined for 304L RSW welded materials on different weld atmosphere. Their results show that the tensile shear load bearing capacity of welded materials increases with increasing heat, the optimum weld quality was obtained for 9kA peak weld current in a nitrogen atmosphere.

Valera *et al.* (2017) conducted RSW process in dissimilar joints of micro-alloyed steels TRIP sheets and they optimized the welding process such as parameters (time and current intensity) had an important effect in the final STR of these kinds of joints. Taguchi design experiment was employed by them in order to optimize the process by the signal-to-noise ratio. Their ANOVA analysis determined the relevance of each parameter in the final mechanical resistance of the welds, the optimum conditions correspond to lower values to those conducting to the metal expulsion phenomenon.

Yanhua Ma *et al.* (2013) gives a review of techniques of monitoring RSW process or weld quality, their advantages, as well as limitations of these techniques, are discussed. The parameters concerning the mechanical response during resistance spot welding including electrode displacement, electrode force, and acoustic emission. Displacement provides the most reliable indication of spot weld quality through weld expansion measurements.

REVIEWS ON THE OPTIMIZATIONS PREDICTION OF ERSW PROCESS PARAMETERS

Goodarzi *et al.* (2008) analyzed the dependence of overload performance on weld attributes for resistance spot welded galvanized low carbon steel. The failure mode, peak load, and energy absorption are obtained in the tensile shear test. They found that weld fusion zone size, electrode indentation, and expansion can significantly affect the mechanical performance of spot welds. Failure mechanism of spot weld which fails through pull out mode during tensile shear test through thickness localized necking in the base metal.

Panchakshari *et al.* (2013) worked to find out a comparative study of the response of RSW process obtained from three methodologies of the

Genetic algorithm, Design of experiments and Response surface method. LCS is the material selected. Their results showed that the obtained high-quality result, nugget diameter and strength of the weld to be equal to 5.4mm and 290N/mm² respectively weld posses the optimum result it should always at in mid value of the range of 20 cycles.

Manoj Raut & Vishal Achwal (2014) investigated the effect and optimization of welding parameters on the tensile shear strength in the RSW process by varying electrode forces, welding currents and welding times. Their results showed that it is possible to increase the tensile shear strength of the joint by the combination of the suitable welding parameters, the validity of the Taguchi method was checked for enhancing the welding performance and optimizing the welding parameters.

Boriwal Lokesh *et al.* (2015) studied the available methods of coupled models for RSW and critical analysis of the process done. The quality of the weld depends upon the optimum process variables such as current, time and pressure. Their results showed that these phenomenon should be interconnected with each other to simulate heat generation and growth in the nugget formation.

Mircea BURCA & Ioan LUCACIU (2013) work presented the principle of projection welding deriving from spot welding by resistance. The outcomes were the shortcomings in achieving quality welds as compared to thin plate welding (<3mm) with applications in welding the required parts of M8 nuts welding technology.

Mat Din *et al.* (2015) worked on PSW of the dissimilar thickness of AA5052 aluminum alloy in order to investigate the effect of metal thickness on weldments strength for lap joint. Their microstructure results showed that this joint has coarse grains of HAZ. As the thickness of the sheet metal

increased, the failure load of the joints increased and there were no linear correlations established between joint strength and metal thickness.

Anurag Tewari & Ekta Rawat (2017) optimized the process parameter of RSW which depends on the current flowing, the resistance of the base metal to produce the heat necessary to make the spot weld. Their outputs showed that increasing the weld current leads to the nugget size increase, but it doesn't increase the hardness distribution. The weld time and welding current increments had resulted in diameters increment at the weld zones.

Min Jou (2003) the main objectives in his research is to explore the phenomenon of how changes happen in controllable parameters that affect a measurable output signal and to create a relationship between the input and output quality of welds. The output shows that the ideal nugget will not be developed until the heat input reaches a certain level. If the applied heat becomes too high the nugget will overdevelop and result in the expulsion of molten metal from the joint which provides important information for process representation.

Shih-Fu-Ling *et al.* (2010) introduced the real-time and in-situ RSW quality monitoring method, which takes the input electrical impedance of the welding system as monitoring signature. The signature is obtained by probing and processing the input voltage and monitoring screen and it's being in-situ because monitoring actions don't jeopardize the welding operations or alter any of the parameters in general.

Luo Yi *et al.* (2009) carried out the regression modeling and process analysis of RSW on the galvanized steel sheet. They studied the nugget geometry and tensile shear strength of spot welds by considering four parameters namely current, electrode force, and welding duration and preheat current. Their results showed that there was a more accurate prediction on nugget size and mechanical properties of spot welds by model analysis.

Oscar Martin *et al.* (2009) developed a tool capable of reliably predicting the TSLBC of RSW from three welding parameters i.e. electrode force weld time and current. Their conclusive evidence proves that the nugget grows with increase with increasing WT and WC. The hardness values of nugget don't decrease and its higher than HAZ and base metal due to the strain hardening. Their development made produces a good result in a prediction of TSLBC of the RSW joints.

Oikawa *et al.* (1999) reported the RSW of steel and aluminum sheets using aluminum clad steel sheets as insert metals. Intermetallic compound layers were formed in the weld zone in direct spot welding sheets. The fatigue strength of joints using insert metals was somewhat lower than that of the aluminum joints for which suitable current is the most essential parameter. Using aluminum clad steel sheets as insert metals are beneficial in spot welding of steel sheets to aluminum sheets.

Pandey *et al.* (2013) optimized the of various parameters of RSW, the investigation reveals that the quality characteristic has been considered using the Taguchi method. The experimental results showed that the right section of the input parameters is medium current, medium pressure and holding time. The contribution of welding current, holding time and pressure towards tensile strength is 61%, 28.7%, and 4% respectively as determined by ANOVA.

Pouranvari *et al.* (2011) the investigated of the effects of the Welding parameters on the overload failure on the mechanical performance of dissimilar RSW between drawing quality special AISI 1008 low carbon steel and DP600 dual plate steel. Their results showed three distinct failure modes as observed during the tensile shear test. The effect of expulsion on the mechanical performance of welds is also investigated. The correlations among the various parameters are also investigated.

Rageon *et al.* (2008) analyzed the interfacial conditions encountered in electrode and sheets assemblies used in RSW process are characterized. Their results show that the primary electrical contact resistances measurements depend on the temperature and pressure that have been carried out on the specific device. Secondly the repetition of the welding, the electrode surface profile that initially curved and quickly presented a flat part whose size increases with the number of welds.

Wei & Wu (2012) carried out an electromagnetic force analysis heat generation and contact resistances at the faying surface and electrode-workpiece interfaces and bulk resistance in workpieces. Their computed results showed that the bulk dynamic electrical resistance cannot reliably reflect transport processes of the nugget shape unless the local constriction resistance and electric current density are known. A decrease in constriction resistance delays the nugget formation enhances convection and solute mixing changes circulation direction of the stronger convection cell during the cooling period.

Dickinson *et al.* (1980) characterized the spot welding behavior by dynamic electrical parameter monitoring. They showed an occurrence of predominant β peak signified the production of an acceptable size nugget and the critical energy level for expulsion was observed. Using their results the dynamic resistance and critical expulsion energy of spot weld control mechanism were proposed.

Hao *et al.* (1996) made a study on the development for characterization of RSW of aluminum. The statistical analysis has applied to investigate the relationship between the extracted features and conventional physical parameters. Their results of Al-Mg alloy AA5754 had shown that the monitoring methods developed previously for steel do not appear to be generally applicable to aluminum and no single parameter can accurately

quantify weld quality and provide a good prediction of nugget diameter and static strength.

Dawei Zhao *et al.* (2013) deals with the real-time monitoring of weld quality small scale RSW for titanium alloy. They performed a systematic research on the voltage curve which turned out to be an indication for the weld quality of SSRSW. They demonstrated that the dynamic voltage during a welding process could be identified as a good signature for weld quality monitoring process.

REVIEW ON THE MECHANICAL AND METALLURGICAL PROPERTIES OF ERSW WELDED JOINTS

Pouranvari *et al.* (2018) in their work addressed the microstructure and tensile – shear mechanical performance of MS1200 Giga-grade martensite advanced high strength steel joints welded by resistance spot welding process. They have concluded that the most predominant feature of MS1200 Martensitic steel spot welds was the HAZ softening which led to producing a local under-match across the weld zone and the large area of SCHAZ was observed when compared to the ICHAZ. The martensite tempering plays an important role in the mechanical properties of the welds. Despite the fact that load-bearing capacity of spot welds failed in interfacial mode was not affected by the HAZ softening phenomena, it significantly affects the peak load of welds failed in pullout mode.

Emel Taban *et al.* (2009) studied the dissimilar materials joining using Aluminium and steel, said that it's of wide interest to the current trend. They made a microstructural analysis and the results of the structures of inertia friction welds between 6061-T6 aluminium alloy and 1018 steel is the best performed at either 170MPa and 250 MPa, also their study includes the upset pressure of the order of 60MPa, results the max thickness of

intermetallic compound layer at 350nm, and the two intermetallic elements were present which included Fe-rich FeAl and Al-rich Fe₂Al₅.

Pouranvari *et al.* (2008) conducted their work on the behavior of dissimilar resistance spot welded joints of low carbon and austenitic stainless steel. They studied the under tensile-shear test with focuses on the failure mode. The results showed that necking is initiated at the nugget circumference and then the failure propagates along the nuggets circumference in the sheet to final fracture. There is a critical fusion zone to ensure pullout failure mode in the shear tensile test which mainly controlled by the ratio of fusion zone hardness and failure location hardness. They concluded that the fusion zone size and failure mode are the most critical factors in the weld quality in terms of peak load and energy absorption, which is governed by welding parameters such a welding current, welding time and electrode force.

Weihua Zhang *et al.* (2014) conducted experiments on dissimilar materials of H220 Zn-coated high strength steel and 6008 aluminum alloy, welded by the median frequency resistant spot welding process. Interfacial characteristics and kinetics of growth of intermetallic compound layer at the steel/aluminum interface in the welded joints were investigated. They concluded that the formation and growth of the intermetallic compound were controlled by reactive diffusion between solid steel and liquid aluminum alloy during resistant spot welding and its exhibited unusual thickness. The welded joints exhibited interfacial failure mode during tensile sheet testing and brittle intermetallic compound layer had crakes propagating near the weak zones

Mathew Vinoth & Saravanan (2016) in their research made a parametric study in spot welding for dissimilar weld joints of AISI 202 and AISI 1018. They investigated the mechanical properties in the different region of the spot-welded stainless steel sheet and mild steel sheet subjected to various welding parameters. Their conclusion includes the optimization of

process parameters of dissimilar sheet joining and the observation was that welding current and welding time has more significant effects than the electrode force is also responsible for tensile strength and hardness.

Verma *et al.* (2014) performed a work about the resistance welding of AISI 304 with AISI 316, the quality and strength of the spot welds are very important to the durability and safety design of the vehicles. They concluded that the tensile strength for different austenitic stainless steel was found to be comparatively more than the similar sheets and the weld currents are the major governing factor affecting the tensile shear strength of the resistant spot welded specimen. As the weld current increases, the nugget size also increases, also the hardness of the weld zones are greater than the hardness of the unwelded zone for dissimilar joints. But the marginal increase was obtained for similar metallic joints.

Ladislav Kolarik *et al.* (2012) deals with the properties of resistance spot welding of low carbon steel and austenitic CrNi stainless steel. The thickness of the welded materials was 2mm. They inferred that the size of the weld metal increases with an increase in welding current. The HAZ of low carbon steel sheet was broader than the HAZ of the austenitic stainless steel, also the hardness was increased in the fusion zone. An increase in iron content in the direction from weld metals towards DC01 steel was also observed.

Honggang Dong *et al.* (2012) carried out research work for joining dissimilar metals of Aluminum alloys to galvanized steel with Al-Si, Al-Cu, Al-Si-Cu and Zn-Al filler wires. They made joints of aluminum alloys sheets and galvanized steel sheets. Their results showed that the 5A02 alloy after it was gas tungsten arc welded with Al-Si, Al-Cu, Al-Si-Cu and Zn-Al fillers wires respectively gives the tensile strength of about 136MPa, and the addition of Cu and Al filler wire into the weld increases the thickness of the interfacial layer.

Akkas *et al.* (2016) performed an experimental study on the resistance spot welding of SPA-C steel sheet used in the side wall and roof in rail vehicles, which were joined by resistant spot welding as lap joints. Their outcomes were in low welding current intensity small nuggets widths were obtained and in high welding current intensities the cross-section area decreased and the welded nuggets spurt out between two sheets resulting in the decrease in nugget width.

Milan Brozek *et al.* (2017) conducted resistance spot welding of steel sheets of the same and different thickness which aims to determine the dependence between the rupture forces of spot welds made using steel sheets of the same thickness for different welding conditions. The spot welds were made from low carbon steel and the spot weld rupture was characterized by the welded sheets thickness from 0.8 to 2.4kN. They concluded that the welding times increases the welds process of higher rupture force namely of 3 to 21%, when compared to the producer, recommended variables.

Alizadeh-Sh *et al.* (2013) the investigation aims that the process-microstructure-performance relationship in resistance spots welding of AISI 430 ferritic stainless steel. Their obtained result shows that the fusion zone was featured by columnar ferrite grains and fine dispersion of carbide precipitates. The MTHAZ exhibited the highest hardness in the HAZ which shows ferrite-martensitic dual microstructure with limited grain growth due to the formation of Υ phase at grain boundaries.

Alizadeh-Sh *et al.* (2014) address the phase transformations and mechanical response of martensitic stainless steel resistance spot welds. The fusion zone microstructure consists of carbon-rich martensitic as the fusion zone which featured the retained eutectic delta ferrite were found along the solidification grain boundaries and all the samples studied are failed in partial interfacial failure mode. The high hardness of FZ provides low fracture

toughness crack propagation path coupled with the presence of sharp notch at the weld nugget FZ/HAZ boundary.

Aslanlar (2004) studied about the effect of welding current time on the tensile peel strength and tensile shear strength of welded joints in electrical resistance spot welding. They selected chromided micro-alloy steel sheets having a 0.8mm thickness and galvanized chromided micro-alloyed steel sheet having 1.0mm thickness were investigated. They inferred that the depth of electrode indentation into the material is not exceeded the 20% of sheet thickness limit accepted for good results, deep electrode indentations, excessive deformations color changes in welding zone and over melting was due to excessive heat input may be occurred.

Baca *et al.* (2013) carried out small-scale resistance spot welding of $\text{Cu}_{47}\text{Ti}_{34}\text{Zr}_{11}\text{Ni}_8$ bulk metallic glass and they also carried out mechanical testing scanning electron microscopy, Differential Scanning Calorimetry (DSC) and X-Ray Diffraction (XRD). The tests obtained outcomes were that the welds were moderately strong and mechanical failure was occurred in peel and in the shear strength test which was likely due to the crystallization or embrittlement. They suggested that this region is of critical importance in generating optimum welds.

Brauser *et al.* (2010) worked on the deformation behavior of spot welded high strength steels for automotive applications. Numerical simulation of the component and assembly behavior under different loading conditions is a main safety tool design in automotive body shell mass production. Their outcome on the failure load doesn't show a linear increase with the base metal strength. SEM results show no indication of reduced deformability of TRIP steel compared to the micro-alloyed steel HX340LAD. The EBSD analysis of austenite content reveals that elimination of austenite in the fracture region of spot welded HCT690T joints.

Darwish (2002) carried out resistance spot welding on similar and dissimilar thickness sheets and they have also used finite techniques for analyzing their work. Their final results from the test show that the stresses are concentrated towards the far ends of the spot welding nugget of similar and dissimilar thickness joints and the introduction of adhesive layer resulted in strengthening as well as in balancing the stress in the dissimilar thickness joints.

Florea *et al.* (2012) conducted the fatigue behavior of analysis of RSW welded aluminum 6061-T6 alloy and experimentally investigated the three welding conditions of low, normal, high to determine the microstructure of the weld nuggets. Their conclusive evidence are that the welding process parameters have great influence upon the quality of the RSW of Aluminum 6061-T6 alloy. The welding currents have great influence on the nuggets dimension and lap joint material behavior and no fatigue initiation sites were observed in the porous area formed from rapid solidification.

Shinji Fukumoto *et al.* (2008) in this work the small-scale RSW was carried out for austenitic stainless steel, the cooling rate that was estimated from the solidification cell size is almost similar to that produced by laser beam welding. The outcome of their research was the shear force increases with the welding current increase owing to the nugget growth. Hot cracking was not observed despite delta ferrite in the weld nuggets and sensitization was not observed in HAZ welded under any conditions.

Ahmet Hasanbasoglu *et al.* (2006) stated that resistance spot weld of dissimilar material is generally more challenging than that the dissimilar metal in which the influence of primary welding parameters affecting the heat input such as peak current on the morphology, microhardness and tensile shear load bearing capacity of dissimilar welds. Their conclusive evidence state that weld current increases result in enlargement of nugget size, failure

occurred by tearing of interstitial free steel metal side of spot welded materials. The increase in energy input caused coarsening of the microstructure of the weld nuggets and also of HAZ.

Fatih Hayat (2010) had an objective of investigating the joining capacity of magnesium AZ31 alloy sheets and aluminum 1350 alloy sheets with the applications of resistance spot welding. Their optimum results obtained was the current increases the nugget diameter increases on both sides and the TLBC values are also increased. The aluminum alloy's indentation depth was more due to its lower strength value and hardness and the EDS analysis carried out on fractured specimen was showed the ratio of Al% and Mg% as varied in the fracture area of specimens welded at low currents and high currents.

Faezeen Shahid *et al.* (2015) investigated the two dissimilar metals which involved in the welding shows different mechanical properties and microstructures which in turn may affect due to welding parameters like weld current, holding time, weld force etc. Their conclusion states that the tensile strength of the weld and the factors affecting the strength of the weld are the major problems occurred with dissimilar metal welds in the formation of intermetallic compounds at the interface which affect the properties of the weld and intermediate layers at the interface.

Choughule *et al.* (2016) carried out on (SS-75-600) spot welding machine is used for welding of dissimilar metals to cope up with the industrial demand for low cost, lightweight and excellent weld strength in automotive industries. Their conclusive evidence states that two plates of mild steel and austenitic stainless steel were placed as a lap joint and spot welded by varying welding current. Increasing the weld current increases the nugget size and doesn't increase the hardness distribution.

REVIEW ON ANALYSING THE ERSW PROCESS USING VARIOUS SOFTWARES

Jan VINAS *et al.* (2012) deals with the metallographic analysis of welding tip materials and workpiece used in production. The experimental tests were carried out and the results confirm the positive influence was an alloying element. The possibility of increasing the strength characteristics without the support of alloying elements comes into a limiting range. The lifetime of the tip can be increased by the combination of alloying elements in the copper alloys.

Sun & Dong (2000) made an analysis on of aluminum resistance spot welding process using coupled finite element procedure. They took the following process parameters into account shows the incremental changes in a sheet – deformed shape, contact area and current density profile as well as large deformations effects. They found that lower electrode force or higher welding current generates a bigger nugget where the weld residual stresses and final sheet deformation are predicted as measure quality within the range analyzed.

Kishore *et al.* (2014) made the parametric studies and FEA on welded steel using RSW process. They stated that the electrode travels on a predetermined path and make contact with the sheets at selected weld points to apply force. They were observed that the tensile strength is maximum for stainless steel and minimum in mild steel and also increases with increases in welding current and weld time irrespective of the materials. Nugget diameter is maximum in SS and minimum in dissimilar materials due to different mechanical and thermal properties.

Sumit Chaudhart *et al.* (2014) deals with an approach for optimization of the RSW. The complicated behavior is studies based on the four important parameters namely Weld Current (WC), Welding Time (WT),

material and thickness are considered as the influencing factors for the quality of the joints.

Hamid Eisazadeh *et al.* (2010) developed a mechanical-electrical-thermal coupled model in an FEA environment. They used this analysis for identifying the shape and size of weld nuggets are computed and validated by comparing with the experimental results. Their results showed that quality and shape of the weld nugget with a variation of each process parameters are the economically optimized to manufacture quality automotive bodies.

Zhigang Hou *et al.* (2007) made a 2D axisymmetric model of thermo-elastic-plastic FEM is used to analyze the mechanical behavior of RSW process with the help of commercial software ANSYS. The temperature and plastic behavior is taken into account. The stress and strain distribution in the weldment and their changes during the RSW process are determined and the deformation of the weldment and the electrode displacement are also calculated.

Yi Luo & Jinglong Li (2014) studied the nugget formation of RSW on dissimilar material sheets of Al and Mg alloys and the element distribution, microstructure and microhardness distribution near the joint interface are also analyzed. The main technical problem of RSW on dissimilar metal sheets of Al and Mg alloys was the brittle-hard $\text{Al}_{12}\text{Mg}_{17}$ intermetallic compounds distributed in the nugget with hardness much higher than either side of the base materials. Microcracks tended to generate at the interface of the nugget and base materials which affected weld quality and strength.

Hessamoddin Moshayedi & Iradj Sattari-Far (2012) carried out the numerical and experimental study of nugget size growth in RSW of Austenitic SS to study the effects of welding time and current intensity on nugget size of AISI 304L using ANSYS. Their outcome states that increasing welding time and current is accompanied by an increase in the fusion zone size with decreasing slope, nugget size also reduces due to melting spattering.

TAO Jian-feng *et al.* (2012) explored the influence of welding parameters and to investigate the Al alloy (AA) nugget formation. The FEM framework and an empirical sub-model were built to analyze the affecting factors on weld nugget. Their numerical and experimental results show that their proposed multi-field FEM model agrees with the measured AA welding feature and the modified dynamics resistance model can able to capture and explore the relationship between dynamic resistance and nugget formation more accurately.

Nied (1983) developed the model which was used for analyzing the squeeze and weld cycles to determine the electrical, thermal and mechanical responses. The temperature – thermal expansion and associated stresses on the weld nugget geometry were also obtained. Their FEM analysis provides a better understanding of the welding physics which would have been difficult to determine by experiment alone.

Tsai *et al.* (1990) modeled the RSW nugget growth using FEM. The ring-like weld nugget expands inward and outward during welding cycles. The weld nugget formed mostly on the thicker workpiece when in the thinner workpiece. When spot welding of dissimilar materials showed that the weld nugget formed more in the workpiece of the lower thermal conductivity or higher electrical resistivity.

Sun & Khaleel (2004) summarized either work on FEM based on nugget growth for RSW of Al alloy to steel. Their coupled thermal-electrical-mechanical FEA models were performed to stimulate the nugget growth and heat generation patterns during the welding process. The prediction nugget growth is compared with experimental weld cross section. Reasonable comparisons of nugget size were achieved.

REVIEW ON THE VARIOUS TYPE OF CORROSION TESTS ON ERSW JOINTS

Emil Spisak *et al.* (2011) analyzed the influence of corrosive environment on the surface quality of spot welds of Hot dip galvanized steel sheets made of DX54D+Z. Alloy the electrochemical properties of used materials were observed. Then carrying capacity is measured before as well as after exposure in the corrosive environment. The tensile test results were used to evaluate the carrying capacity. The qualities of the weld were evaluated based on the microhardness measurement results realized on the scratch pattern too.

Mustafa ACARER *et al.* (2013) made a study to investigate the microstructure, micro-hardness, tensile shear tests and corrosion properties of DP450 dual phase steel sheet welded using spot welding under both uncoated and hot dip galvanized conditions. Their experimental results concluded that there was an increase in joining strength with an increase in welding current and weld time, welding parameters didn't have any significant effect on corrosion properties, the uncoated specimen had more corrosion resistance in comparison to hot-dip galvanized specimens.

Jamasri *et al.* (2011) conducted a corrosion behavior study on RSW dissimilar metal welds between Carbon steel and Austenitic Stainless Steel with different thickness. The corrosion fatigue tests were carried out at room temperature, fatigue tests were also performed. The results showed that the corrosion fatigue strength of RSW in seawater is lower than that performed in the air. The hydrogen enhanced plasticity mechanism tends to ease the generation of dislocations is the cause of corrosion fatigue strength weakening.

Liang *et al.* (2010) analyzed the effect of the modified filler metal that replaces Pd with Ru. The initial stress conducted on the button- metal samples and bead-on-plate welds indicated that Ni-Cu-Ru exhibited good corrosion properties. Ni-Cu-Ru is far better the Ni-Cu-Pd welds. They found that these welds are a suitable replacement for welds made with standard 300-series consumables.

Martin *et al.* (2012) studied the combined effect of RSW and post-welding sensitization on the pitting corrosion behavior of AISI 304 using cyclic potentiodynamic polarization tests. The behavior caused on the weld metal zone was a cast dendritic microstructure with δ - ferrite in interdendritic regions, whose microstructural regeneration kinetics is faster than that of HAZ. The HAZ metal possesses the chromium-rich phases and are more homogeneously distributed than in the parent metal.

Paswuale Russo Spina *et al.* (2017) investigated the effects of main RSW welding parameters on mechanical strength and corrosion behavior of galvanized quenching and partitioning and transformation induced in the plasticity of spot welds. The welding current and time play the strongest influence on the shear strength of the spot weld. Where clamping force is of minor importance. The clamping force has a good influence on corrosion resistance because it hinders the permeation of corrosive environment towards the spot welds.

Somervuori *et al.* (2004) made a characterization on corrosion study of spot welds of austenitic stainless steel. Their results indicate the yellow, red and blue oxides formed having double-layered structures with an iron-rich and chromium depleted outer layer and a less iron and more chromium containing inner layer. Chromium depleted layer was found in the base material under the yellow hear tinted oxide layer, and a significant amount of copper contaminations were found on the spot weld surface near the weld edge.

INFERENCE FROM LITERATURE SURVEY AND PROBLEM IDENTIFICATION

- From the literature survey, it is identified that the RSW process was widely used in welding of different metal sheets such as AISI1020, AIS5052, AL alloys etc.
- The more research work was already carried out in analyzing the mechanical properties and metallurgical characterizations of various types of weld joints.
- Very few works were identified in analyzing the application of weld joints in corrosion environment.
- The few works were already carried out in analyzing the effect TIG and GAS welding on welding of AISI 304 (SS), AISI 1020 (MS) and AA 1008 alloys no works were carried out in analyzing the effect of RSW process on welding of above alloy.
- No works have been carried out in analyzing the effect of various RSW process parameter on welding of AISI 304 (SS), AISI 1020 (MS) and AA 1008 alloys on its mechanical & metallurgical properties.
- A lot of works has been identified on optimization of RSW process parameter on various of type joints.
- The application RSW model (CCRD) in the optimization process parameter was yet carried out. It also observed that no works have been conducted on predicting the RSW parameters using ANOVA for AISI 304 (SS), AISI 1020 (MS) and AA 1008.

SUMMARY

This chapter clearly reviews the various research work that was done by a researcher in the field of RSW process. This chapter also illustrates the various process parameters selected for the RSW process in welding of various materials for obtaining better quality joints. The various mechanical & metallurgical characterizations carried out on RSW welded joints by various researchers are also discussed. The application of various optimization and prediction tools carried out by various researchers on RSW weld joints in optimization and prediction of its input and output parameters are also illustrated in detail in this chapter.

The literature survey related to the analysis of the RSW process using various software carried out in various research works is also discussed. Finally, the literature survey related to the study of corrosion behavior on RSW joints carried out by various researchers is also studied. The next chapter illustrates in detail about the objective and methodology employed in this research work.

CHAPTER 3

OBJECTIVES AND METHODOLOGIES

This chapter describes the prime objectives of the current work and various methodologies followed during the course of this investigation. Based on the data collected from the detailed literature survey as put forth in Chapter 2, it is evident and clearly understood that there has been in-depth loads of research work which have been already carried through by earlier researchers in the field of various welding techniques and the materials which are been used in different welding processes. Similarly, the analyses of the mechanical and metallurgical characterization in the weldments, applications of weldments in numerous environmental conditions, weld process simulations using various software's and parameter optimization and prediction of welding process parameter using various models are also carried out by previous researchers are discussed. The most valuable learnings and the apparent limitations in the field of electric resistance spot welding are put forth as follows.

1. The ERSW process has gained more focus and importance in the field of engineering automobile and household appliances in welding of similar and dissimilar materials. The characteristic properties of ERSW both mechanical and metallurgical properties of the welds obtained are been widely discussed by various researchers all over the globe.

2. The ERSW provides the easy adaptability in the Automation of High-rate Production of various sheet metal combinations assemblies for various applications.
3. ERSW can be operated at High Speed and good accuracy.
4. ESRW is one of the few most economical processes.
5. ERSW provides a predominant level of dimensional accuracy

The Limitations of Electrical Resistance Spot Welding process which are been taken into considerations are as follows.

1. There is the possibility of difficulty in the maintenance or the repair works.
2. It leads to additional weight and material cost to the product, compared with other welded joint.
3. ESRW, in general, has a higher cost than most of the arc welding set-ups.
4. The full strength of the sheet cannot prevail across a spot welded joint.

From the various research reviews, it is observed that the welding of dissimilar materials has gained tremendous importance in the field of engineering and they are been widely employed in different industrials usages such as aerospace and defense-oriented department applications. Few of the weldments failure are also been identified and reported in different material alloys by various scholars.

From the above literature it is clearly identified that the ERSW process was widely used for welding of sheet material like Low carbon steel, galvanized chromided sheets, stainless steel, low carbon cold rolled EDD grade material and AISI1008. It is also identified that very few works were conducted in the welding of AIS5052, AISI1020, and AA1008 by various welding processes. No work has been conducted in welding of RSW process on AIS5052, AISI1020 and AA1008 materials under similar and dissimilar conditions.

It is noted that more works were carried out in analyzing the mechanical properties such as hardness on ERSW welded lap joints. A limited number of works were conducted in identifying the corrosion resistance behavior of RSW welded joints. The implementations of the design of experiments using RSM, ANN, and ANOVA on ERSW process for different materials were carried out by various researchers. It is observed that no works had been identified in implementing RSM and ANOVA for the prediction and optimization of RSW process on welding of AIS5052, AISI1020 and AA1008 similar and dissimilar joints.

The extensive usage of ERSW welding process in the welding of AIS5052, AISI1020, and AA1008 combinational dissimilar sheet metal alloys is scarce. In this context, it is understood that AIS5052, AISI1020, and AA1008 were enormously used for automobile and household appliances. A large no of weld defects was stated in the above alloys welded by a various welding process such as TIG, Arc etc. has reported in other researches. The selection of ERSW welding process for welding of the above alloys is scarce. In this context, the ERSW welding process was finally opt as a welding process in the welding of similar and dissimilar sheet metal alloys combinations of AIS5052-AISI1020, AIS5052-AL, AISI1020-AL which is chosen as a parent material for this present combinational investigation from the various literature reviews it is also found that only limited work has been

carried out in applying various optimization and predictions techniques on the process parameters of ERSW welding in dissimilar sheet metal alloys.

OBJECTIVES

The primary objective of this work is to ensure the feasibility in welding of AIS5052-AIS5052, AISI1020-AISI1020, AIS5052-AISI1020, AISI1020-AL similar and dissimilar joints by ERSW process. Similarly, this research work also concentrates on identifying suitable RSW weld process parameters for obtaining better mechanical and nugget dimensions for weldments using RSM and ANOVA tools. The individual investigation includes

- An experimental investigation has been carried out on welding of AIS5052, AISI1020 and AA1008 similar joints using ERSW process by varying the weld pressure and keeping weld time and current as constant.
- To ensure the quality of similar and dissimilar ERSW joints, mechanical tests such as Tensile Shear Fracture Load (TSFL) and microhardness test were carried out. Similarly, the metallurgical test such as Scanning Electron Microscope (SEM), EDAX, Micro & Macro Examinations was conducted. The factography examination was carried out on the failed tensile test samples.
- The corrosion test was carried out on the ERSW joints using potentiodynamic polarization.
- In order to investigate the effect of ERSW weld process parameters on welding of AIS5052, AISI1020, and AA1008 dissimilar joints. The weld trails were conducted by varying

welding current (55W- 65W), Time (1.5 sec to 2.5 sec) and pressure (3.3 to 3.7kgf).

- To optimize the RSW weld input process parameters such as current, voltage and pressure on the welding of dissimilar AIS5052, AISI1020, and AA1008 joints was carried out using RSM. Based on the input data obtained from RSM model the weld trails were conducted. The welded samples were subjected to TSFL and microhardness test. The nugget diameter was measured by video captured model (VCM) for all the joints. Similarly the metallurgical test EDAX, SEM etc. and the factography test was also carried out on dissimilar joints.
- To predict the better ERSW weld process parameters for welding of dissimilar AIS5052, AISI1020, and AA1008 joints was carried out using ANOVA model for obtaining good mechanical properties and nugget diameter.
- To validate the optimized process parameters confirmation test was conducted and experimentally obtained results were compared with the RSM and ANOVA results.
- Similarly, the corrosion test was conducted on the samples welded at the optimum condition and the obtained results were compared with the results unoptimized weld samples for ERSW joints.
- From the detailed literature review on ERSW welding process on optimization and prediction of its process parameters for different materials. The major problem had been identified and presented as a detailed workflow chart as given in three phases presented in Figure 3.1 (a), 3.1 (b), 3.1 (c) and the entire workflow chart given in 3.1 (d).

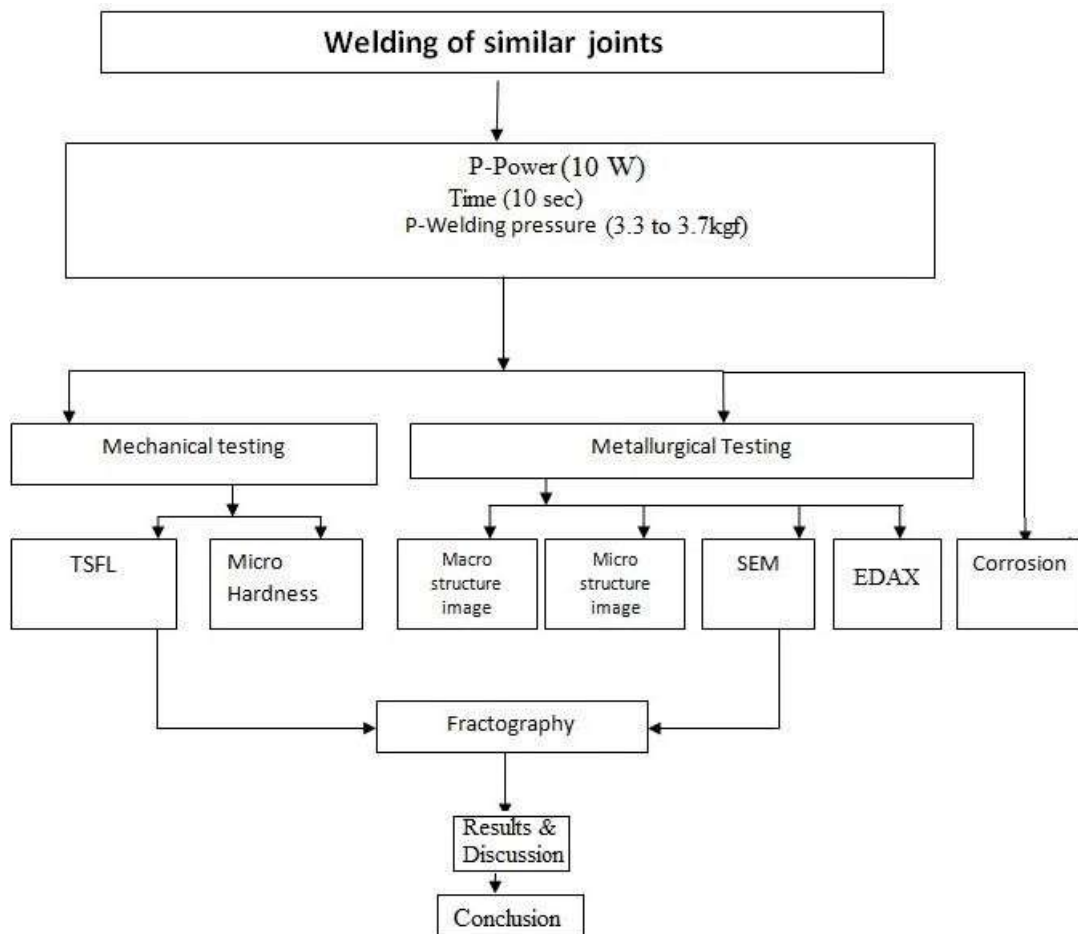


Figure 3.1(a) Schematic workflow chart phase-1

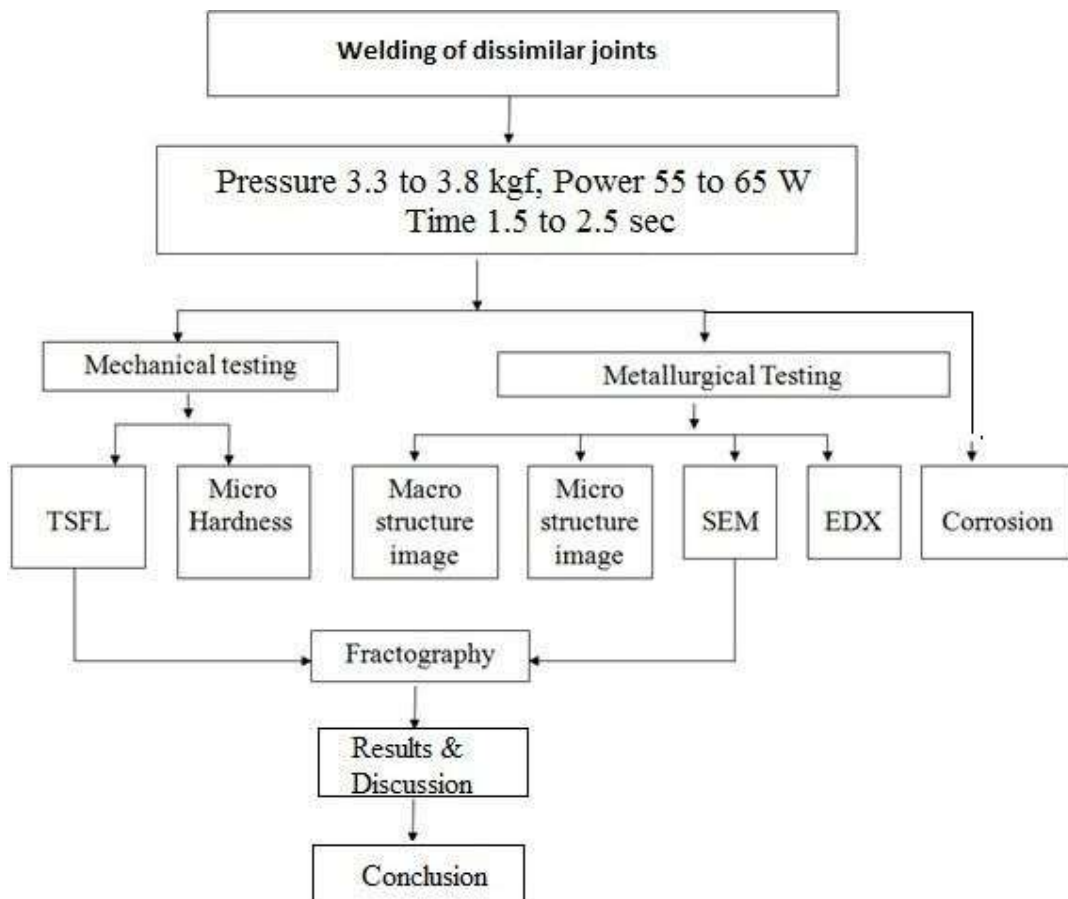


Figure 3.1(b) Schematic workflow chart phase-II

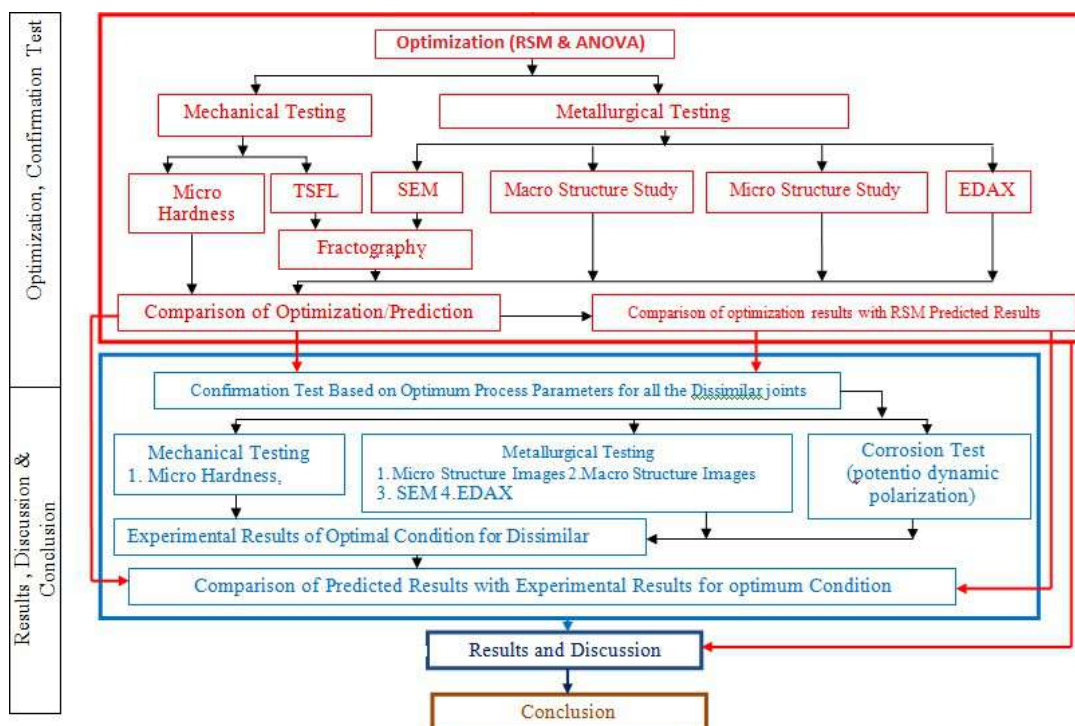


Figure 3.1(c) Schematic workflow chart phase-III

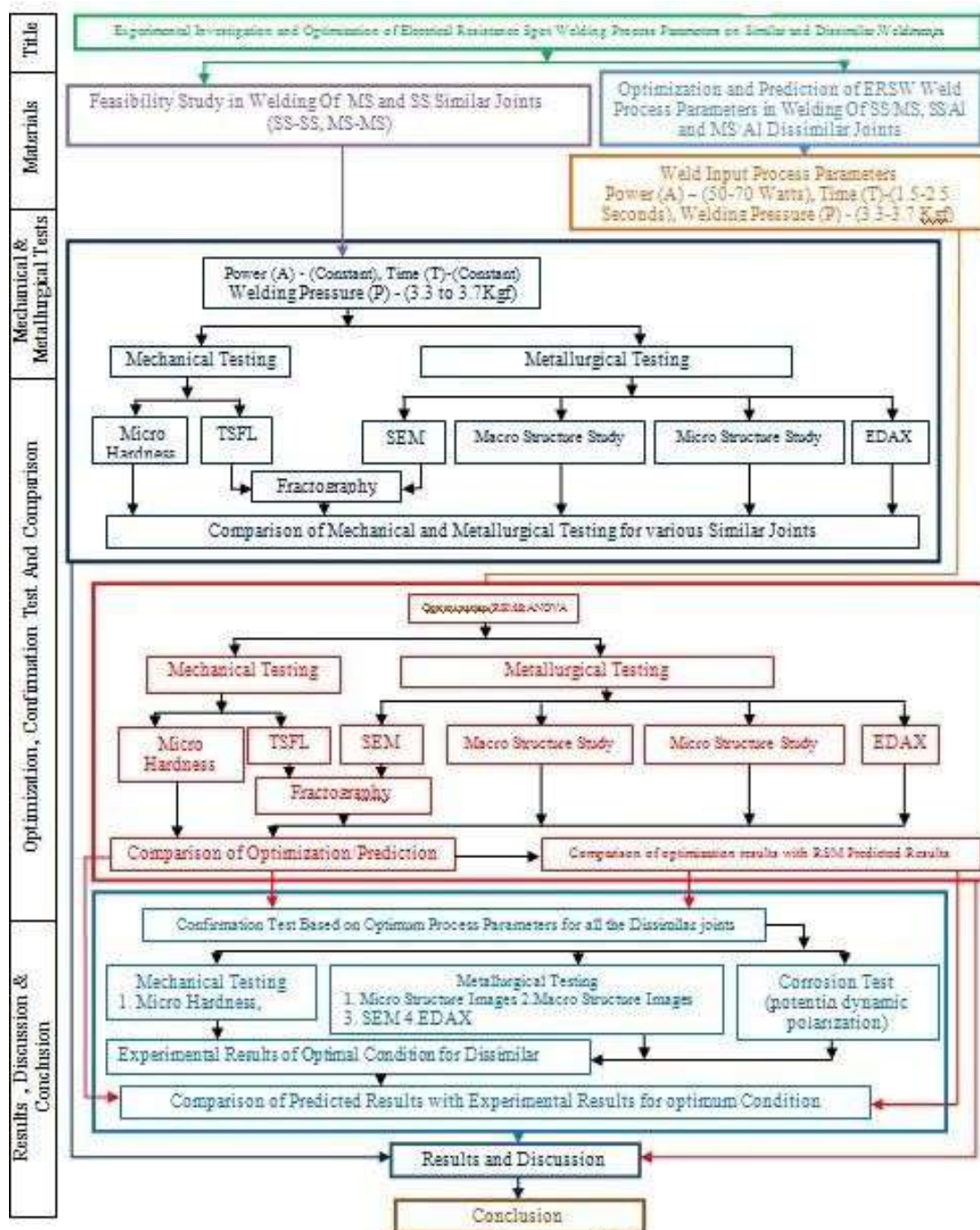


Figure 3.1(d) Schematic workflow chart

METHODOLOGY

The total and complete experimental methodology is described in the form of the workflow chart in this section and illustrated in Figures 3.1(a), 3.1(b), 3.1(c) and 3.1 (d). The sequence of the methodology which was followed in the present investigation is given below:

- Initially, the base material was prepared from the AIS5052, AISI1020, and AA1008, for welding of similar and dissimilar joints using ERS Welding process.
- Welding of similar joints was carried out by keeping pressure and time as constant and the pressure was varied from to 3.9 kgf.
- Then the welded samples are tested using the radiographic test to check and confirm that the samples contain no defect on them.
- According to the various ASTM standards the TSFL and microhardness test samples were prepared from welded joints and tested.
- The metallographic test like micro, macro, SEM and EDAX were carried out on the welded samples to study the structural changes happened in the grains during welding in the nugget zone.
- Factography test was carried out on the failed TSFL samples to study the mode of failure occurred.

- A corrosion test was conducted on the ERSW joints using potentiodynamic polarization to analyze the effect of corrosion on the welded joints.
- Similarly, welding of dissimilar joints was carried out at various RSW weld parameter such as current (50A-30kA), voltage (50-70W) and pressure (3.4 to 3.9kgf) and the mechanical, metallurgical, factography and corrosion tests were conducted for the dissimilar joints.
- In order to identify the optimum ERSW weld process parameters, the RSM model was used.
- The RSM model was developed based on Central Composite Rotatable Design (CCRD) for optimization of the three important process parameters such as power time and pressure.
- Similarly, the welded sample was initially tested using radiographic test for the confirmation of defect-free joints. The various mechanical test's such as TSFL and Microhardness test was carried out on all the samples prepared based on various ASTM standards from the ERSW welded joints.
- The metallographic test such as SEM, EDAX, micro, and macro was conducted on the welded samples and the factography test was carried out TSFL on fractured samples.
- The prediction of ERSW weld process parameters was carried out using ANOVA model.
- A corrosion test was carried out on the samples welded at optimum process parameters and obtained results were compared with the non-optimized corrosion test results.

3.3 SUMMARY

The prime objectives and methodology of this stipulated research work are clearly explained in detail in this chapter. The developed workflow chart implicated the step by step work to be followed and the target work to be achieved based on the above-mentioned objectives. The next subsequently following chapter deals with the experimental methods required for the present work.

CHAPTER 4

EXPERIMENTAL METHODS AND MATERIALS

Based on the inference from the objectives and methodologies discussed in the third chapter, the experimental methods to be deployed and followed are framed and discussed in an elaborate manner. This current chapter emphasizes the material selection and the base materials preparations for welding. It further discusses in depth about the welding machine, welding procedure followed and the welding process parameters incorporated in this research work.

The different mechanical testing machines used for various tests like the TSFL and microhardness test and their necessary appropriate ASTM standards are used for the preparation of the sample's has been put forth in this chapter. This chapter also discussed in detail the necessary metallurgical testing machines used for this research work required to analyze like the macro, micro, SEM and EDAX tests.

MATERIALS SELECTION

In this work AISI 304 (SS), AISI 1020 (MS) and AA 1008 (Al) was selected as base materials for this investigation because they are widely used in automobile and household applications.

In this work, AISI 304 (SS), AISI 1020 (MS) and AA 1008 (Al) selected as base materials for this investigation because of they are widely applied in different engineering industries and their corresponding chemical composition and mechanical properties are tested and tabulated in Tables 4.1 and 4.2 respectively.

Table 4.1 Chemical Compositions of the Selected Base Materials

Materials	Weight %											
	C	Fe	Mn	P	S	Cr	Ni	Si	Al	Cu	Mg	Zn
AISI1020	0.17-0.23	99.08-99.53	0.30-0.60	≤0.040	≤0.05	-	-	-	-	-	-	-
AIS5052	0.08	66.3-74	2	0.045	0.03	18-20	8-10.5	1	-	-	-	-
AA1008	-	0.5	0.3-0.9	-	-	0.1	-	0.5	90-94	4-5	1-2	.25

Table 4.2 Mechanical Properties of the Selected Base Materials

Materials	Properties				
	Tensile Strength, Ultimate (MPa)	Modulus of Elasticity (GPa)	Bulk Modulus (GPa)	Poissons Ratio	Shear Modulus (GPa)
AISI1020	394.72	200	140	0.290	80.0
AIS5052	505	193-200	-	0.29	86
AA1008	324	73.1	-	0.33	28

ERSW WELDING MACHINE

The joining of metal sheets was carried out in Resistance spot welding machine with the configuration of pedestal type inverter base medium frequency DC machine (Model PACI TECH-ERSW) of capacity 90kV. It has the flexibility of welding sheets up to 6 mm thickness with a

maximum current of 20 kVA capacities. The photographs views of the ERSW welding machine deployed for this investigations were shown in figure 4.1.



Figure 4.1 Photographic View of the ERSW machine deployed in this study

WELD PROCESS PARAMETERS

The weld process parameters selected for feasibility trails and optimization in welding of AISI 304 and AISI 1020 AA1008 similar and dissimilar joints was discussed detailed in this section below.

Selected ERSW Process Parameters for Trail Experiments

The feasibility study was conducted by varying the weld pressure and keeping the weld time and current as constant for AISI 304 and AISI 102 similar joints. The parameters selected for the feasibility study was discussed in section.

ERSW Process Parameters for Optimization and Prediction Techniques

The optimization and prediction of ERSW process parameters were carried out on AISI5052-AISI1020, AISI1020-AA1008, and AIS5052-AA1008 dissimilar joints by varying the welding current (55-65W), Time (1.5 to 2.5 sec) and pressure (3.4 to 3.9kgf). The parameter range was selected from the results obtained from the feasibility study experiments as explained in section 4.3.1 and based on a literature survey.

MECHANICAL TESTING

The mechanical properties of the ERSW welded joints were identified by conducting TSFL and Microhardness tests on the specimens prepared from the ERSW welded joints according to various ASTM standards.

TSFL Test

The TSFL specimens were prepared from the welded joints based on ISO14273 standards as given in Figure 4.2. The TSFL test was conducted using UTM of 20kVA as given in Figure 4.3.

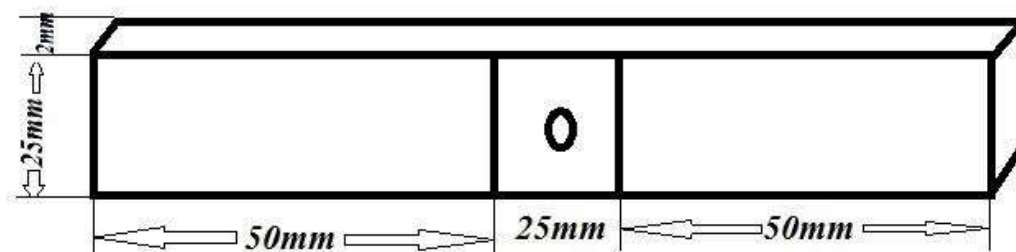


Figure 4.2 Specimen Dimensions (all dimensions are in mm)



Figure 4.3 TSFL machine

Micro Hardness test

The microhardness test samples were prepared from the ERSW weld samples based on the ASTM standards as shown in Figure (4.5). Figure 4.6 shows the base and nugget zone of the welded samples. The microhardness test was carried out by using a Micro Vickers Hardness Tester machine by applying a 1Kg load shown in Figure 4.5.

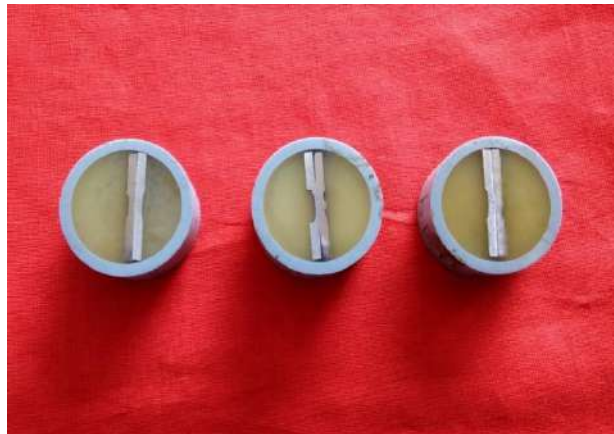


Figure 4.4 Hardness sample



Machine Name: Micro Vickers Hardness Tester

Testing load range: 10 grams to 1 Kg Load

Make: Wilson Wolpert – Germany

Vernier caliper least count: 0.01 mm

Available Hardness testing Scale: HV, HRA, HRC, 15N, 30N etc.

Figure 4.5 Micro Vickers Hardness Tester Machine

METALLURGICAL TESTING

The metallurgical investigation was carried out on the specimen prepared from ERSW welded joints using an optical microscope and scanning electron microscope for analyzing the structural changes occurred in the weld nugget zone. The factography test was carried out on a failed TSFL sample using SEM in order to identify the mode of failure and the result was correlated with mechanical properties. The EDAX test was carried out on the nugget zone in order to examine the elemental changes occurred during welding.

The optical microscope was used for macro and micro was shown in Figure 4.6. The SEM and EDAX test conducted by using SEM machine shown in Figure 4.7.



Figure 4.6 Photographic image of Optical Microscope



Figure 4.7 Photographic image of Scanning Electron Microscope (SEM)

POTENTIO DYNAMIC POLARISATION TEST

The corrosion test was carried out using potentiodynamic polarization methods and the corresponding experimental setup as shown in Figure 4.8. The corrosion samples were prepared from the joints welded at the optimized condition for dissimilar joints and on the similar joints welded at high weld pressure according to the specification of potentiodynamic polarization the sample dimensions are 10mm × 10mm and the nugget zone has been polished by mirror polished method, which is shown in Figure 4.9

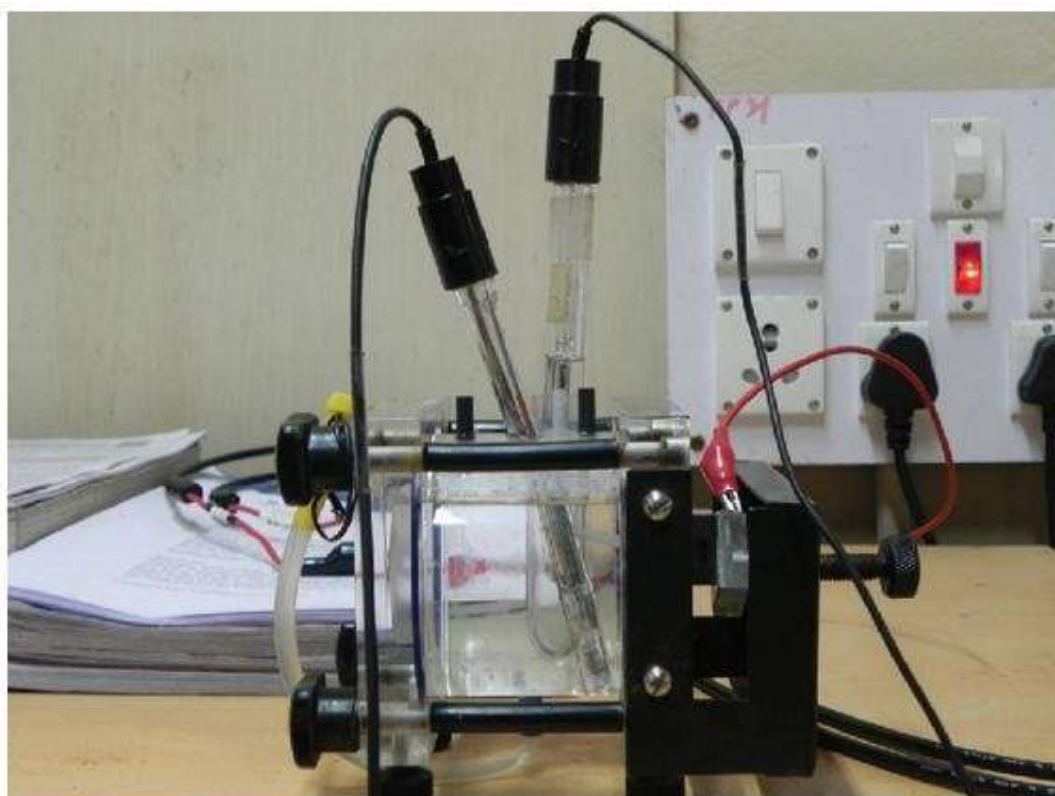


Figure 4.8 Experimental setup for potentiodynamic polarization test



Figure 4.9 Samples of Corrosion Test

SUMMARY

This chapter describes in details about the selected various material, weld procedures and various mechanical metallurgical and corrosion test methods are employed in this work. This chapter also discussed in detail about the ERSW weld machine and the various weld input process parameters identified for experimental works. This chapter also explains various ASTM standards employed in the preparation of the sample test in this work, the next chapter describes in details about various weld process parameters selected for similar and dissimilar joints.

CHAPTER 5

SELECTED WELDING PROCESS PARAMETERS

This chapter describes in detail about the various ranges of weld process parameters selected for welding of AISI 304, AISI 1020 and AA1008 similar and dissimilar joints.

In this section, it deals with the different range of input process parameters selected for welding of AIS5052-AISI1020 and AISI1020-Al and AIS5052-Al joint using optimization techniques.

TRIAL EXPERIMENTAL STUDY ON SIMILAR JOINTS

This chapter illustrates in detail about the various weld process parameters selected for welding of AIS5052-AIS5052 and AISI1020-AISI1020 similar joints.

Trial Experimental Studied for AIS5052-AIS5052 Similar Joints

To determine the suitable welding pressure range for welding of AIS5052-AIS5052 similar joints. These trial experiments were conducted. The base materials $75 \times 25 \times 2$ mm³ sheet were prepared from the AIS5052-AIS5052 material for investigation as given in Figure 5.1. The lap joint was prepared using ERSW machine by keeping power and time as constant and varying the weld pressure at various levels. The weld process parameters are tabulated in Table 5.1. The welded samples were shown in Figure 5.2. After welding the sample was subjected to a radiographic test to identify the

defects. TSFL and

microhardness specimens prepared from each welded samples welded at different weld pressure 3.3 to 3.7 kgf. The various metallurgical test such as Macro, Micro, SEM, EDAX, and factography were examined and its corresponding results were discussed in section7.1.1

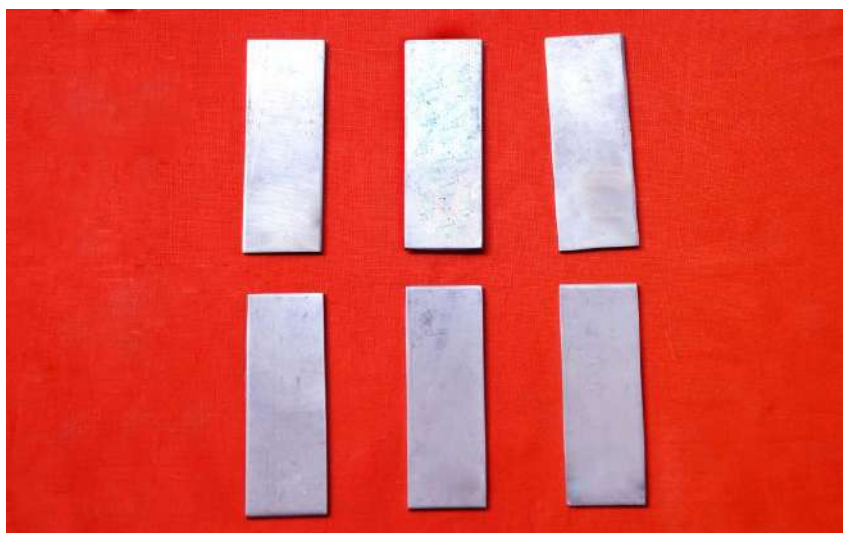


Figure 5.1 Photographic view of the AISI1020-AISI1020 samples before the weld

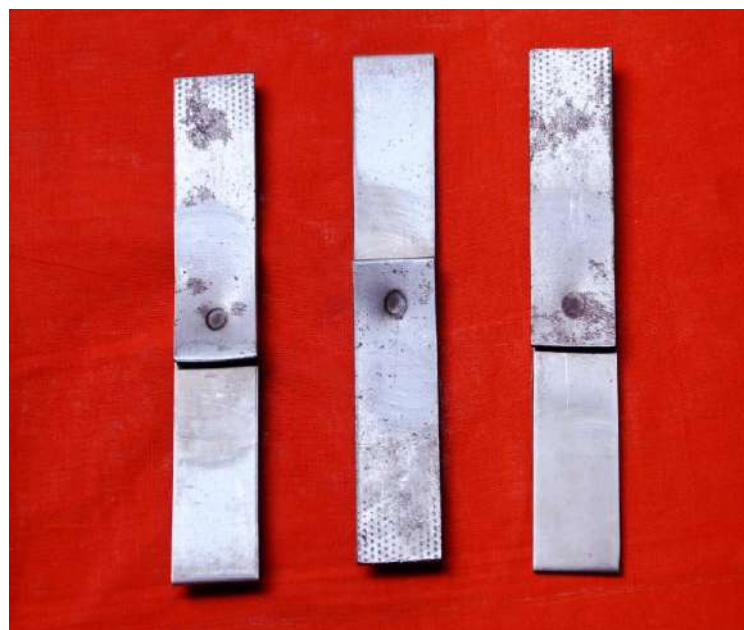


Figure 5.2 Photographic view of the AISI1020-AISI1020 samples after the weld

Table 5.1 The weld process parameters AISI1020-AISI1020 similar joints

Sample No	Power (W)	Time (sec)	Pressure (kgf)
1	15	10	3.3
2	15	10	3.5
3	15	10	3.7

Trial Experimental AIS5052-AIS5052 Similar Joints

To determine the suitable welding pressure range for welding of AIS5052-AIS5052 similar joints. These trial experiments were conducted. The base materials $75 \times 25 \times 2 \text{mm}^3$ sheet was prepared from the AIS5052-AIS5052 material. For investigation as given in Figure 5.3. the lap joint was prepared using ERSW machine by keeping power and time as constant and varying the weld pressure at various levels. The weld process parameters are tabulated in Table 5.2. The welded samples are shown in Figure 5.4. After welding the sample was subjected to a radiographic test to identify the defects. TSFL and microhardness specimens prepared from each welded samples welded at different weld pressure 3.3 to 3.9 kgf. The various metallurgical test such as Macro, Micro, SEM, EDAX, and factography were examined and its corresponding results are discussed in section 7.1.2.



Figure 5.3 Photographic view of the AIS5052-AIS5052 samples before the weld



Figure 5.4 Photographic view of the AIS5052-AIS5052 samples after the weld

Table 5.2 The weld process parameters of AIS5052-AIS5052

Sample No	Power (W)	Time (sec)	Pressure (kgf)
1	15	10	3.3
2	15	10	3.5
3	15	10	3.7

TRIAL EXPERIMENTAL DISSIMILAR JOINTS

This chapter illustrates in detail about the various weld process parameters selected for welding of AIS5052-AISI1020, AISI1020-AA1008 and AIS5052-AA1008 dissimilar joints.

Trial Experimental of AIS5052-AISI1020

In order to optimize the ERSW weld pressure parameter weld trails are conducted by varying welding power (55W- 65W), Time (1.5 to 2.5 sec) and pressure (3.3 to 3.8kgf) at various levels based on RSM model. The base metals size of $75 \times 25 \times 2 \text{mm}^3$ of AIS5052-AISI1020 was prepared as shown in Figure 5.5. the weld input process parameters were given in Table 7.7. The lap joints were performed using ERSW machine at various weld conditions based on RSM model as given in Figure 5.6. The samples are subjected to radiographic test after welding. The TSFL and microhardness specimen were prepared from the 17 welded samples and tested. Similarly, the various metallurgical test was carried out on the samples and results were discussed detailed in section 7.2.1.1 and 7.2.1.2 respectively.

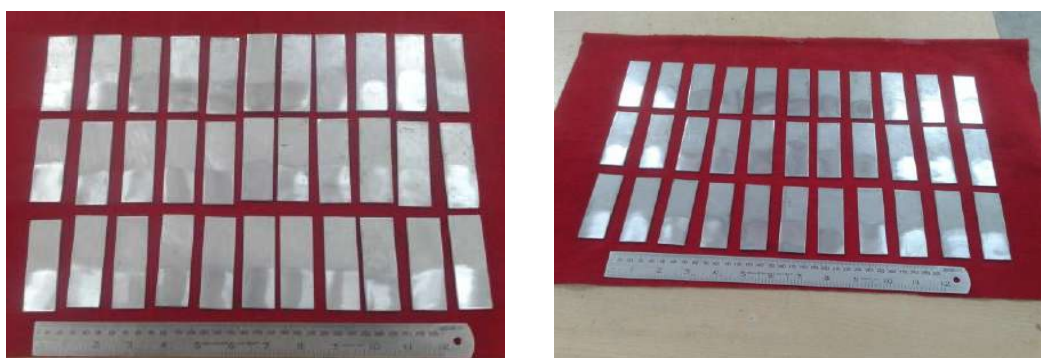


Figure 5.5 Photographic view of the AIS5052-AISI1020 samples before the weld



Figure 5.6 Photographic view of the AIS5052-AISI1020 samples after the weld

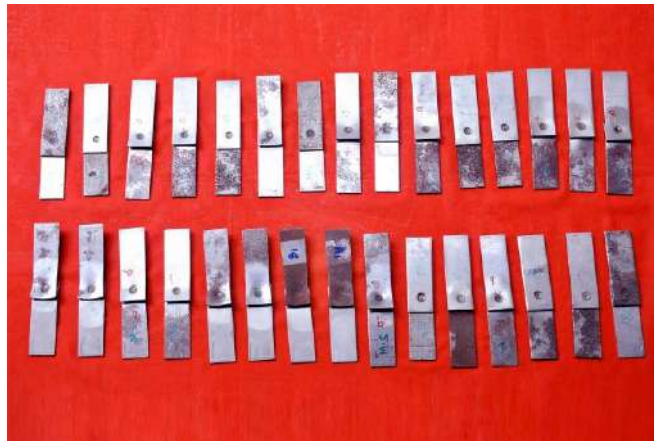


Figure 5.6.1 Photographic view of the AIS5052-AISI1020 samples before TSFL Test



Figure 5.6.2 Top view of AIS5052-AISI1020 samples after TSFL Test

Trial Experimental AISI1020 –AA1008

In order to optimize the ERSW weld pressure parameter weld trails are conducted by varying welding current (50A- 30kA), voltage (50-70W) and pressure (3.4 to 3.9kgf) at various levels based on RSM model. The base metals size of $75 \times 25 \times 2 \text{mm}^3$ of AIS5052-AISI1020 was prepared as shown in Figure 5.7. the weld input process parameters were given in table 7.7. The lap joints were performed using ERSW machine at various weld conditions based

on RSM model as given in Figure 5.8. The samples are subjected to radiographic test after welding. The TSFL and microhardness specimen were prepared from the 17 welded samples and tested. Similarly, the various metallurgical test was carried out on the samples and results were discussed detailed in section 7.2.2.1 and 7.2.2.2 respectively.

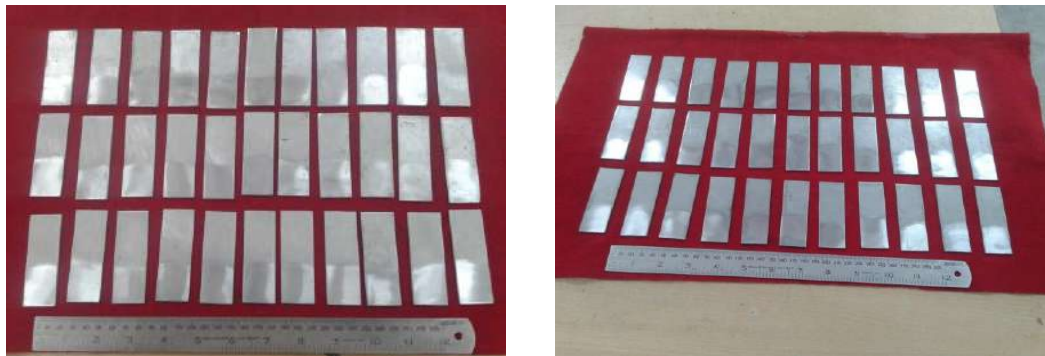


Figure 5.7 Photographic view of the AISI1020-AA1008 samples before the weld



Figure 5.8 Photographic view of the AISI1020-AA1008 samples after the weld



Figure 5.8.1 Photographic view of the AISI1020-AA1008 samples after TSFL test

Trial Experimental AIS5052-AA1008

In order to optimize the ERSW weld pressure parameter weld trails are conducted by varying welding current (50A-30kA), voltage (50-70W) and pressure (3.4 to 3.9kgf) at various levels based on RSM model. The base metals size of $75 \times 25 \times 2 \text{mm}^3$ of AIS5052-AISI1020 was prepared as shown in Figure 5.9. The weld input process parameters were given in table 7.7. The lap joints were performed using ERSW machine at various weld conditions based on RSM model as given in Figure 5.10. The samples are subjected to radiographic test after welding. The TSFL and microhardness specimen were prepared from the 17 welded samples and tested. Similarly, the various metallurgical test was carried out on the samples and results were discussed detailed in section 7.2.3.1 and 7.2.3.2 respectively.



Figure 5.9 Photographic view of the AIS5052-AA1008 samples before the weld



Figure 5.10 Photographic view of the AIS5052-AA1008 samples after the weld



Figure 5.10.1 Photographic view of the AIS5052-AA1008 samples after TSFL Test

SUMMARY

This chapter clearly reveals that weld pressure is having a major role in welding of similar and dissimilar joints using the ERSW process based on the feasibility trails. Similarly, the various weld process parameters at various levels selected for the welding of dissimilar joints was also discussed. The next chapter illustrates the optimization techniques using the RSM model to optimize the weld process parameters and ANOVA model to predict the mechanical properties, nugget diameter of the welded joints.

CHAPTER 6

OPTIMIZATION AND PREDICTION MODEL FOR ERSW PROCESS USING RSM AND ANOVA TECHNIQUES

OPTIMIZATION OF ERSW INPUT PROCESS PARAMETERS FOR WELDING OF AIS5052-AISI1020, AISI1020-AA1008, AND AIS5052- AA1008 DISSIMILAR JOINTS

The RSM optimization techniques are used for optimizing the ERSW welding input process parameters for welding of AIS5052-AISI1020, AISI1020-AA1008 and AIS5052- AA1008 dissimilar joints. The ANOVA model was also developed to predict the TSFL, microhardness and nugget diameter were also discussed in detail in this chapter. The various ERSW input process parameters for the joining of metals was identified by conducting the feasibility trail experiments. In this work power, pressure and time are considered as important input process parameters for welding of AIS5052-AISI1020, AISI1020-AA1008, and AIS5052- AA1008 dissimilar joints. In this work, the design of the experiment was carried out using RSM to optimize the various input process parameters for identifying the better mechanical properties and nugget diameter of the joints. Similarly, ANOVA is used to predict the various mechanical properties and nugget diameter.

An overview of Design of Experiments (DOE)

DOE is the statistical techniques in which a large number of test trial were conducted by varying the input process at various levels and to find out the changes occurred in the output responses. This study is used to identify the effect multiple selected at the same time and to determine the factor arrangement for optimum result. The experimental trails were carried out using one factor at a time approach in which one of the factors is varied over its range while the other factor is kept at the base level. The result obtained from the reveals the most influencing parameters that are to be considered for identifying the exact variation of information of experiments. The DOE is also having a major role for prediction of the responses and predesign the experiments by altering of the input process parameter of the experiments. In DOE the predictor variable and response variable plays an important role. The analysis of variance ANOVA is the collection of a statistical model with related procedures that used to examine the variance.

Response surface methodology (RSM)

The RSM is a mathematical model is used for modeling and analyzing the various engineering applications. This DOE method established by George E.P. Box and Wilson K.B in the year of 1951. This method is used to identifying the optimal values for the designed experiments. RSM is using the second-degree polynomial model. In this method to get accurate and optimum values by varying the parameters.

RSM properties

RSM has three important properties namely Orthogonality, Rotatability, and Uniformity as discussed below.

Orthogonality: The effect individual property of k-factors is to be calculated without confusing.

Rotatability: The center of the factor space is occupied by the rotating points and its property and moreover design points are considered as constant.

Uniformity: The CCD designs follow the uniform precision by a number of center points.

The main goal of this technique is to optimize the output responses which is mainly influenced by various input parameters based on the experimental data. It also deals with and measures the connection between the various input process parameters and output responses. The RSM deals with

- Analyzing the effect of input process parameters on the selected output responses.
- The identification of a correlation between the various input variables.
- It also characterizes the combined effect of all the input variable which have the influence on output process responses.

Analysis of variance (ANOVA)

Analysis of variance is the statistical method in which models will be analyzed to know the variance or difference among group means. A selected variable will be sectioned and it is about to a number of variables to the various source of variation. Many groups are equal and therefore simplifies the t-test into greater than two groups. It is very useful to compare any numbers of variables for the statistical mean.

➤ Model Classification

In this ANOVA there are three classifications in terms of the model. Fixed effect model, the random effect model, and mixed effects models.

➤ Fixed-effects models

In this model, one or more actions considered for the corresponding experiment to validate the variable changes or variance.

➤ Random-effects models

Random effects model is applicable for large data application and it takes various influencing factors for the experiments. Based on the large data experiments the variance has been compared with fixed effect models.

➤ Mixed-effects models

Mixed effect model adopted for both the fixed and random effect model procedure, In which both models has been compared with one another to get the exact and right values in the variance.

➤ F-Test

The F-test is used to compare the factors of total deviation

$$F \text{ test} = \text{variance between treatments} / \text{variance within treatment} \quad (6.1)$$

The ANOVA is applied in five steps.

- **Step 1.** Set up hypotheses and determine the level of significance

- **Step 2.** Select the appropriate test statistic.
- **Step 3.** Set up a decision rule.
- **Step 4.** Compute the test statistic.
- **Step 5.** Conclusion

DEVELOPMENT OF RSM MODEL FOR OPTIMIZATION OF ERSW PROCESS PARAMETERS

The design expert software 9.0.3.1 was used in this study for designing the input process parameters and to analyze the output responses statistically. In this work the experiments were designed based on the Central Composite Rotatable Design (CCRD) a three-level, three-factor CCRD is selected. Based on the CCRD experimental design matrix 17 experimental trials (1 center point, at the Centre, axial points outside the cube, four factorial point and four replicated center points), which gives suitable information to fit a full second-order polynomial (Montgomeri 2001). The parameters which affect the selected TSFL microhardness and nugget diameter were selected based on the feasibility study and literature review. The RSM flowchart is used in this work as shown in Appendix-I. From the various literature it is identified that the various input process parameters for the ERSW process are power, weld time, diameter, electrode tip angle and electrode material etc. to identify the various mechanical properties such as TSFL strength, hardness and nugget diameter of the ERSW joints using various materials. For welding of AIS5052, AISI1020 and 1008 material using ERSW process the researchers are mainly focusing the three important parameters such as weld power, time and pressure. The effect of ERSW input process parameter which is selected to determine the mechanical properties and nugget diameter is analyzed by using RSM. The ranges of the selected ERSW input parameters selected for identifying the output responses are confirmed by conducting feasibility experiments and from the detailed literature

DEVELOPMENT OF ANOVA MODEL FOR PREDICTION OF MECHANICAL AND NUGGET DIAMETER FOR ERSW JOINTS

The ANOVA model is developed in order to understand the statistical model. The model was finalized based on the assumptions made and it is mandatory that selection of suitable assumptions in order to get the accurate variance for the chosen data. The Minitab steps have been utilized for the experiment to check the relationship and regression of ANOVA. To conduct the various input parameter by Minitab software. In this investigation, ANOVA is applied in five steps.

- **Step 1.** Set up hypotheses and determine the level of significance
- **Step 2.** Select the appropriate test statistic.
- **Step 3.** Set up a decision rule.
- **Step 4.** Compute the test statistic.
- **Step 5.** Conclusion

In this study, the ANOVA has been incorporated with 17 trials were allowed to find out the null hypothesis variation, which states that error variance indicates the equal magnitude in this study.

SUMMARY

This chapter deals with the optimization and prediction methods followed in this work and its corresponding procedure and steps for obtaining optimum input process parameters for the ERSW process have been

discussed. The RSM and ANOVA steps have been discussed in detail. the assumptions and procedures for selected input process parameters were also discussed. The next chapter will discuss the various result and discussion of ERSW joints welded based on different weld input process parameters selected for this investigation.

CHAPTER 7

RESULTS AND DISCUSSION

The results obtained from TSFL, microhardness, nugget diameter, metallographic study and corrosion test on AIS5052 and AISI1020 similar joints welded using ERSW process was discussed in detail in this section. Similarly, optimization and prediction of ERSW weld input process parameter for welding of AIS5052, AISI1020 and AA1008 dissimilar joints on various mechanical properties and nugget diameter are also illustrated detail in this section.

EXPERIMENTAL INVESTIGATION ON THE EFFECT OF WELD PRESSURE ON MECHANICAL AND METALLURGICAL PROPERTIES OF ERSW WELDED AIS5052 –AIS5052 AND AISI1020-AISI1020 SIMILAR JOINTS

This section discusses in detail about the results obtained from TSFL, microhardness, nugget diameter and corrosion test for AIS5052 and AISI1020 similar joints welded using ERSW process. In order to assess the effect of weld pressure on ERSW process, the weld pressure range of 3.3 kgf to 3.7kgf was selected for the welding of AIS5052- AIS5052 and AISI1020- AISI1020 similar joints. The literature review shows clearly that the mechanical properties and its associated parameters are influenced by the current, electrode pressure and weld time. In this similar joints study, initially, weld trails were conducted by varying the weld pressure and keeping the time and power as constant. The ERSW process was used for welding of the joints by keeping the current at 10A and voltage at 15kVA as constant while

varying the welding pressure from 3.3 kgf to 3.7kgf. Finally, the Mechanical, metallurgical and corrosion tests were carried out on the welded joints to identify the better weld pressure parameter as discussed in the following sections.

Mechanical and Metallurgical Investigation of AIS5052 – AIS5052 similar Joints

This section discusses in detail about the results obtained from TSFL, microhardness, nugget diameter and corrosion test for AIS5052-AIS5052 similar joints.

Analysis of TSFL and hardness

The TSFL test samples were prepared from ERSW welded joints according to ISO14273 standard as shown in Figure 7.1, then the samples were tested using Instron 250 kN. The failed TSFL specimens are shown in Figure 7.2. From the Figure 7.2, it is identified that all the samples are failed at the weld nugget region.



Figure 7.1 Photographic view of TSFL test samples of AIS5052 Similar joints before testing



Figure 7.2 Photographic image of TSFL tested samples of AIS5052 – AIS5052 similar welded joints after testing.

The TSFL test results for the samples welded at three different weld pressure are shown in Figure 7.3.

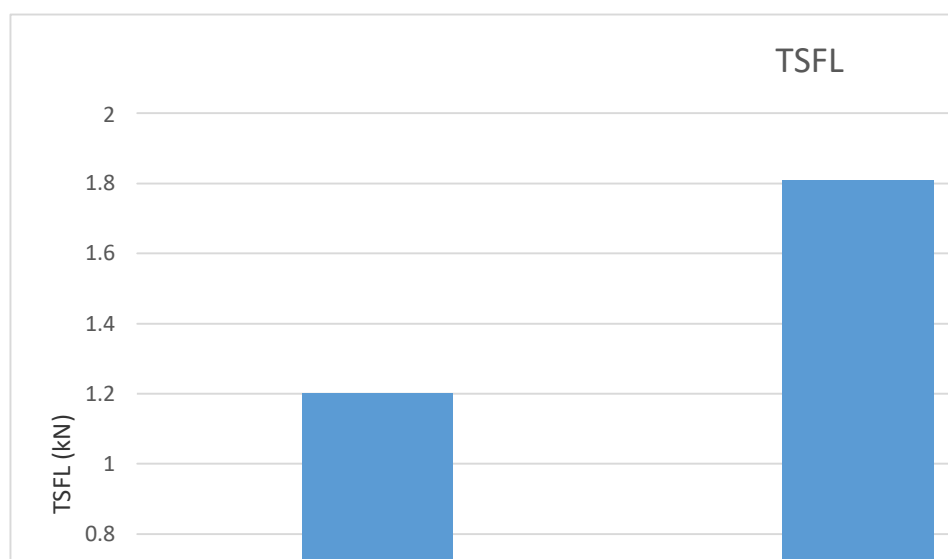


Figure 7.3 TSFL test results for the samples welded at three different weld pressure conditions for AIS5052 Similar joints.

From the Figure 7.3, it is noted that the maximum TSFL was obtained for the sample welded at the weld pressure 3.7kgf.

The results obtained from the TSFL and microhardness tests were given in Table 7.1.

Table 7.1 Results obtained from TSFL and microhardness tests for AIS5052 similar joints

Sample No	Weld Parameters			TSFL (kN)	Micro Hardness (VHN)
	Power (W)	Time (seconds)	Pressure (kgf)		
AIS5052–AIS5052-1	15	10	3.3	1.20	214.8
AIS5052–AIS5052-2	15	10	3.5	1.81	215.2
AIS5052–AIS5052-3	15	10	3.7	1.85	220.2

From the Table 7.1, it is clearly identified that increase in weld pressure increases the TSFL strength.

Similarly, the microhardness samples were prepared from the ERSW joints welded at three different weld pressure and it was etched by sodium hydroxide solution as shown in Figure 7.4 (a).



Figure 7.4 (a) Photographic view of microhardness samples of AIS5052 similar joints

The hardness test was conducted using a Vickers microhardness tester for a load of 1 kg. The results obtained from the test are shown in Figure 7.4 (b).

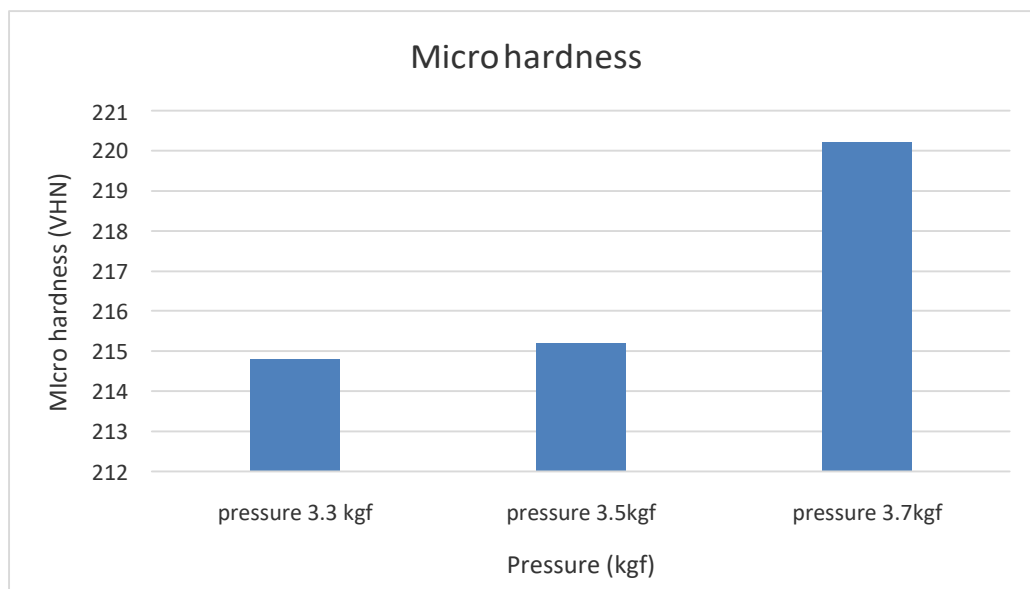


Figure 7.4(b) Microhardness test result for the samples welded at various weld pressures

From the Figure 7.4(b) it is identified that maximum hardness values were obtained for the sample welded at the maximum weld pressure of 3.7kgf. Therefore, it was observed that the hardness values are directly proportional to the weld pressure as tabulated in Table 7.1.

Analysis of metallurgical results

The macro, micro, SEM, EDAX and factography analysis test was carried out on the AIS5052- AIS5052 joints and the results are discussed in the section below.

Macro, Microstructural and nugget dimension examinations

The macro and microstructural examinations were carried out on AIS5052- AIS5052 joints welded at different weld pressure 3.3 kgf, 3.5 kgf and 3.7kgf and their corresponding images are shown in Figure 7.5(a) to (f).




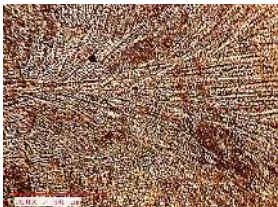

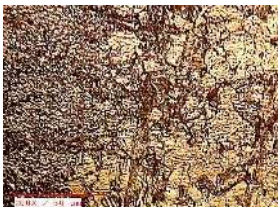
Pressure (kgf)	Macro Image	Micro Image	Nugget Diameter (mm)
3.3	 (a)	 (d)	3.8
3.5	 (b)	 (e)	4.2
3.7	 (c)	 (f)	4.9

Figure 7.5 (a) to (f) shows the Macro-micro image and Nugget diameter of the AIS5052- AIS5052 similar joints welded at various weld pressure

The macrostructural images show that the sample welded at the weld pressure 3.7kgf is having defect free nugget and no holes were

identified. Similarly, while comparing the nugget zone macro structures it is identified that the sample welded at pressure 3.3kgf possess small holes, which clearly reveals that the sample welded at the weld pressure 3.7kgf weld pressure is better as shown in figure 7.5 (a), 7.5 (b) & 7.5 (c). The same result was proved in the TSFL, hardness and nugget diameter examinations.

The microstructural study shows that the sample welded at a pressure of 3.7kgf is having very fine grains when compared with the samples welded at the pressure at 3.3kgf and 3.5 kgf as shown in Figure 7.5 (d, e & f). The microstructural images show the occurrence of coarse austenite and ferrite mode. In addition to that, the presence of high chromium content in AIS5052 promotes more ferrite content. The presence of dendritic ferrite on the nugget zone was also identified and this dendrite ferrite was almost normal to weld interface as presented in the above Figure 7.5(d, e & f).

The nugget diameter was measured using a video measurement system (VMS) 2010F and the measured values of the nugget diameter of the samples welded at three different weld pressure are tabulated in Figure 7.5. From the nugget diameter values, it is identified that the maximum nugget diameter was obtained for the sample welded at maximum weld pressure of 3.7kgf.

SEM & EDAX analysis

The SEM and EDAX tests were carried using Scanning Electron Microscope on the sample welded at the maximum weld pressure at 3.7kgf and its corresponding SEM images and EDS plot are shown are shown in Figure 7.6 (a) and (b) respectively.

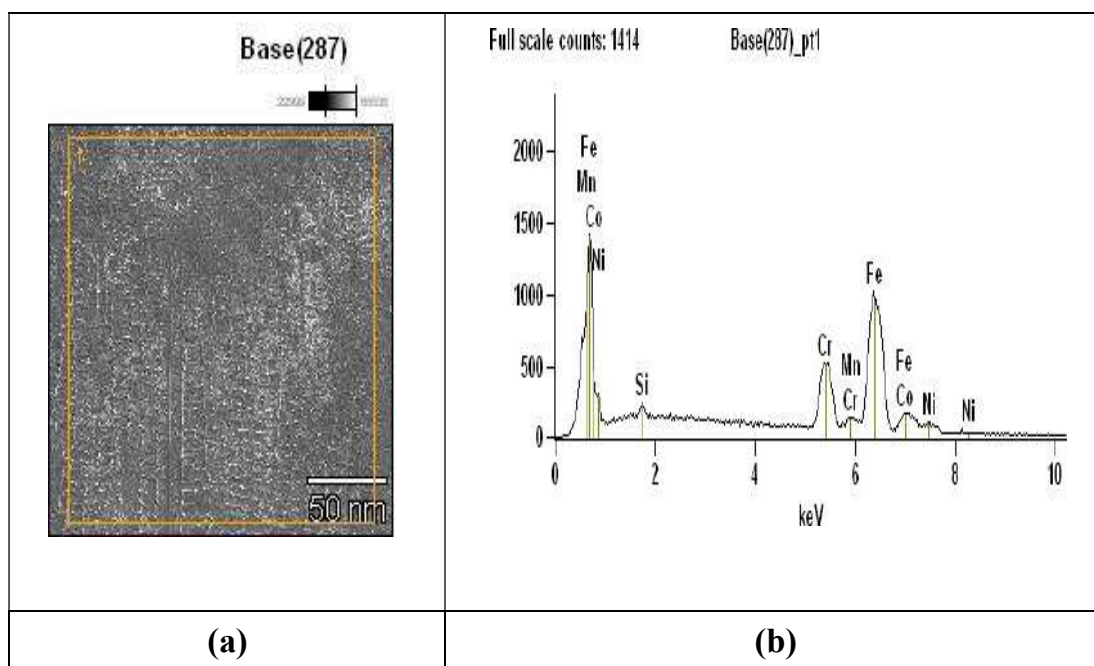


Figure 7.6 (a) SEM image of the sample welded at the weld pressure of 3.7kgf (b) EDS plot of the sample welded at weld pressure 3.7kgf

From the Figure 7.6 (a) and (b) it is identified that the no elemental changes occur in the samples and the elemental table shows the presence of chromium and Magnesium at a high percentage in the plot. The elements present in the sample welded at maximum weld pressure of 3.7kgf are given in Table 7.2.

Table 7.2 Weight percentage of elements on the sample welded at 3.7kgf

	<i>Si</i>	<i>Cr</i>	<i>Mn</i>	<i>Fe</i>	<i>Co</i>	<i>Ni</i>
<i>Base(287)_pt1</i>	0.78	17.19	5.75	66.12	8.23	1.93

Factography test

The fracture surface of the TSFL sample welded at the maximum weld pressure of 3.7kgf was analyzed using SEM to reveal the fracture surface morphology and the fracture surface image was shown in Figure 7.7. From the figure 7.7, it is identified that the grains are elongated and possess a lot of crest and trough-like appearance. Which clearly indicates the ductile mode of failure.

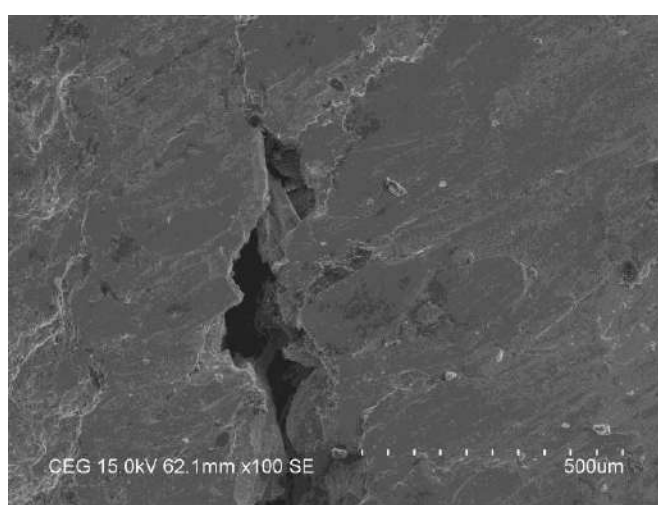


Figure 7.7 Factography images of TSFL tested sample welded at the weld pressure 3.7kgf.

7.1.3 Analysis of corrosion test results

The corrosion test was carried out based on the potentiodynamic polarization method for the sample welded at the maximum weld pressure of 3.7kgf. and their corresponding TAFEL data model was listed in table 7.3. The obtained TAFEL plot for AIS5052 similar joints welded at 3.7 kgf as shown in figure 7.8. From the table 7.3 & figure 7.8, it is identified that the maximum corrosion rate is found to be about 6.294mm/Year.

Table 7.3 TAFEL Data Model Data for AIS5052 similar joint welded at the weld pressure 3.7kgf

Tafel data model for AISI 304-AIS5052 for 3.7KN weld pressure	
E. Corr V	-0.0751
I Cor. A	1.17E-05
I Cor. A/cm ²	0.000732
Rp ohm	3641
ba V/dec	0.204
bc V/dec	0.189
C. Rate mm/y	6.294

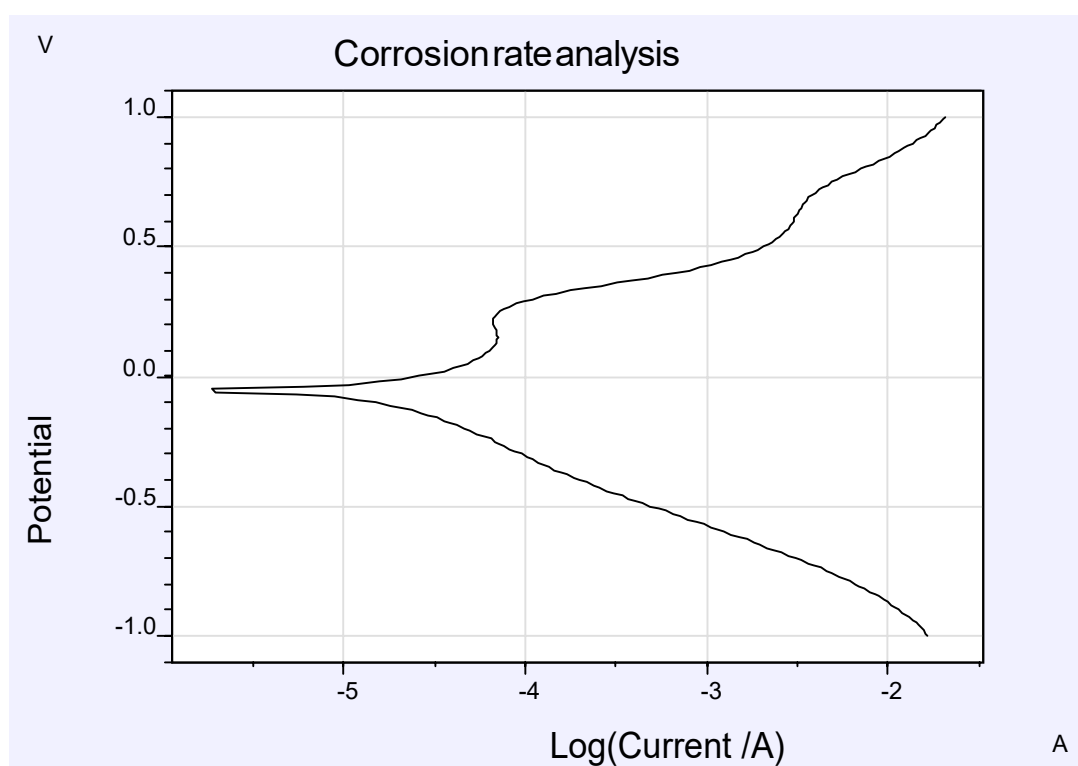


Figure 7.8 TAFEL plot for AISI 304 similar joints welded at 3.7Kgf weld pressure

Mechanical and Metallurgical Investigation of AISI1020 – AISI1020 Joints

This section discusses in detail about the results obtained from TSFL, microhardness, nugget diameter and corrosion test for AISI1020-AISI1020 similar joints.

Analysis of TSFL and hardness

The TSFL test samples were prepared from ERSW welded joints according to ISO14273 standard as shown in Figure 7.9, then the samples were tested using Instron 250 kN. The failed TSFL specimens are shown in Figure 7.9. From the Figure 7.9, it is identified that all the samples are failed at the weld nugget region.



Figure 7.9 Photographic view of TSFL test samples of AISI1020 Similar joints before testing.



Figure 7.10 Photographic image of TSFL tested samples of AISI1020 – AISI1020 similar welded joints after testing.

The TSFL test results for the samples welded at three different weld pressure are shown in Figure 7.11.

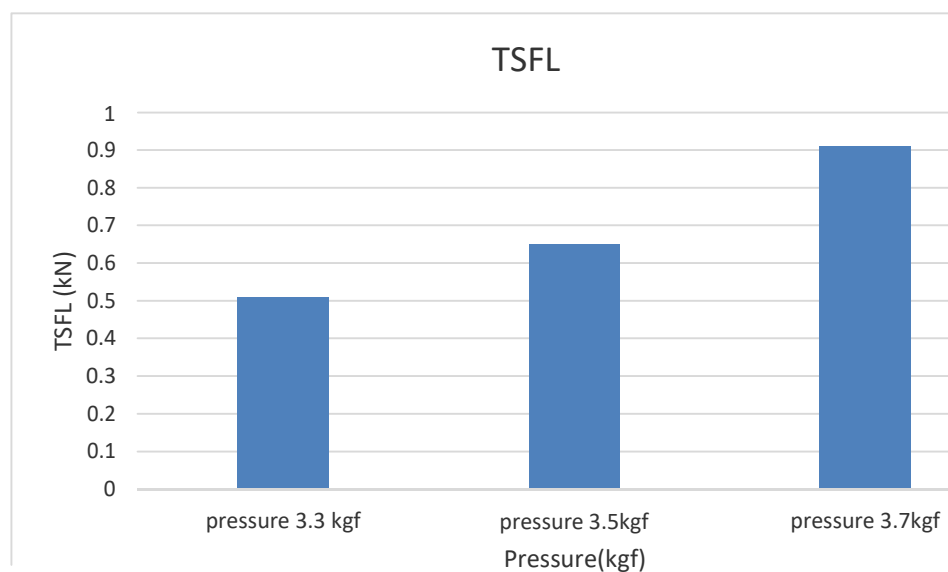


Figure 7.11 TSFL test results for the samples welded at three different weld pressure conditions for AISI1020 Similar joints.

From the Figure 7.11, it is noted that the maximum ultimate tensile strength was obtained for the sample welded at pressure 3.7kgf.

The results obtained from the TSFL and microhardness tests were given in Table 7.4.

Table 7.4 Results obtained from TSFL and microhardness tests for AISI1020 similar joints

Sample no	Weld Parameters			TSFL (kN)	Micro Hardness (VHN)
	Power (W)	Time (sec)	Pressure (kgf)		
AISI1020– AISI1020 -1	15	10	3.3	0.51	191.5
AISI1020 – AISI1020 -2	15	10	3.5	0.65	208.8
AISI1020 – AISI1020 -3	15	10	3.7	0.91	267.5

From the Table 7.4, it is clearly identified that increase in weld pressure increases the TSFL strength.

Similarly, the microhardness samples were prepared from the ERSW joints welded at three different weld pressure and it was etched by sodium hydroxide solution as shown in Figure 7.12 (a).

The hardness test was conducted using a Vickers microhardness tester for a load of 1 kg. The results obtained from the test are shown in Figure 7.12 (b).



Figure 7.12(a) Photographic view of microhardness samples of AISI1020 similar joints

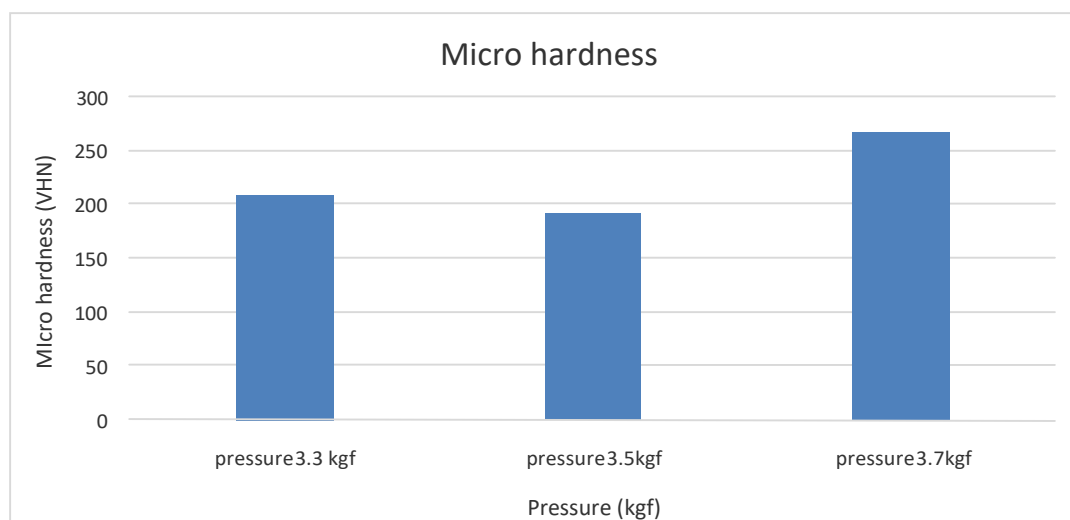


Figure 7.12(b) Microhardness test result for the samples welded at various weld pressures

From the Figure 7.12(b) it is identified that maximum hardness values were obtained for the sample welded at the maximum weld pressure of 3.7kgf. Therefore, it was observed that the hardness values are directly proportional to the weld pressure as tabulated in Table 7.6.

Analysis of Metallurgical results

The macro, micro, SEM, EDAX and factography analysis test was carried out on the AISI1020- AISI1020 joints and the results are discussed in the section below.

Macro, Microstructural study, and nugget dimension study

The macro and microstructural examinations were carried out on AISI1020- AISI1020 joints welded at different weld pressure 3.3 kgf, 3.5 kgf and 3.7kgf and their corresponding images are shown in Figure 7.13(a) to (f).

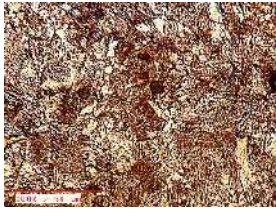





Pressure (kN)	Micro Image	Macro Image	Nugget Diameter (mm)
3.3	 (a)	 (b)	4.0
3.5	 (c)	 (d)	4.5
3.7	 (e)	 (f)	5.1

Figure 7.13 (a) to (f) shows the Macro-micro image and Nugget diameter of the AISI1020 similar joints welded at various weld pressure

The macrostructural images show that the sample welded at the weld pressure 3.7kgf is having defect free nugget and no holes were identified. Similarly, while comparing the nugget zone macro structures it is identified that the sample welded at pressure 3.3kgf possess small holes, which clearly reveals that the sample welded at the weld pressure 3.7kgf weld pressure is better as shown in figure 7.13 (b), 7.13 (d) & 7.13(f). The same result was proved in the TSFL, hardness and nugget diameter examinations.

The microstructural study shows that the sample welded at a pressure of 3.7kgf is having very fine grains when compared with the samples welded at the pressure at 3.3kgf and 3.5 kgf as shown in Figure 7.13 (a, c & e). The microstructural images show the occurrence of course austenite and ferrite mode. In addition to that, the presence of high chromium content in AISI1020 promotes more ferrite content. The presence of dendritic ferrite on the nugget zone was also identified and this dendrite ferrite was almost normal to weld interface as presented in the above Figure 7.13(a, c& e).

The nugget diameter was measured using a video measurement system (VMS) 2010F and the measured values of the nugget diameter of the samples welded at three different weld pressure are tabulated in Figure 7.13. From the nugget diameter values, it is identified that the maximum nugget diameter was obtained for the sample welded at maximum weld pressure of 3.7kgf.

SEM & EDAX analysis

The SEM and EDAX tests were carried using Scanning Electron Microscope on the sample welded at the maximum weld pressure at 3.7kgf and its corresponding SEM images and EDS plot are shown are shown in Figure 7.14 (a) and (b) respectively.

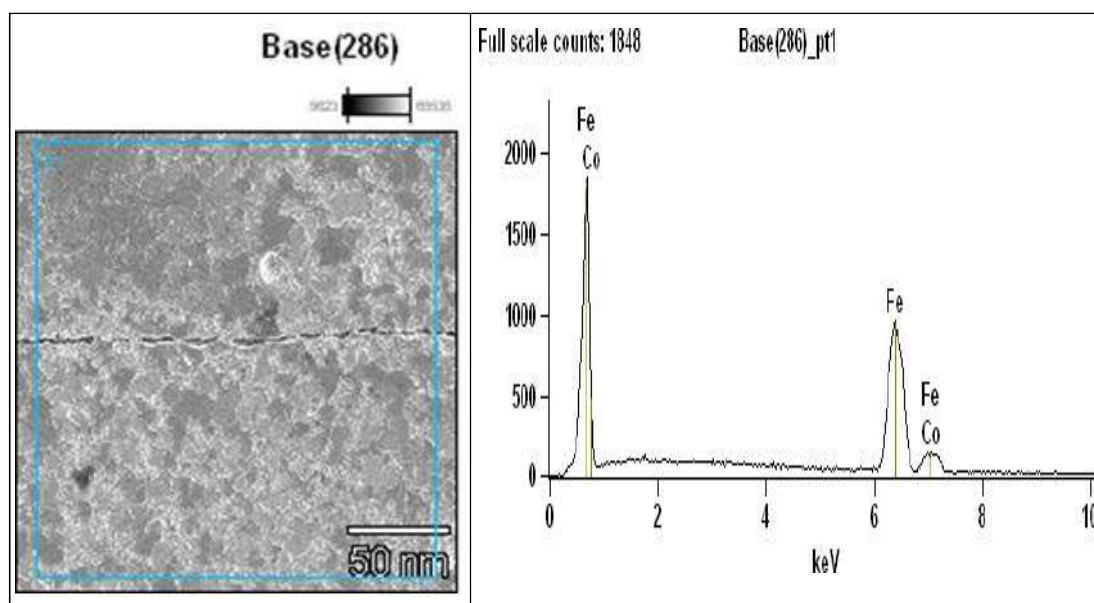


Figure 7.14 (a) SEM image of the sample welded at the weld pressure of 3.7kgf (b) EDS plot of the sample welded at weld pressure 3.7kgf

From the Figure 7.14 (a) and (b) it is identified that the no elemental changes occur in the samples and the elemental table shows the presence of chromium and Magnesium at a high percentage in the plot. The elements present in the sample welded at maximum weld pressure of 3.7kgf are given in Table 7.5.

Table 7.5 Weight percentage of elements on the sample welded at 3.7kgf

				<i>Fe</i>	<i>Co</i>
<i>Base(286)_pt1</i>				92.20	7.80

Factography test

The fracture surface of the TSFL sample welded at the maximum weld pressure of 3.7kgf was analyzed using SEM to reveal the fracture surface morphology and the fracture surface image was shown in Figure 7.15. From the figure 7.15, it is identified that the grains are elongated and possess a lot of crest and trough-like appearance. Which clearly indicates the ductile mode of failure.

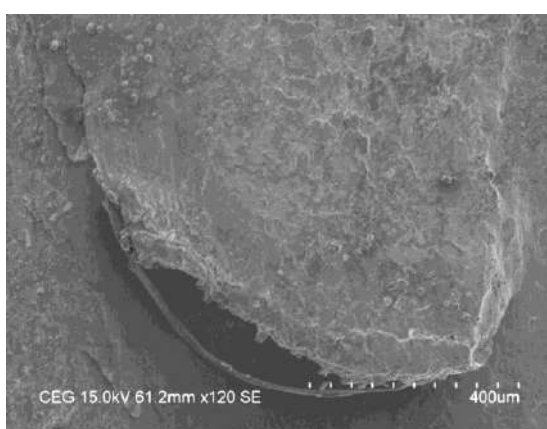


Figure 7.15 Factography images of the TSFL tested sample welded at weld pressure 3.7kgf.

Analysis of corrosion results

The corrosion test was carried out based on the potentiodynamic polarization method for the sample welded at the maximum weld pressure of 3.7kgf. and their corresponding TAFEL data model was listed in table 7.6. The obtained TAFEL plot for AISI1020 similar joints welded at 3.7 kgf as shown in figure 7.16. From the table 7.6 & figure 7.16, it is identified that the maximum corrosion rate is found to be about 3.032mm/Year.

Table 7.6 TAFEL Data Model Data for AISI1020 similar joint welded at the weld pressure 3.7kgf

Tafel data model for AISI1020-AISI1020 for 3.7kgf weld pressure	
E. Corr V	-0.7135
I Cor. A	5.64E-06
I Cor. A/cm ²	0.000352
Rp ohm	4091
ba V/dec	0.069
bc V/dec	0.227
C. Rate mm/y	3.032

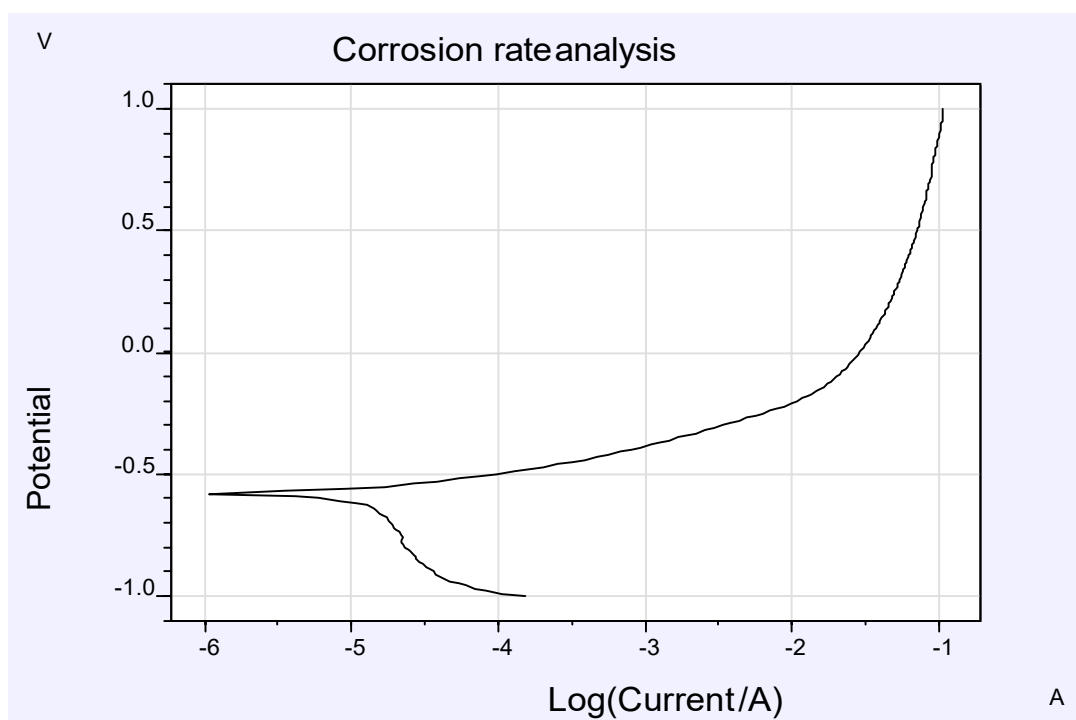


Figure 7.16 TAFEL plot for AISI1020 for welded at 3.7Kgf weld pressure

**OPTIMIZATION OF ERSW PROCESS PARAMETERS FOR
AIS5052(SS)-AISI1020(MS), AISI1020(MS)- AA1008(AI)
AND AIS5052(SS)-AA1008(AI) DISSIMILAR JOINTS
USING RSM**

Based on the feasibility study conducted the main operational parameters and their levels were selected. In this work, three input process parameters at three levels (i.e.) weld power, weld time and weld pressure are considered. In the RSM model the CCRD design was selected for this analysis. The interaction effect between the various weld input process parameter on mechanical properties and nugget diameter was validated with the developed model. In this work, the optimization process was carried out on AIS5052(SS)-AISI1020(MS), AISI1020(MS)-AA1008(AI) and AIS5052(SS)-AA1008(AI) dissimilar joints and the obtained results were discussed in the section below.

RSM Results for AIS5052-AISI1020 Dissimilar Joints

The RSM model was created based on CCRD model by considering three important process parameter with three levels (i.e.) power(55 to 65 W), pressure (3.4 to 3.8 kgf) and time (1.5 to 2.5 seconds) was considered for welding of AIS5052(SS)-AISI1020(MS) dissimilar joints. The various process parameters and their levels selected for the present study were listed in Table 7.7.

Table 7.7 Process Parameters and their levels for AIS5052(SS)-AISI1020(MS) dissimilar joints

Parameters	Unit	Symbol	Levels		
			Low (-1)	Medium (0)	High (+1)
POWER	(W)	A	55	60	65
PRESSURE	(kgf)	B	3.4	3.6	3.8

TIME	(second)	C	1.5	2	2.5
------	-----------------	---	-----	---	-----

Based on Table 7.7, the mathematical model was developed for optimizing the weld process parameters by taking power (55-65W), Pressure (3.3 to 3.8kgf) and time (1.5 to 2.5sec) as input parameters as stated in various literature and trail experiments conducted. The 17 experimental runs were performed in a randomized order based on CCRD design matrix as given in table7.17.1. The TSFL and hardness samples were prepared as shown in figure 7.16.1 (a) and (b) respectively.

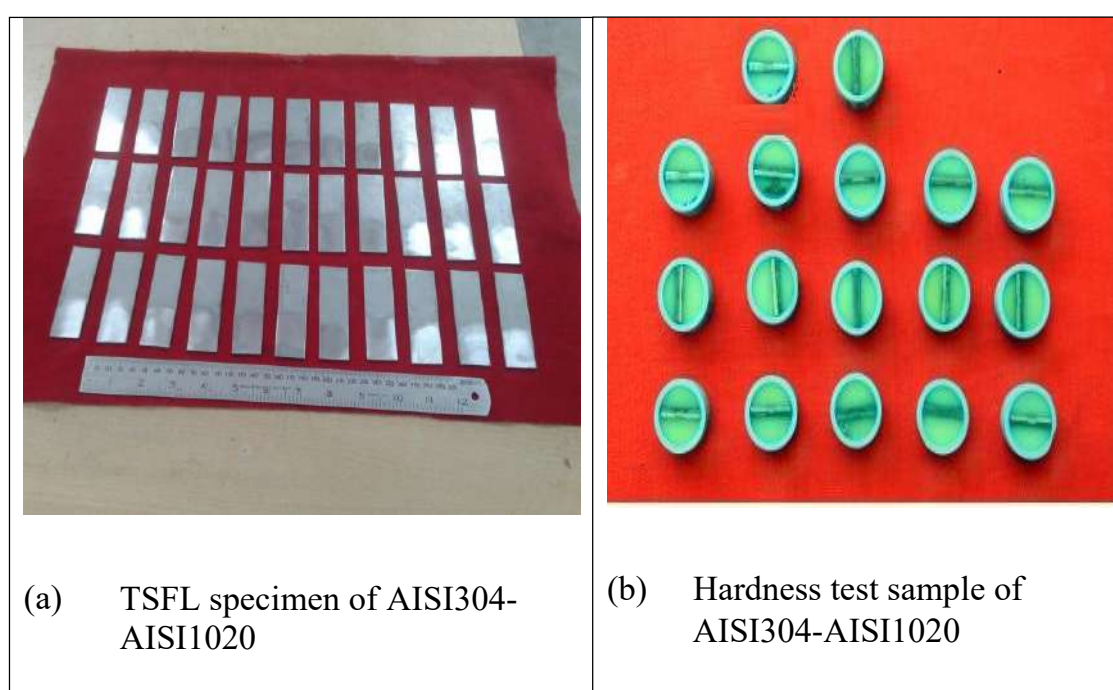


Figure 7.16.1 (a) and (b) TSFL specimen of AIS5052-AISI1020 and Hardness test sample of AIS5052-AISI1020

The tested TSFL sample, hardness sample and nugget images were shown in Figure 7.17(a) to 7.17(o).
















TSFL (KN)	Cross-sectional macrostructure	Nugget (mm)	Top view of the top sheet	Bottom view of the top sheet	Top view of the bottom sheet
High (9.8)					
	(a)	(d)	(g)	(j)	(m)
Medium (7.3)					
	(b)	(e)	(h)	(k)	(n)
Low (5)					
	(c)	(f)	(i)	(l)	(o)

Figure 7.17(a) to (o) Cross-Sectional Macrostructure and Nugget images of the TSFL samples

The welded AIS5052-AISI1020 dissimilar joint possess high, medium and low TSFL values were analyzed using macrostructural and nugget images as shown in Figure 7.17(a) to (o). from the figure it is identified that the depth of penetration of the sample possess high TSFL joint

is higher when compared to medium and low TSFL samples as shown in Figure 7.17 (a) to (c) similarly, the nugget diameter of the sample possess high TSFL strength is higher when compared to other TSFL samples.

Table 7.17.1 L17 (3³) Orthogonal array used in design experiments with three parameters at three levels for AIS5052-AISI1020

Std	Run	Coded values			Actual values		
		A:Power	B:Pressure	C:Time	A:Power	B:Pressure	C:Time
		W	kgf	S	W	kgf	S
2	1	1	-1	0	65	3.4	2
11	2	0	-1	1	60	3.4	2.5
3	3	-1	1	0	55	3.8	2
6	4	1	0	-1	65	3.6	1.5
14	5	0	0	0	60	3.6	2
4	6	1	1	0	65	3.8	2
16	7	0	0	0	60	3.6	2
5	8	-1	0	-1	55	3.6	1.5
1	9	-1	-1	0	55	3.4	2
12	10	0	1	1	60	3.8	2.5
15	11	0	0	0	60	3.6	2
13	12	0	0	0	60	3.6	2
9	13	0	-1	-1	60	3.4	1.5
7	14	-1	0	1	55	3.6	2.5
8	15	1	0	1	65	3.6	2.5
10	16	0	1	-1	60	3.8	1.5
17	17	0	0	0	60	3.6	2

The TSFL, microhardness and nugget diameter values are tabulated in Table 7.17.2.

Table 7.17.2 TSFL, micro Hardness and Nugget diameter values of AIS5052-AISI1020 dissimilar joints

		Factor 1	Factor 2	Factor 3	Response 1	Response 2	Response 3
Std	Run	A: Power	B: Pressure	C: Time	Hardness	Nugget Diameter	TSFL
		W	kgf	S	VHN	mm	kN
2	1	65	3.4	2	490	5.652	9.2
11	2	60	3.4	2.5	423	5.012	7.9
3	3	55	3.8	2	421	4.662	7.3
6	4	65	3.6	1.5	509	5.897	9.5
14	5	60	3.6	2	320	6.39	9.3
4	6	65	3.8	2	546	6.45	9.8
16	7	60	3.6	2	320	6.39	9.3
5	8	55	3.6	1.5	359	4.604	5.8
1	9	55	3.4	2	335	4.876	5
12	10	60	3.8	2.5	530	5.431	9
15	11	60	3.6	2	320	6.39	9.3
13	12	60	3.6	2	320	6.39	9.3
9	13	60	3.4	1.5	420	5.015	7.2
7	14	55	3.6	2.5	369	4.612	6.5
8	15	65	3.6	2.5	530	5.924	9.5
10	16	60	3.8	1.5	504	4.949	9.2
17	17	60	3.6	2	320	6.39	9.3

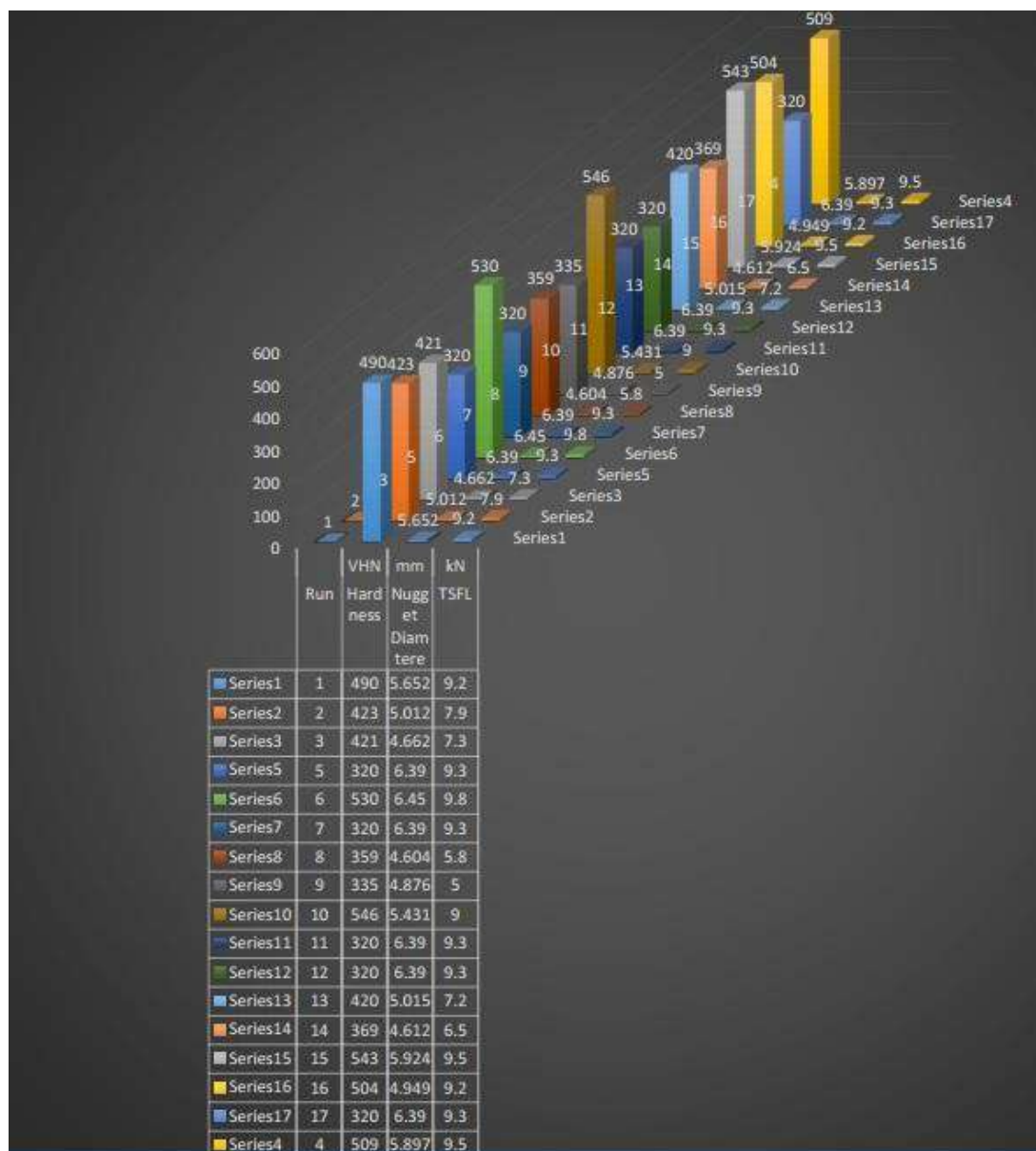


Figure 7.17.1 The TSFL, microhardness and nugget diameter values of AIS5052 and AISI1020

The Table7.17.2 and Figure 7.17.1 both clearly show the TSFL 9.8kN, Microhardness 543 VHN and nugget diameter 6.45 at the maximum weld the pressure of 3.7kgf.

Optimizing weld input process parameter for TSFL strength

To obtain the influencing ERS welding process parameter for TSFL strength. The interaction effects plots were obtained. The interaction effect results obtained from DOE software for the 3D response, 2D contour effects of the input process parameters such as pressure, power, time on the nugget diameter, TSFL, hardness are given in Figure 7.18 (a) to 7.18 (f). The Figure 7.18 (a) to (e) shows the interaction effects between power versus pressure, power versus time and pressure versus time.

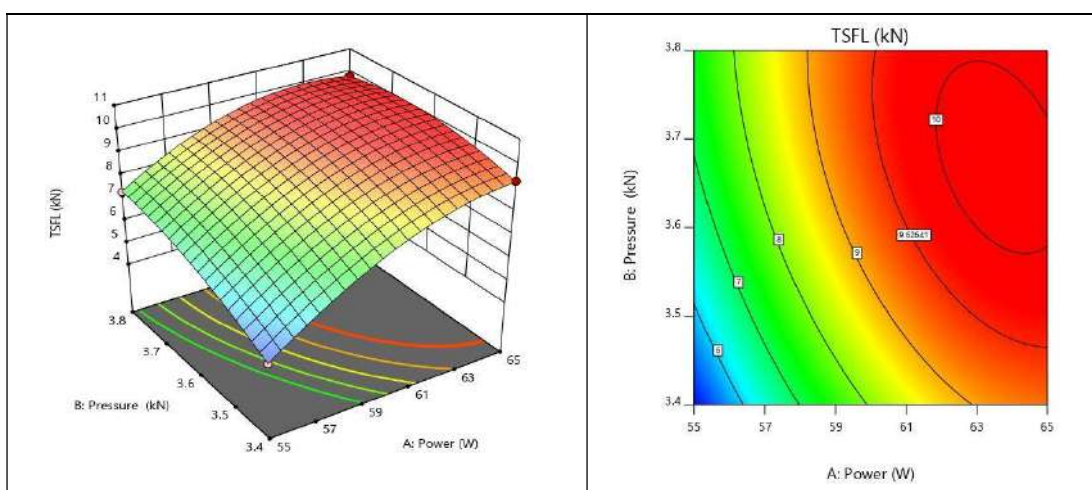


Figure 7.18 (a)

Figure 7.18 (b)

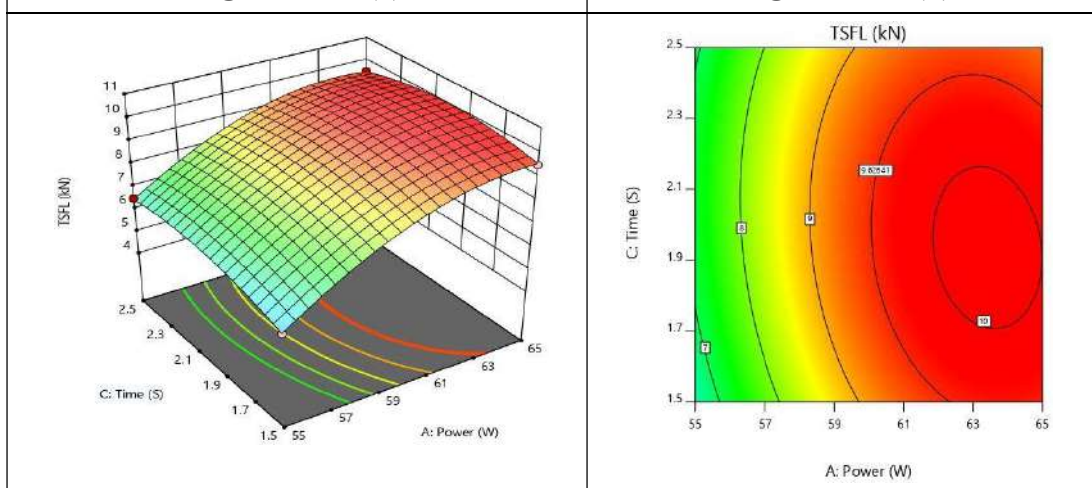


Figure 7.18 (c)

Figure 7.18 (d)

Figure 7.18 (Continued)

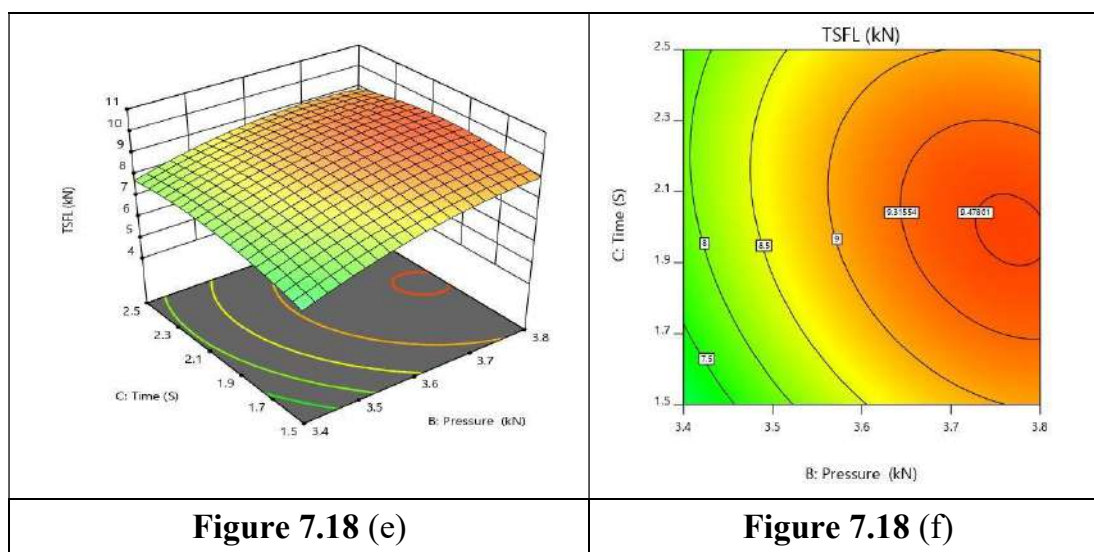


Figure 7.18 (a) to (f) Various interaction plots 3D (a, c, e) and 2D (b, d, f) plots for TSFL.

Interaction effect on ERSW weld input process parameters for TSFL strength

The interaction effect was achieved by the design of expert software for both the 2D and 3D responses of input process parameters such as pressure, time and power on TSFL are shown in Figures 7.18 (a) to (7.18 f).

The Figure 7.18 (a) shows the 3D surface plot which indicates all the points are within the plot. Similarly, 7.18 (b) indicates the 2D contour plot between power versus pressure. The plotted results show blue colored value is lesser and green colored values are average and red colored value is higher which indicates that the TSFL decreases with the increase in power. The TSFL is high at power 65w. It has good agreement with various works discussed literature reviews.

The Figure 7.18 (c) shows the 3D surface plot where indicates all the points are within the plot. Similarly, 7.18 (d) indicates the 2D contour plot between power versus Time. The plotted results show blue colored value is lesser and green colored values are average and red colored value is higher, which indicates that the TSFL decreases with the increase in power. The TSFL is high at higher at the power of 65w. It has good agreement with various literary works reviews.

The Figure 7.18 (e) is 3D surface plot indicates all the points are within the plot. Similarly, 7.18 (f) indicates the 2D contour plot between pressure versus time. The plotted results show blue colored value is lesser and green colored values are average and red colored value is higher and the TSFL decreases with the pressure. The TSFL is high at pressure 3.8kgf. it has good agreement with various literature reviews.

Optimizing weld input process parameter for microhardness

To obtain the influencing ERS welding process parameter for Microhardness strength. The interaction effects plots were obtained. The interaction effect results obtained from DOE software for the 3D response, 2D contour effects of the input process parameters such as pressure, power, time on the hardness are given in Figure 7.19 (a) to 7.19 (f). The Figure 7.19 (a) to 7.19 (f) shows the interaction effects between power versus pressure, power versus time and pressure versus time.

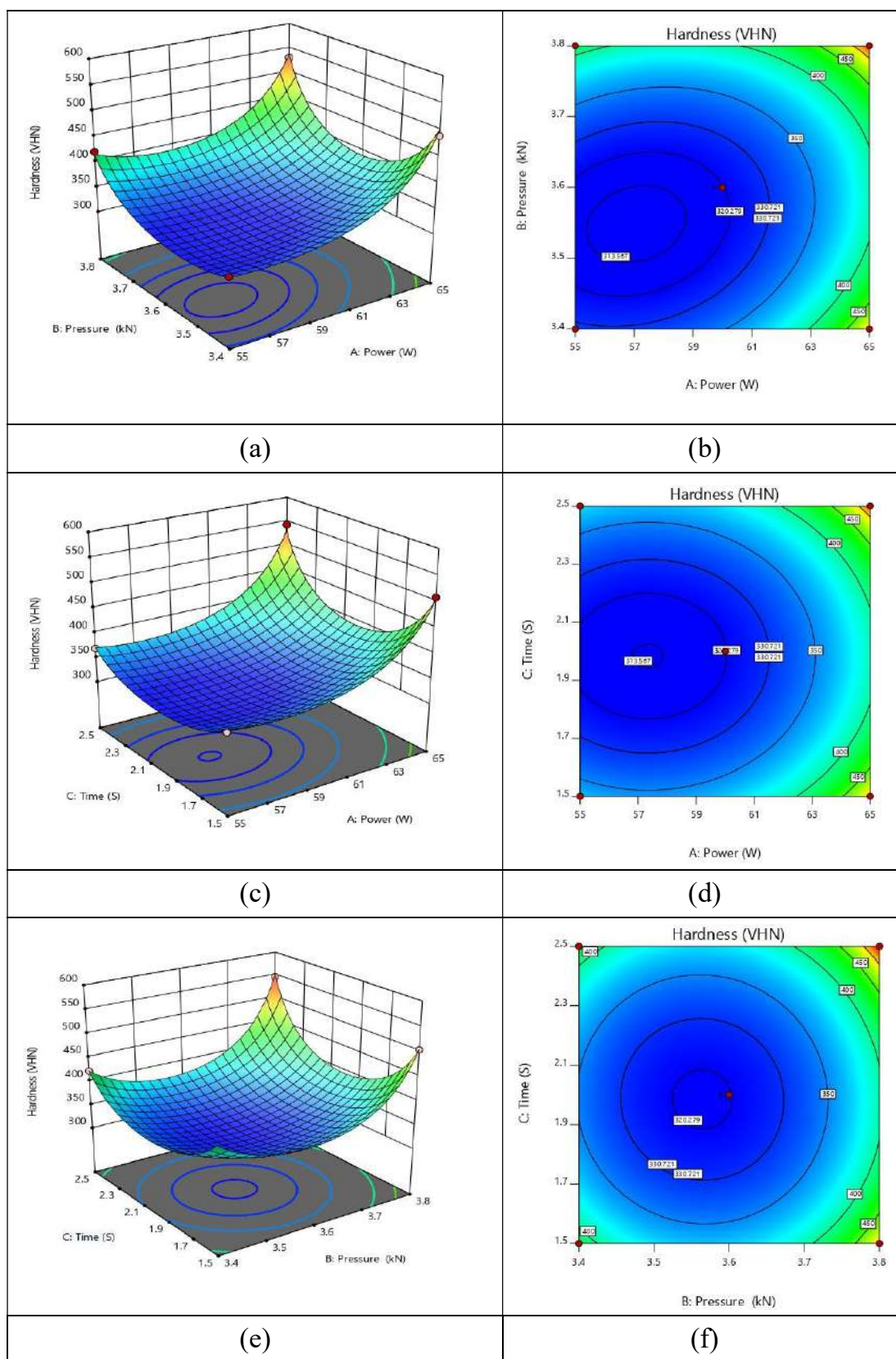


Figure 7.19 (a) to (e) Various interaction plots for hardness, figure (a,c,e) shows 3D plots and figures (b,d,f) shows the 2D plots.

Interaction effect weld input process parameter for microhardness

The interaction effect was achieved by the design of expert software for both the 2D and 3D responses of input process parameters are pressure, time and power on hardness are listed in Figures 7.19 (a) to (7.19 f).

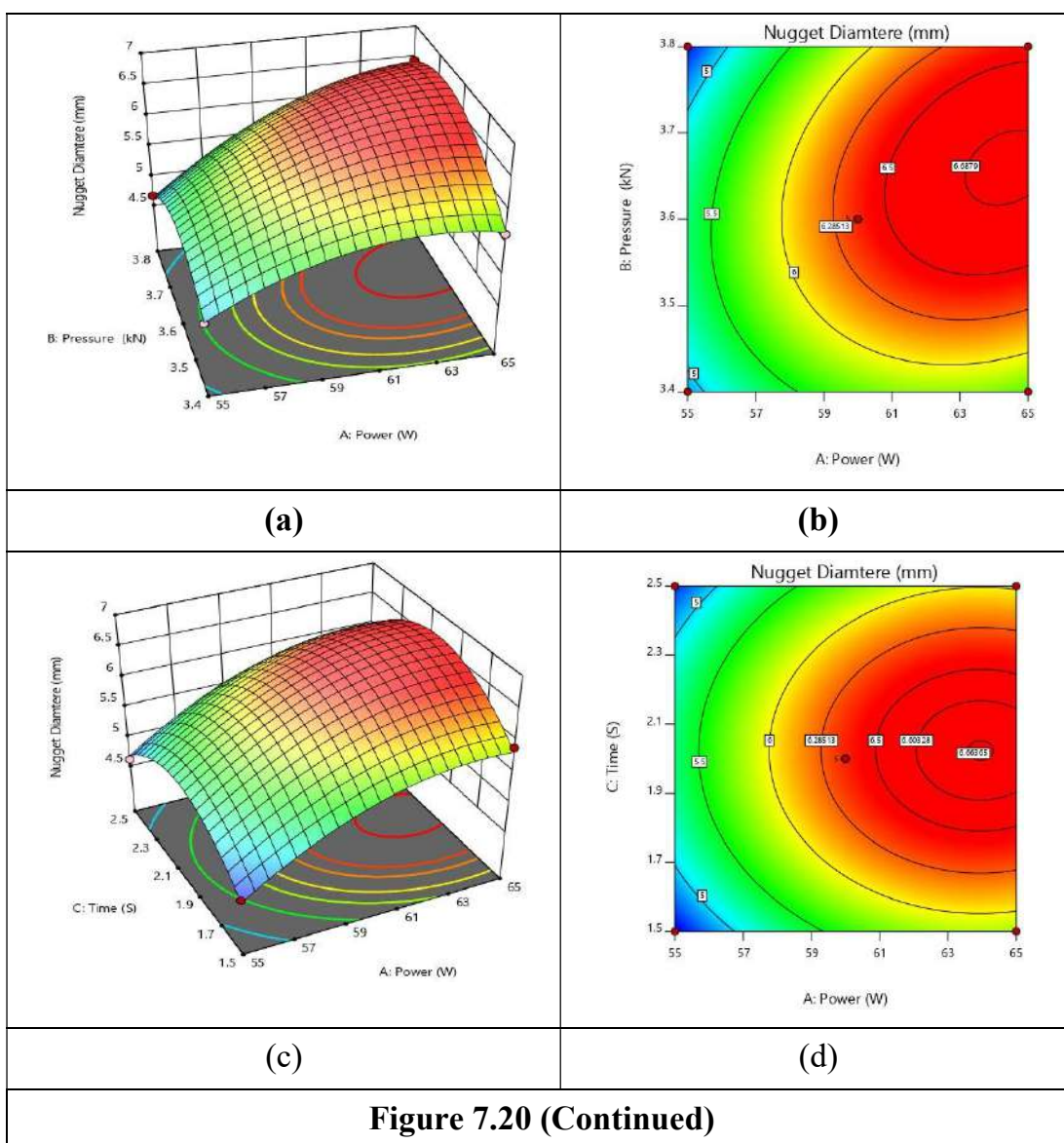
The Figure 7.19 (a) to (7.19 f). shows 3d and 2D responses of hardness. The Figure 7.19 (a) is 3D surface plot indicates all the points are within the plot. Similarly, 7.19 (b) indicates the 2D contour plot between power versus pressure. The plotted results show blue colored value is lesser and green colored values are average and red colored value is higher and the hardness decreases with the power. The hardness is high at power 65w. it has good agreement with various literature reviews.

The Figure 7.19 (c) is 3D surface plot indicates all the points are within the plot. Similarly, 7.19 (d) indicates the 2D contour plot between power versus Time. The plotted results show blue colored value is lesser and green colored values are average and red colored value is higher and the hardness decreases with the power. The hardness is high at power 65w. it has good agreement with various literature reviews.

The Figure 7.19 (e) is 3D surface plot indicates all the points are within the plot. Similarly, 7.19 (f) indicates the 2D contour plot between pressure versus time. The plotted results show blue colored value is lesser and green colored values are average and red colored value is higher and the hardness decreases with the pressure. The hardness is high at pressure 65w. it has good agreement with various literature reviews.

Optimizing weld input process parameter for nugget diameter

To obtain the influencing ERS welding process parameter for nugget diameter. The interaction effects plots were obtained. The interaction effect results obtained from DOE software for the 3D response, 2D contour effects of the input process parameters such as pressure, power, time on the nugget diameter, TSFL, hardness are given in Figure 7.20(a) to 7.20(f). The Figure 7.20(a) to 7.20(f) shows the interaction effects between power versus pressure, power versus time and pressure versus time.



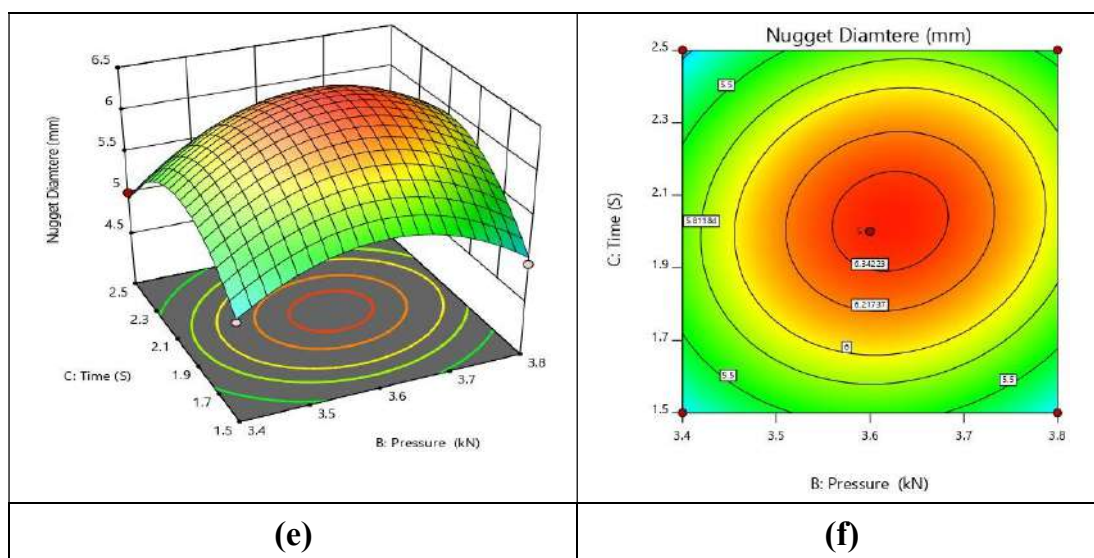


Figure 7.20 (a) to (f) Various interaction plots for nugget diameter. figure (a,c,e) shows 3D plots and figures (b,d,f) shows the 2D plots.

Interaction effect weld input process parameter for nugget diameter

The interaction effect was achieved by the design of expert software for both the 2D and 3D responses of input process parameters are pressure, time and power on Nugget diameter are listed in Figures 7.20 (a) to (7.20 f).

The Figure 7.20 (a) to (7.20 f). shows 3d and 2D responses of Nugget diameter. The Figure 7.20 (a) is 3D surface plot indicates all the points are within the plot. Similarly, 7.20 (b) indicates the 2D contour plot between power versus pressure. The plotted results show blue colored value is lesser and green colored values are average and red colored value is higher and the Nugget diameter decreases with the power. The Nugget diameter is high at power 65w. It has good agreement with various literature reviews.

The Figure 7.20 (c) is 3D surface plot indicates all the points are within the plot. Similarly, 7.20 (d) indicates the 2D contour plot between power versus Time. The plotted results show blue colored value is lesser and green colored values are average and red colored value is higher and the Nugget diameter decreases with the power. The Nugget diameter is high at power 65w. it has good agreement with various literature reviews.

The Figure 7.20 (e) is 3D surface plot indicates all the points are within the plot. Similarly, 7.20 (f) indicates the 2D contour plot between pressure versus time. The plotted results show blue colored value is lesser and green colored values are average and red colored value is higher and the Nugget diameter decreases with the pressure. The Nugget diameter is high at pressure 65w. It has good agreement with various literature reviews.

RSM Results for AISI1020-AA1008 Dissimilar Joints

The RSM model was created based on CCRD model by considering three important process parameter with three levels (i.e.) power (55 to 65 W), pressure (3.4 to 3.8 kgf) and time (1.5 to 2.5 seconds) was considered for welding of AISI1020-AA1008 dissimilar joints. The various process parameters and their levels selected for the present study were listed in Table 7.7.

Based on Table 7.7, the mathematical model was developed for optimizing the weld process parameters by taking power (55-65W), Pressure (3.3 to 3.8kgf) and time (1.5 to 2.5sec) as input parameters as stated in various literature and trail experiments conducted. The 17 experimental runs were performed in a randomized order based on CCRD design matrix as given in table7.17.3. The TSFL and hardness samples were prepared as shown in figure 7.20.1 (a) and (b) respectively.



Figure 7.20.1 (a) and (b) TSFL specimen of AISI1020-AA1008 and Hardness test sample of AISI1020-AA1008

The tested TSFL sample, hardness sample and nugget images were shown in Figure 7.20.2 (a) to 7.20.2(o).

The welded AISI1020-AA1008 dissimilar joint possess high, medium and low TSFL values were analyzed using macrostructural and nugget images as shown in Figure 7.20.2(a) to (o). from the figure it is identified that the depth of penetration of the sample possess high TSFL joint is higher when compared to medium and low TSFL samples as shown in Figure 7.20.2 (a) to (c). similarly, the nugget diameter of the sample possesses high TSFL strength is higher when compared to other TSFL samples.






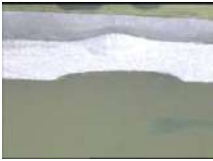









TSFL (KN)	Cross-sectional macrostructure	Nugget (mm)	Top view of the top sheet	Bottom view of the top sheet	Top view of the bottom sheet
High (2.615)					
	(a)	(d)	(g)	(j)	(m)
Medium (1.489)					
	(b)	(e)	(h)	(k)	(n)
Low (0.555)					
	(c)	(f)	(i)	(l)	(o)

Figure 7.20.2(a) to (o) Cross-Sectional Macrostructure and Nugget images of the TSFL samples

Table 7.17.3 L17 (3³) Orthogonal array used to design experiments with three parameters at three levels AISI1020-AA1008

Std	Run	Coded Values			A:Power	B:Pressure	C:time
		A: Power	B: Pressure	C:time			
		W	Kgf	S	W	Kgf	S
1	16	-1	-1	0	55	3.4	2
5	17	-1	0	-1	55	3.6	1.5
7	3	-1	0	1	55	3.6	2.5
3	9	-1	1	0	55	3.8	2
9	4	0	-1	-1	60	3.4	1.5
11	13	0	-1	1	60	3.4	2.5
15	1	0	0	0	60	3.6	2
17	2	0	0	0	60	3.6	2
16	6	0	0	0	60	3.6	2
14	7	0	0	0	60	3.6	2
13	14	0	0	0	60	3.6	2
10	12	0	1	-1	60	3.8	1.5
12	11	0	1	1	60	3.8	2.5
2	8	1	-1	0	65	3.4	2
6	5	1	0	-1	65	3.6	1.5
8	10	1	0	1	65	3.6	2.5
4	15	1	1	0	65	3.8	2

Table 7.17.4 TSFL, micro Hardness and Nugget diameter values of AISI1020-AA1008 dissimilar joints

		Factor 1	Factor 2	Factor 3	Response 1	Response 2	Response 3
Std	Run	A: Power	B: Pressure	C:time	Hardness	Nugget Diameter	TSFL
		W	Kgf	S	VHN	mm	kN
1	16	55	3.4	2	104.8	4.945	0.555
5	17	55	3.6	1.5	112	4.644	0.814
7	3	55	3.6	2.5	118	4.712	0.708
3	9	55	3.8	2	121.3	4.722	1.489
9	4	60	3.4	1.5	124	5.128	1.218
11	13	60	3.4	2.5	122	5.109	1.411
15	1	60	3.6	2	95	6.889	2.615
17	2	60	3.6	2	95	6.889	2.615
16	6	60	3.6	2	95	6.889	2.615
14	7	60	3.6	2	95	6.889	2.615
13	14	60	3.6	2	95	6.889	2.615
10	12	60	3.8	1.5	134	4.822	2.173
12	11	60	3.8	2.5	159.4	5.568	2.145
2	8	65	3.4	2	152	5.654	2.221
6	5	65	3.6	1.5	137.8	5.944	2.324
8	10	65	3.6	2.5	178	5.934	2.334
4	15	65	3.8	2	154	6.459	2.378

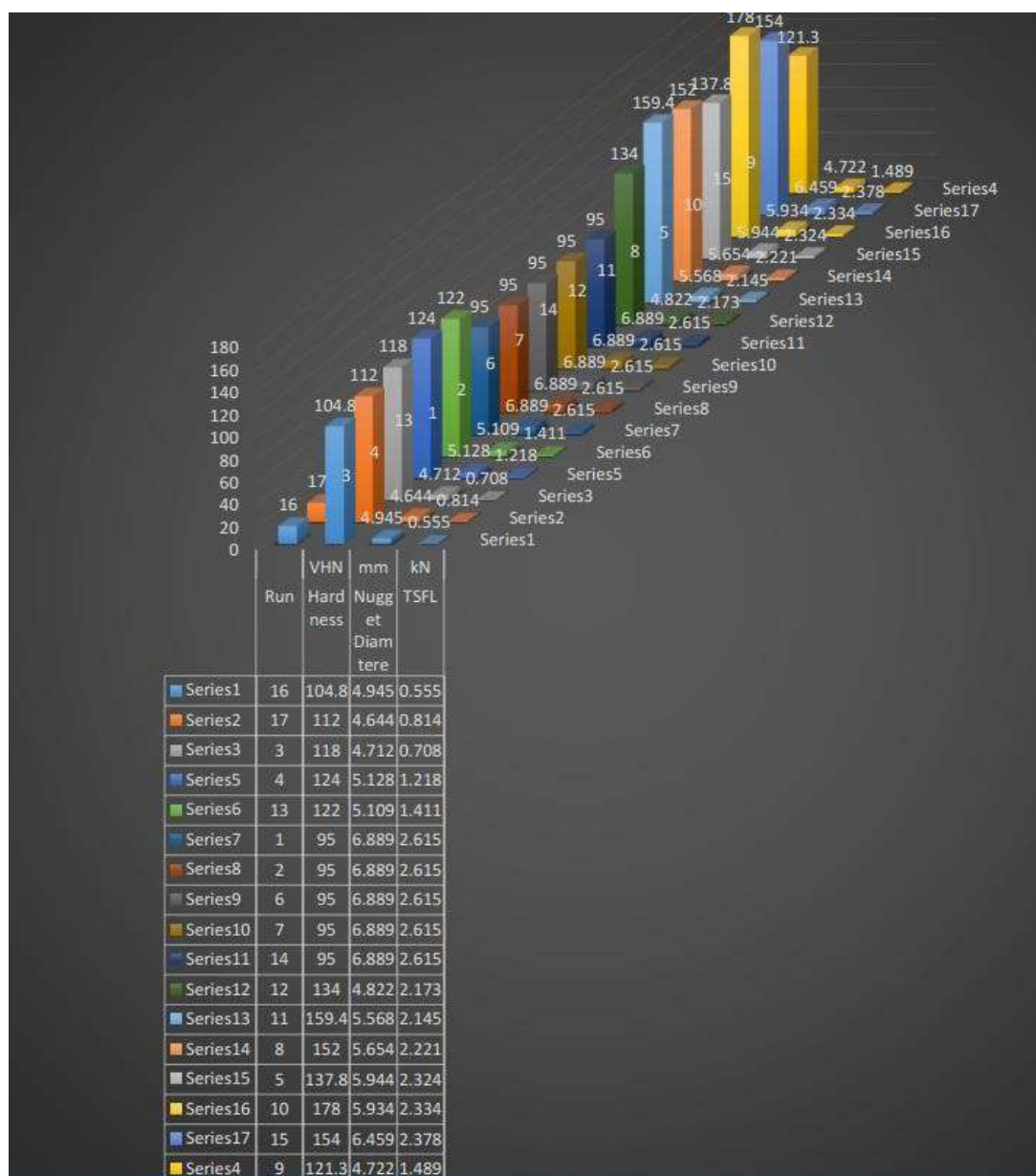


Figure 7.20.3 The TSFL, microhardness and nugget diameter values of AISI1020-AA1008

The Table 7.20.1.1 and Figure 7.20.3 both clearly show the TSFL 2.615kN, Microhardness 159.4 VHN and nugget diameter 6.889mm at the maximum weld pressure of 3.7kgf.

Optimizing weld input process parameter for TSFL strength

To obtain the influencing ERS welding process parameter for TSFL strength. The interaction effects plots were obtained. The interaction effect results obtained from DOE software for the 3D response, 2D contour effects of the input process parameters such as pressure, power, time on the nugget diameter, TSFL, hardness are given in Figure 7.21(a) to (f). The Figure 7.21 (a) to (e) shows the interaction effects between power versus pressure, power versus time and pressure versus time.

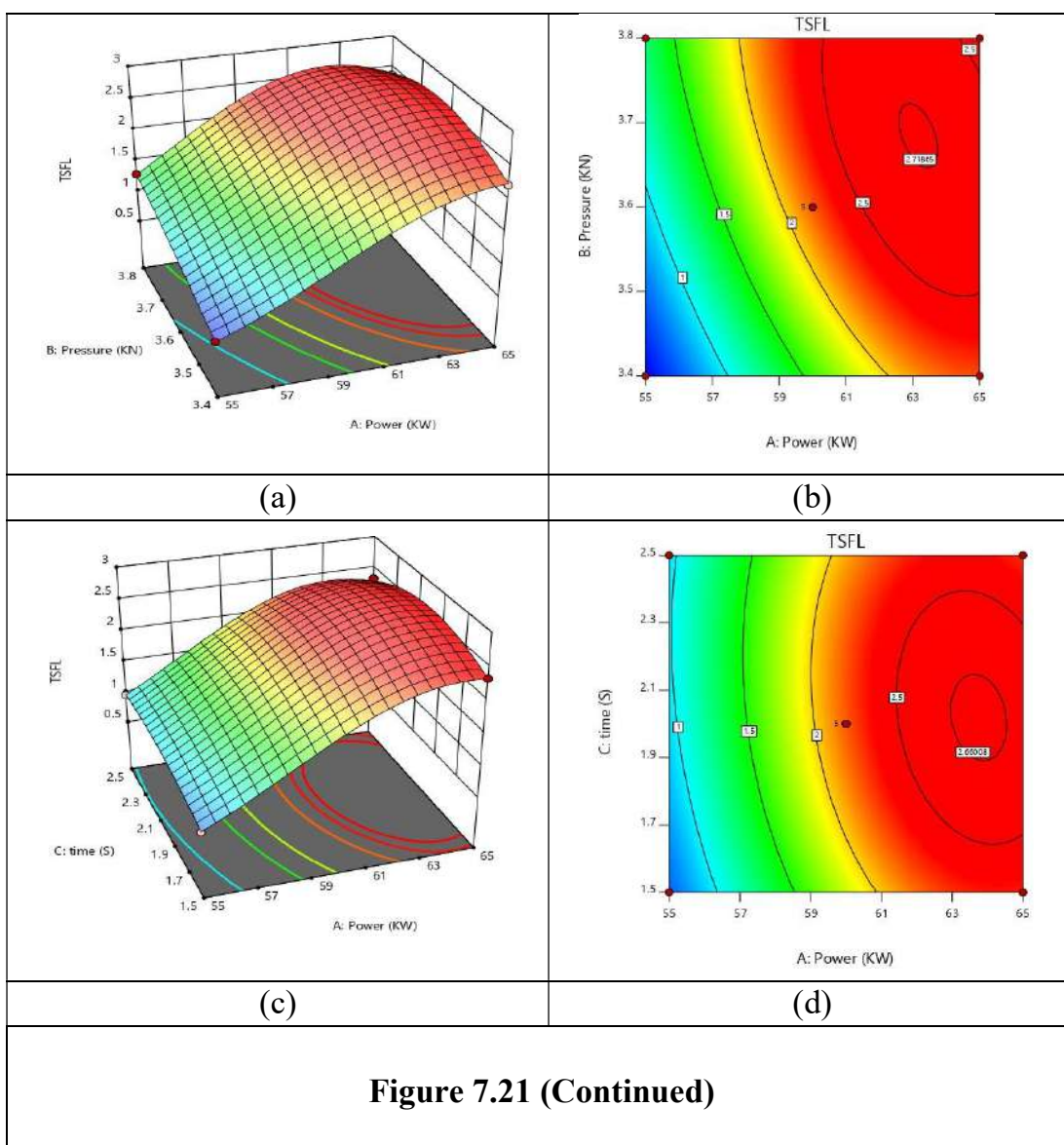


Figure 7.21 (Continued)

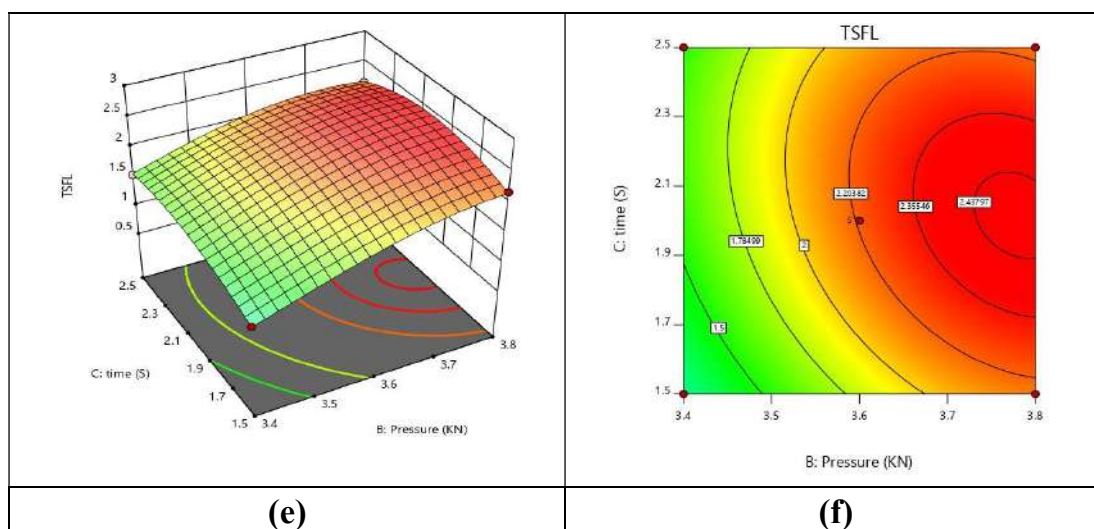


Figure 7.21 (a) to (f) Various interaction 3D (a,c,e) and 2D (b,d,f) plots for TSFL.

Interaction effect on ERSW weld input process parameters for TSFL strength

The interaction effect was achieved by the design of expert software for both the 2D and 3D responses of input process parameters are pressure, time and power on TSFL are listed in Figures 7.21 (a) to (7.21 f).

The Figure 7.21 (a) to (7.21 f). shows 3d and 2D responses of TSFL. The Figure 7.21 (a) is 3D surface plot indicates all the points are within the plot. Similarly, 7.21 (b) indicates the 2D contour plot between power versus pressure. The plotted results show blue colored value is lesser and green colored values are average and red colored value is higher and the TSFL decreases with the power. The TSFL is high at power 65w. It has good agreement with various literature reviews.

The Figure 7.21 (c) is 3D surface plot indicates all the points are within the plot. Similarly, 7.21 (d) indicates the 2D contour plot between power versus Time. The plotted results show blue colored value is lesser and green colored values are average and red colored value is higher and the TSFL decreases with the power. The TSFL is high at power 65w. It has good agreement with various literature reviews.

The Figure 7.21 (e) is 3D surface plot indicates all the points are within the plot. Similarly, 7.21 (f) indicates the 2D contour plot between pressure versus time. The plotted results show blue colored value is lesser and green colored values are average and red colored value is higher and the TSFL decreases with the pressure. The TSFL is high at pressure 65w. it has good agreement with various literature reviews.

Optimizing weld input process parameter for microhardness

To obtain the influencing ERS welding process parameter for Microhardness strength. The interaction effects plots were obtained. The interaction effect results obtained from DOE software for the 3D response, 2D contour effects of the input process parameters such as pressure, power, time on the hardness are given in Figure 7.22 (a) to 7.22 (f). The Figure 7.22 (a) to 7.22 (f) shows the interaction effects between power versus pressure, power versus time and pressure versus time.

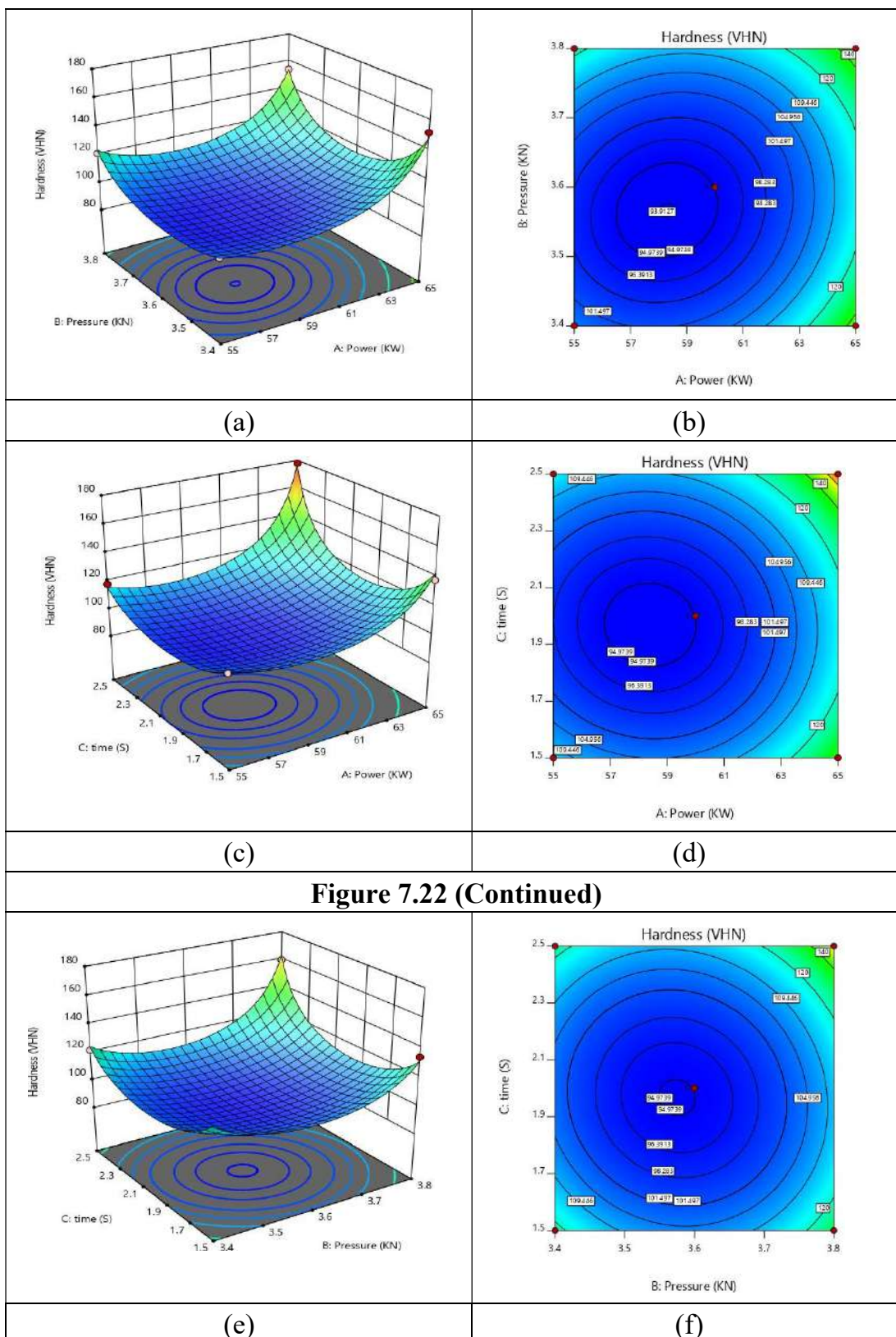


Figure 7.22 (a) to (e) Various interaction plots for hardness, figure (a,c,e) shows 3D plots and figures (b,d,f) shows the 2D plots.

Interaction effect weld input process parameter for microhardness

The interaction effect was achieved by the design of expert software for both the 2D and 3D responses of input process parameters are pressure, time and power on hardness are listed in Figures 7.22 (a) to (7.22 f).

The Figure 7.22 (a) to (7.22 f). shows 3d and 2D responses of hardness. The Figure 7.22 (a) is 3D surface plot indicates all the points are within the plot. Similarly, 7.22 (b) indicates the 2D contour plot between power versus pressure. The plotted results show blue colored value is lesser and green colored values are average and red colored value is higher and the hardness decreases with the power. The hardness is high at power 65w. it has good agreement with various literature reviews.

The Figure 7.22 (c) is 3D surface plot indicates all the points are within the plot. Similarly, 7.22 (d) indicates the 2D contour plot between power versus Time. The plotted results show blue colored value is lesser and green colored values are average and red colored value is higher and the hardness decreases with the power. The hardness is high at power 65w. it has good agreement with various literature reviews.

The Figure 7.22 (e) is 3D surface plot indicates all the points are within the plot. Similarly, 7.22 (f) indicates the 2D contour plot between pressure versus time. The plotted results show blue colored value is lesser and green colored values are average and red colored value is higher and the hardness decreases with the pressure. The hardness is high at pressure 65w. it has good agreement with various literature reviews.

The Figure 7.22 (c) is 3D surface plot indicates all the points are within the plot. Similarly, 7.22 (d) indicates the 2D contour plot between power versus Time. The plotted results show blue colored value is lesser and green colored values are average and red colored value is higher and the hardness decreases with the power. The hardness is high at power 65w. it has good agreement with various literature reviews.

The Figure 7.22 (e) is 3D surface plot indicates all the points are within the plot. Similarly, 7.22 (f) indicates the 2D contour plot between pressure versus time. The plotted results show blue colored value is lesser and green colored values are average and red colored value is higher and the hardness decreases with the pressure. The hardness is high at pressure 65w. it has good agreement with various literature reviews.

Optimizing weld input process parameter for nugget diameter

To obtain the influencing ERS welding process parameter for nugget diameter. The interaction effects plots were obtained. The interaction effect results obtained from DOE software for the 3D response, 2D contour effects of the input process parameters such as pressure, power, time on the nugget diameter, TSFL, hardness are given in Figure 7.23(a) to 7.23(f). The Figure 7.23(a) to 7.23(f) shows the interaction effects between power versus pressure, power versus time and pressure versus time.

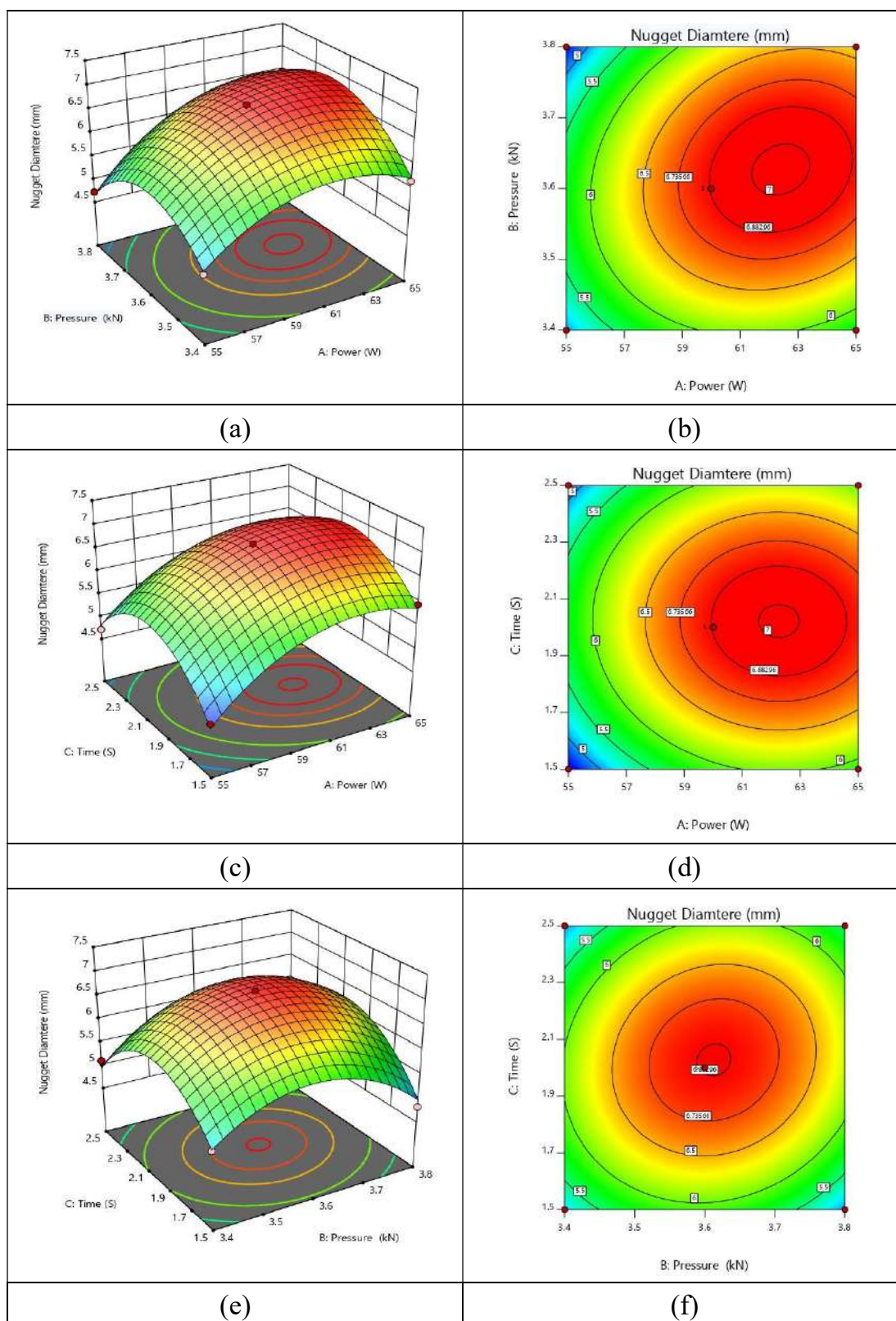


Figure 7.23 (a) to (f) Various interaction plots for nugget diameter. figure (a,c,e) shows 3D plots and figures (b,d,f) shows the 2D plots.

Interaction effect weld input process parameter for Nugget diameter

The interaction effect was achieved by the design of expert software for both the 2D and 3D responses of input process parameters are pressure, time and power on Nugget diameter are listed in Figures 7.23 (a) to (7.23 f).

The Figure 7.23 (a) to (7.23 f). shows 3D and 2D responses of Nugget diameter. The Figure 7.23 (a) is 3D surface plot indicates all the points are within the plot. Similarly, 7.23 (b) indicates the 2D contour plot between power versus pressure. The plotted results show blue colored value is lesser and green colored values are average and red colored value is higher and the Nugget diameter decreases with the power. The Nugget diameter is high at power 65w. It has good agreement with various literature reviews.

The Figure 7.23 (c) is 3D surface plot indicates all the points are within the plot. Similarly, 7.23 (d) indicates the 2D contour plot between power versus Time. The plotted results show blue colored value is lesser and green colored values are average and red colored value is higher and the Nugget diameter decreases with the power. The Nugget diameter is high at power 65w. it has good agreement with various literature reviews.

The Figure 7.23 (e) is 3D surface plot indicates all the points are within the plot. Similarly, 7.23 (f) indicates the 2D contour plot between pressure versus time. The plotted results show blue colored value is lesser and green colored values are average and red colored value is higher and the Nugget diameter decreases with the pressure. The Nugget diameter is high at pressure 65w. It has good agreement with various literature reviews.

RSM Results for AIS5052-AA1008 Dissimilar Joints

The RSM model was created based on CCRD model by considering three important process parameter with three levels (i.e.) power(55 to 65 W), pressure (3.4 to 3.8 kgf) and time (1.5 to 2.5 seconds) was considered for welding of AIS5052-AA1008 dissimilar joints. The various process parameters and their levels selected for the present study were listed in Table 7.7.

Based on Table 7.7, the mathematical model was developed for optimizing the weld process parameters by taking power (55-65W), Pressure (3.3 to 3.8kgf) and time (1.5 to 2.5sec) as input parameters as stated in various literature and trail experiments conducted. The 17 experimental runs were performed in a randomized order based on CCRD design matrix as given in table7.17.6. The TSFL and hardness samples were prepared as shown in figure 7.23.1 (a) and (b) respectively.

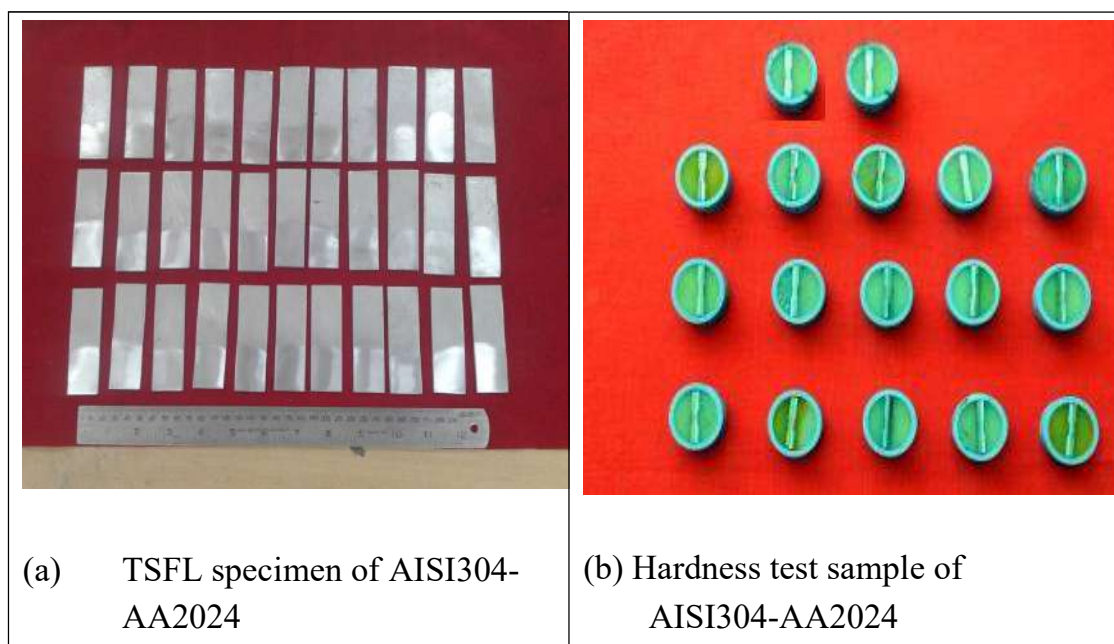


Figure 7.23.1 (a) and (b) TSFL specimen of AIS5052-AA1008 and Hardness test sample of AIS5052- AA1008

The tested TSFL sample, hardness sample and nugget images were shown in Figure 7.23.1.1 (a) to (o).
















TSFL (KN)	Cross-sectional macrostructure	Nugget (mm)	Top view of the top sheet	Bottom view of the top sheet	Top view of the bottom sheet
High (3.648)					
	(a)	(d)	(g)	(j)	(m)
Medium (2.489)					
	(b)	(e)	(h)	(k)	(n)
Low (1.157)					
	(c)	(f)	(i)	(l)	(o)

Figure 7.23.1.1 (a) to (o) Welded TSFL sample, hardness sample, and nugget images

The welded AIS5052-AA1008 dissimilar joint possess high, medium and low TSFL values were analyzed using macrostructural and nugget images as shown in figure 7.23.1.1 (a) to (o). from the figure it is identified that the depth of penetration of the sample possess high TSFL joint is higher when compared to medium and low TSFL samples as shown in figure 7.23.1.1 (a) to (c) similarly, the nugget diameter of the sample possess high TSFL strength is higher when compared to other TSFL samples.

Table 7.17.5 L17 (3³) Orthogonal array used to design experiments with three parameters at three levels SS-AL

Std	Run	Coded Values			A:Power	B:Pressure	C:time
		A: Power	B: Pressure	C:time			
		W	Kgf	S	W	Kgf	S
15	1	0	0	0	60	3.6	2
17	2	0	0	0	60	3.6	2
7	3	-1	0	1	55	3.6	2.5
9	4	0	-1	-1	60	3.4	1.5
6	5	1	0	-1	65	3.6	1.5
16	6	0	0	0	60	3.6	2
14	7	0	0	0	60	3.6	2
2	8	1	-1	0	65	3.4	2
3	9	-1	1	0	55	3.8	2
8	10	1	0	1	65	3.6	2.5
12	11	0	1	1	60	3.8	2.5
10	12	0	1	-1	60	3.8	1.5
11	13	0	-1	1	60	3.4	2.5
13	14	0	0	0	60	3.6	2
4	15	1	1	0	65	3.8	2
1	16	-1	-1	0	55	3.4	2
5	17	-1	0	-1	55	3.6	1.5

The TSFL, microhardness and nugget diameter values are tabulated in Table 7.17.6.

Table 7.17.6 TSFL, micro Hardness and Nugget diameter values of AIS5052-AA1008 dissimilar joints

		Factor 1	Factor 2	Factor 3	Response 1	Response 2	Response 3
Std	Run	A: Power	B: Pressure	C:time	Hardness	Nugget Depth	TSFL
		W	kgf	S	VHN	mm	kN
15	1	60	3.6	2	114	4.335	3.165
17	2	60	3.6	2	114	4.335	3.165
7	3	55	3.6	2.5	135	4.555	2.085
9	4	60	3.4	1.5	133	4.552	2.489
6	5	65	3.6	1.5	143.34	4.622	2.899
16	6	60	3.6	2	114	4.335	3.165
14	7	60	3.6	2	114	4.335	3.165
2	8	65	3.4	2	144	4.814	2.912
3	9	55	3.8	2	132	4.624	1.928
8	10	65	3.6	2.5	166	4.899	3.456
12	11	60	3.8	2.5	172	4.972	3.648
10	12	60	3.8	1.5	155	4.722	2.148
11	13	60	3.4	2.5	148	4.664	2.598
13	14	60	3.6	2	114	4.335	3.165
4	15	65	3.8	2	162	5.112	3.11
1	16	55	3.4	2	120	4.432	1.518
5	17	55	3.6	1.5	136	4.445	1.157

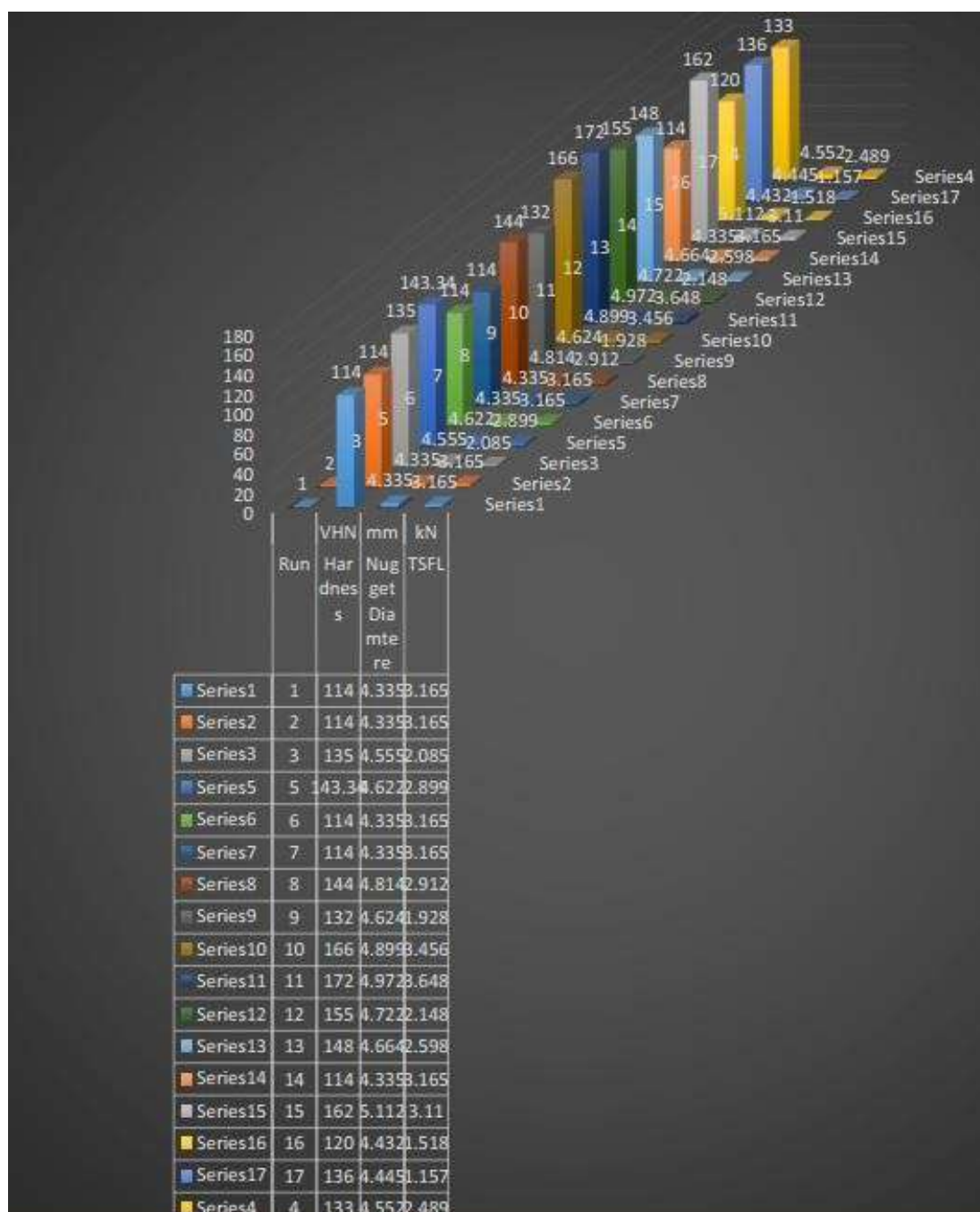


Figure 7.23.2 The TSFL, microhardness and nugget diameter values of AIS5052 and AA1008

The Table 7.17.6 and Figure 7.23.2 both clearly show the TSFL 3.165kgf, Microhardness 172 VHN and nugget diameter 5.113mm at the maximum weld pressure of 3.7kgf.

Optimizing weld input process parameter for TSFL strength

To obtain the influencing ERS welding process parameter for TSFL strength. The interaction effects plots were obtained. The interaction effect results obtained from DOE software for the 3D response, 2D contour effects of the input process parameters such as pressure, power, time on the nugget diameter, TSFL, hardness are given in Figure 7.24 (a) to 7.24 (f). The Figure 7.24 (a) to (e) shows the interaction effects between power versus pressure, power versus time and pressure versus time.

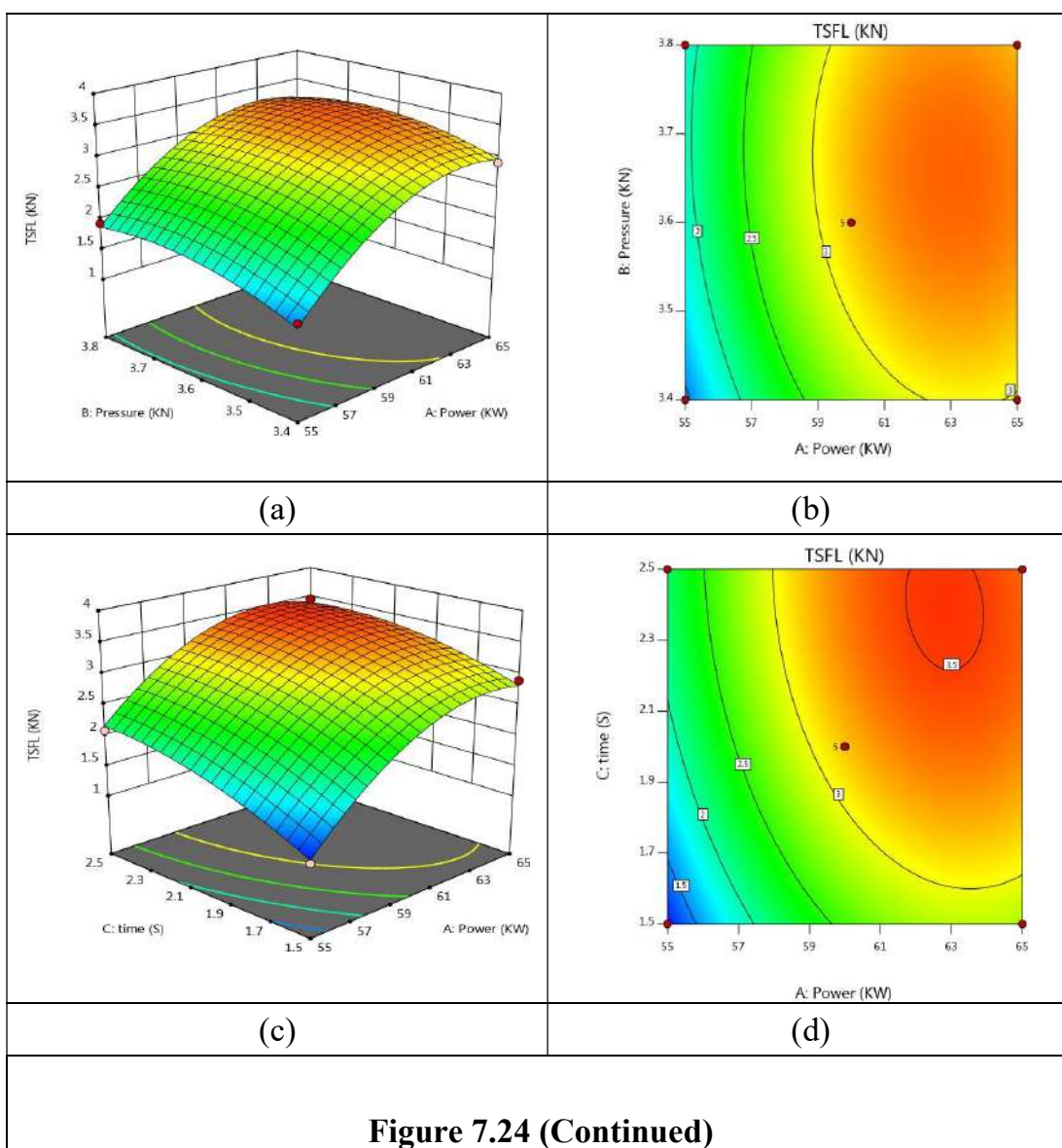


Figure 7.24 (Continued)

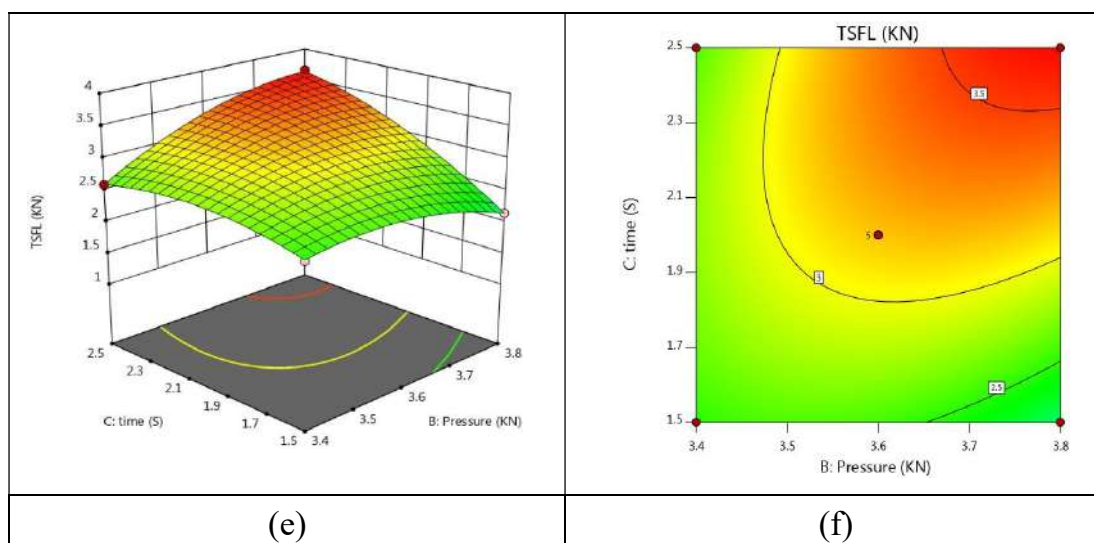


Figure 7.24 (a) to (f) Various interaction plots for TSFL figure (a,c,e) shows 3D plots and figures (b,d,f) shows the 2D plots.

Interaction effect weld input process parameter for TSFL strength

The interaction effect was achieved by the design of expert software for both the 2D and 3D responses of input process parameters such as pressure, time and power on TSFL are shown in Figures 7.24 (a) to (7.24 f).

The Figure 7.24 (a) shows the 3D surface plot which indicates all the points are within the plot. Similarly, 7.24 (b) indicates the 2D contour plot between power versus pressure. The plotted results show blue colored value is lesser and green colored values are average and red colored value is higher which indicates that the TSFL decreases with the increase in power. The TSFL is high at power 65w. It has good agreement with various works discussed literature reviews.

The Figure 7.24 (c) shows the 3D surface plot where indicates all the points are within the plot. Similarly, 7.24 (d) indicates the 2D contour plot between power versus Time. The plotted results show blue colored value is lesser and green colored values are average and red colored value is higher, which indicates that the TSFL decreases with the increase in power. The TSFL is high at higher at the power of 65w. It has good agreement with various literary works reviews.

The Figure 7.24 (e) is 3D surface plot indicates all the points are within the plot. Similarly, 7.24 (f) indicates the 2D contour plot between pressure versus time. The plotted results show blue colored value is lesser and green colored values are average and red colored value is higher and the TSFL decreases with the pressure. The TSFL is high at pressure 3.8kgf. it has good agreement with various literature reviews.

Optimizing weld input process parameter for microhardness

To obtain the influencing ERS welding process parameter for Microhardness strength. The interaction effects plots were obtained. The interaction effect results obtained from DOE software for the 3D response, 2D contour effects of the input process parameters such as pressure, power, time on the hardness are given in Figure 7.25 (a) to 7.25 (f). The Figure 7. 25 (a) to 7.25 (f) shows the interaction effects between power versus pressure, power versus time and pressure versus time.

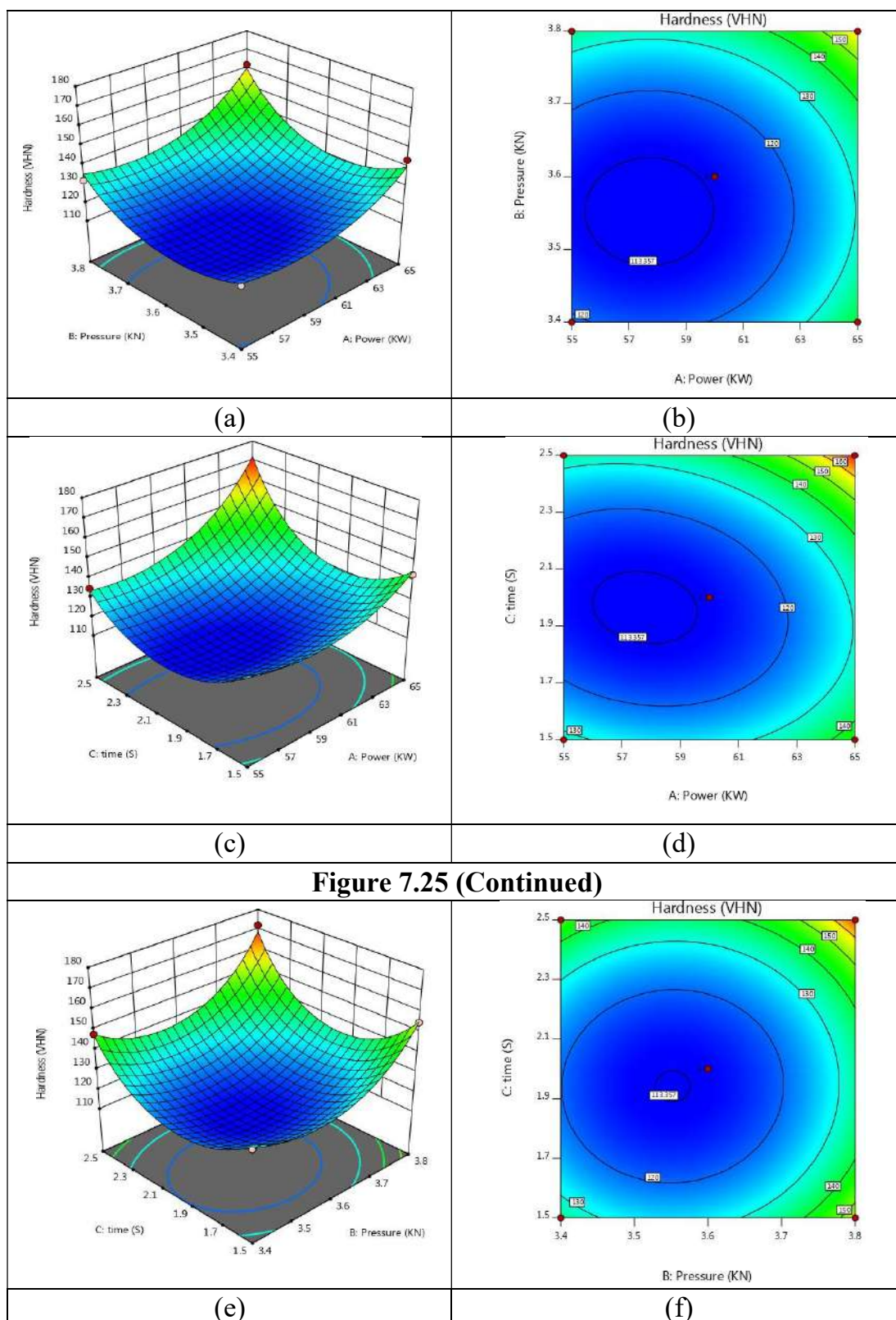


Figure 7.25 (a) to (f) Various interaction plots for TSFL figure (a,c,e) shows 3D plots and figures (b,d,f) shows the 2D plots

Interaction effect weld input process parameter for microhardness

The interaction effect was achieved by the design of expert software for both the 2D and 3D responses of input process parameters are pressure, time and power on hardness are listed in Figures 7.25 (a) to (7.25 f).

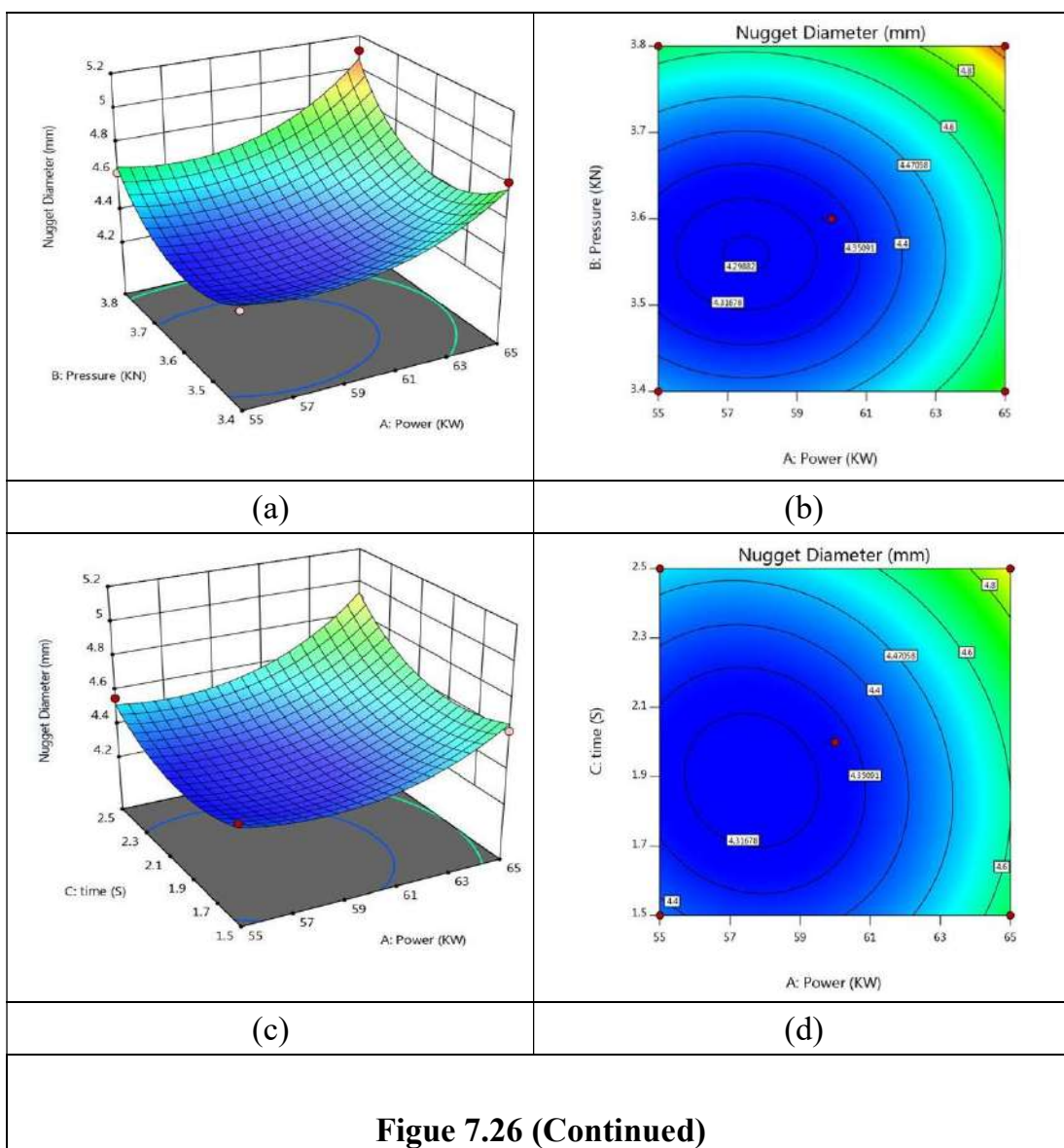
The Figure 7.25 (a) to (7.25 f). shows 3d and 2D responses of hardness. The Figure 7.25 (a) is 3D surface plot indicates all the points are within the plot. Similarly, 7.25 (b) indicates the 2D contour plot between power versus pressure. The plotted results show blue colored value is lesser and green colored values are average and red colored value is higher and the hardness decreases with the power. The hardness is high at power 65w. it has good agreement with various literature reviews.

The Figure 7.25 (c) is 3D surface plot indicates all the points are within the plot. Similarly, 7.25 (d) indicates the 2D contour plot between power versus Time. The plotted results show blue colored value is lesser and green colored values are average and red colored value is higher and the hardness decreases with the power. The hardness is high at power 65w. it has good agreement with various literature reviews.

The Figure 7.25 (e) is 3D surface plot indicates all the points are within the plot. Similarly, 7.25 (f) indicates the 2D contour plot between pressure versus time. The plotted results show blue colored value is lesser and green colored values are average and red colored value is higher and the hardness decreases with the pressure. The hardness is high at pressure 65w. it has good agreement with various literature reviews.

Optimizing weld input process parameter for nugget diameter

To obtain the influencing ERS welding process parameter for TSFL strength. The interaction effects plots were obtained. The interaction effect results obtained from DOE software for the 3D response, 2D contour effects of the input process parameters such as pressure, power, time on the nugget diameter, TSFL, hardness are given in Figure 7.26 (a) to (f). The Figure 7.26 (a) to (f) shows the interaction effects between power versus pressure, power versus time and pressure versus time.



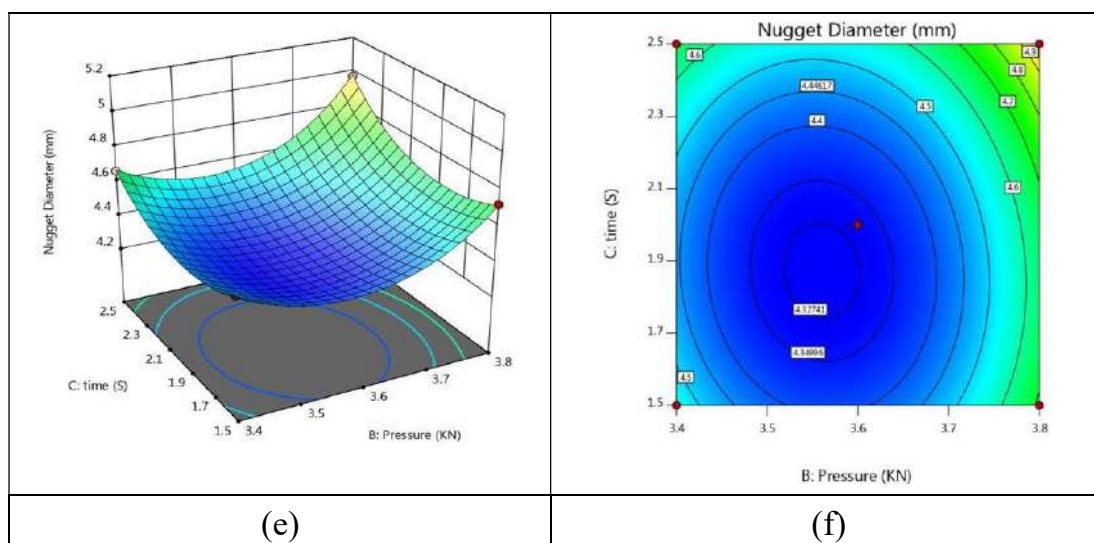


Figure 7.26 (a) to (f) Various interaction plots for TSFL figure (a,c,e) shows 3D plots and figures (b,d,f) shows the 2D plots.

7.2.3.3.3 Interaction effect weld input process parameter for nugget diameter

The interaction effect was achieved by the design of expert software for both the 2D and 3D responses of input process parameters are pressure, time and power on Nugget diameter are listed in Figures 7.26 (a) to (7.26 f).

The Figure 7.26 (a) to (7.26 f). shows 3D and 2D responses of Nugget diameter. The Figure 7.26 (a) is 3D surface plot indicates all the points are within the plot. Similarly, 7.26 (b) indicates the 2D contour plot between power versus pressure. The plotted results show blue colored value is lesser and green colored values are average and red colored value is higher and the Nugget diameter decreases with the power. The Nugget diameter is high at power 65w. It has good agreement with various literature reviews.

The Figure 7.26 (c) is 3D surface plot indicates all the points are within the plot. Similarly, 7.26 (d) indicates the 2D contour plot between power versus Time. The plotted results show blue colored value is lesser and green colored values are average and red colored value is higher and the Nugget diameter decreases with the power. The Nugget diameter is high at power 65w. it has good agreement with various literature reviews.

The Figure 7.26 (e) is 3D surface plot indicates all the points are within the plot. Similarly, 7.26 (f) indicates the 2D contour plot between pressure versus time. The plotted results show blue colored value is lesser and green colored values are average and red colored value is higher and the Nugget diameter decreases with the pressure. The Nugget diameter is high at pressure 65w. It has good agreement with various literature reviews.

Confirmation Test Result for Optimized Condition of Dissimilar Joints

In this work, 8 confirmation test was conducted to check the accuracy of the developed model. The confirmation test was carried out based on the parameters selected randomly that should be within the range selected for the RSM test. The predicted values from the RSM and the experimentally obtained values from the confirmation test conducted are given in Table 7.8.

The Table 7.8 shows the confirmation test results and RSM obtained results to check the desirability of both investigations. Based on the table 7.8 it clearly identified that the pressure time and power are within the range and its corresponding TSFL and hardness values are also within the range of both predicted and experimented data.

Table 7.8 Result of confirmation and predicted values by RSM

Sample No.	Pressure (kgf)	Time (sec)	Power (w)	TSFL (kN)		Hardness (VHN)		Desirability
				RSM	EXP	RSM	EXP	
1.	3.6	2	51.59	6.17	6.14	354	359	0.99513
2.	3.8	1.5	55	7.29	7.24	415	412	0.99314
3.	3.4	2.5	55	7.19	7.15	408	409	0.99443
4.	3.4	1.5	55	6.54	6.52	364	365	0.99692
5.	3.8	2.5	55	8.94	8.91	472	473	0.99662
6.	3.6	2	60	8.75	8.71	450	456	0.99542
7.	3.26	2	60	7.93	7.91	421	423	0.99745
8.	3.6	2	60	8.60	8.58	451	455	0.99767

The Table 7.8, it is clearly identified that the predicted values from RSM for each response are much closer to the experimental results. The error percentage between predicted and experimental value are within the allowable range, hence it is evident that the developed RSM model can able to predict the TSFL, hardness and nugget diameter for any combination of weld pressure, weld power and weld time within the range of parameters selected for experimentation.

The Confirmation experiments have been conducted to validate the weld input process parameters and the optimum value for obtaining better TSFL, Hardness and nugget diameter.

PREDICTION OF ERSW PROCESS PARAMETER FOR WELDING OF SS-AISI1020, SS-AL, AISI1020-AL DISSIMILAR JOINTS

The ANOVA is used to find out the significance factor statistically. It gives the clear idea about how far the ERSW input process parameters, mechanical properties and the level of significance are to be considered.

Prediction of Process Parameters ERSW Welded SS-AISI1020, Dissimilar Joints Using ANOVA

This section illustrates the ANOVA response for TSFL, Microhardness, nugget diameter of ERSW joints welded at various input conditions for SS-AISI1020 dissimilar joints.

ANOVA results for TSFL analysis

The experimental values arrived according to the CCRD method is mentioned in Table 7.8. The experimental results will be examined through RSM to get the empirical relationship for good responses. The estimated values show that the relationship in or near the local and central point of the model. The all values within the confidence interval is about 99.5% with the adaption of F-test and design expert software package 9.0.31. The end model has been finalized after finding the coefficients of significance. The final mathematical model has been used to find and calculate the TSFL.

The final TSFL mathematical equation has been arrived and given in Equation (7.1), which has the coded variables A, B and C

Table 7.9 Results of ANOVA for TSFL (AIS5052-AISI1020)

Source	Sum of Squares	df	Mean Square	F-value	p-value	
Model	5.14	9	0.5708	2487.68	< 0.0001	significant
A-Power	3.30	1	3.30	14388.51	< 0.0001	
B-Pressure	0.6413	1	0.6413	2795.08	< 0.0001	
C-Time	0.0287	1	0.0287	125.12	< 0.0001	
AB	0.1436	1	0.1436	625.86	< 0.0001	
AC	0.0202	1	0.0202	88.01	< 0.0001	
BC	0.0288	1	0.0288	125.51	< 0.0001	
A ²	0.6152	1	0.6152	2681.42	< 0.0001	
B ²	0.1343	1	0.1343	585.16	< 0.0001	
C ²	0.1384	1	0.1384	603.17	< 0.0001	
Residual	0.0016	7	0.0002			
Lack of Fit	0.0016	3	0.0005			
Pure Error	0.0000	4	0.0000			
Cor Total	5.14	16				
	Std. Dev.	0.0151	R²			0.9997
	Mean	4.41	Adjusted R²			0.9993
	C.V. %	0.3431	Predicted R²			0.9950
			Adeq Precision			159.3328

Coded Equation

$$\begin{aligned}
 (\text{TSFL})^{0.7} = & 4.76363 + 0.642396 * A + 0.283134 * B + 0.0599053 * C + \\
 & - 0.189473 * AB + -0.0710502 * AC + -0.0848507 * BC + -0.382256 * A^2 + \\
 & - 0.17857 * B^2 + -0.181297 * C^2
 \end{aligned}
 \tag{7.1}$$

From the Table 7.9, the actual coefficient of determination of R^2 obtained from ANOVA table is 0.9997, which is less than the 1%. The adjacent coefficient of determination R^2 of the developed model is 0.9993 which is less than the actual R^2 , which indicates that the developed model is highly significant. Similarly the R^2 value and predicted R^2 value are in good agreement. The optimized ANOVA table for TSFL shows that the ability of the developed model to predict the parameters is about 99% confidence level and the p values are less than 0.001. The experimentally obtained values are in good agreement with predicted values. Based on the R^2 value, it is concluded that Equation (7.1) is able to predict the TSFL more accurately and the results are highly reliable as stated in various literature.

Checking of data and adequacy of the model

The plots show the externally studentized residual and internally studentized residuals achieved by design expert software for TSFL as shown in Figure 7.17.1 (a) to (d). In that plots, the residuals are very near to the straight line, which indicates that the errors are normally distributed. Similarly, the plot run number versus internally studentized residuals is shown in Figure 7.17.1 (d). The plot shows that all residuals are falling between -6 to 6 . Which is also has a better agreement when compared with the various literature reviews.

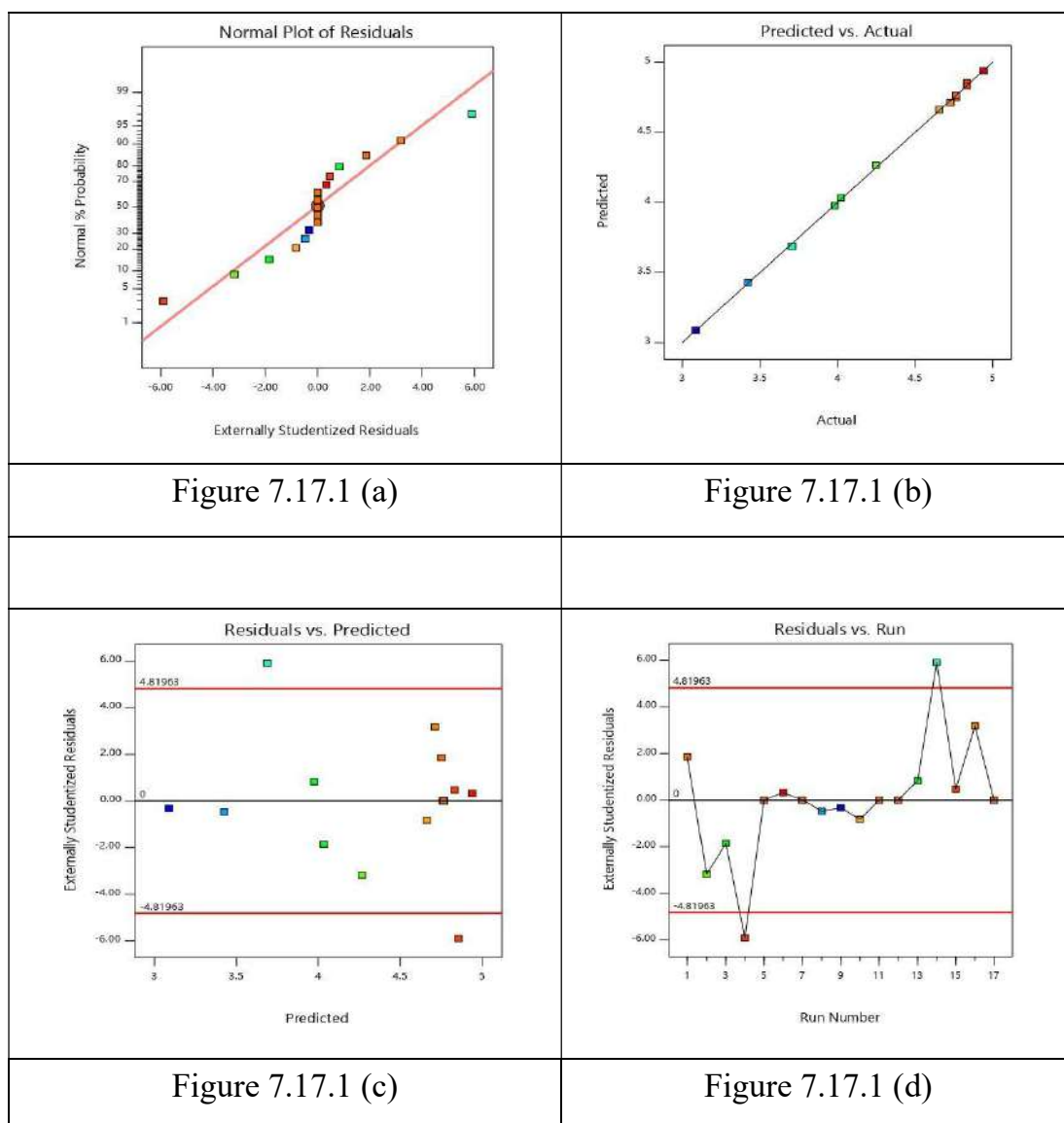


Figure 7.17.1(a)to(d) Various predicted, actual, run number, externally studentized residuals and normal % probability plots

ANOVA results for hardness analysis

The experimental values arrived according to the CCRD method is mentioned in Table 7.10. The experimental results will be examined through RSM to get the empirical relationship for good responses. The estimated values show that the relationship in or near the local and central point of the

model. The all values within the confidence interval is about 99.5% with the adaption of F-test and design expert software package 9.0.31. The end model has been finalized after finding the coefficients of significance. The final mathematical model has been used to find and calculate the TSFL. The final TSFL mathematical equation has been arrived and given in Equation (7.2), which has the coded variables A, B, and C.

Checking of data and adequacy of the model

The plots externally studentized residual and internally studentized residuals are achieved by design expert software for TSFL as shown in Figure 7.18.1 (a) to (d). In that plots, the residuals are very near to the straight line, which indicates that the errors are normally distributed. Similarly, the plot run number versus internally studentized residuals is shown in Figure 7.18.1 (d). The plot shows that all residuals are falling between -6 to 6 . which is also has better agreement with the various literature reviews.

From the Table 7.10, the actual coefficient of determination of R^2 obtained from ANOVA table is 0.9990, which is less than the 1%. The adjacent coefficient of determination R^2 of the developed model is 0.9976 which is less than the actual R^2 , which indicates that the developed model is highly significant. Similarly the R^2 value and predicted R^2 value are in good agreement. the optimized ANOVA table for TSFL shows that the ability of the developed model to predict the parameters is about 99% confidence level and the p values are less than 0.001. The experimentally obtained values are in good agreement with predicted values. Based on the R^2 value, it is concluded that Equation (7.2) is able to predict the TSFL more accurately and the results are highly reliable as stated in various literature.

Table 7.10 Results of ANOVA for hardness(AIS5052-AISI1020)

Source	Sum of Squares	df	Mean Square	F-value	p-value	
Model	3.166E-13	9	3.517E-14	752.40	< 0.0001	significant
A-Power	7.125E-14	1	7.125E-14	1524.25	< 0.0001	
B-Pressure	2.008E-14	1	2.008E-14	429.48	< 0.0001	
C-Time	7.079E-16	1	7.079E-16	15.14	0.0060	
AB	5.730E-15	1	5.730E-15	122.58	< 0.0001	
AC	6.670E-19	1	6.670E-19	0.0143	0.9083	
BC	1.272E-16	1	1.272E-16	2.72	0.1431	
A ²	3.316E-14	1	3.316E-14	709.25	< 0.0001	
B ²	8.225E-14	1	8.225E-14	1759.47	< 0.0001	
C ²	8.131E-14	1	8.131E-14	1739.43	< 0.0001	
Residual	3.272E-16	7	4.675E-17			
Lack of Fit	3.272E-16	3	1.091E-16			
Pure Error	0.0000	4	0.0000			
Cor Total	3.169E-13	16				
		Std. Dev.	6.837E-09	R²	0.9990	
		Mean	2.862E-07	Adjusted R²	0.9976	
		C.V. %	2.39	Predicted R²	0.9835	
				Adeq Precision	65.5763	

Coded equation

$$(\text{Hardness})^{-2.53} = 4.59167\text{e-}07 + -9.43754\text{e-}08 * A + -5.00962\text{e-}08 * B + -9.40689\text{e-}09 * C + 3.78496\text{e-}08 * AB + 4.08347\text{e-}10 * AC + -5.6385\text{e-}09 * BC + -8.87375\text{e-}08 * A^2 + -1.39765\text{e-}07 * B^2 + -1.38967\text{e-}07 * C^2$$

(7.2)

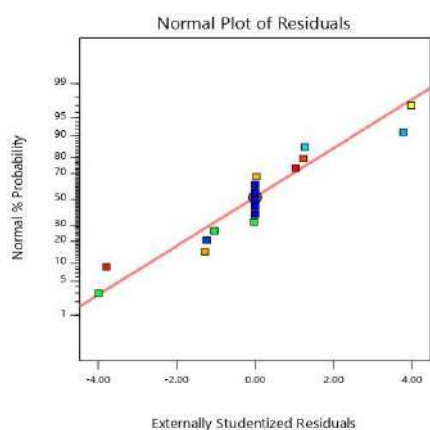


Figure:7.18.1 (a)

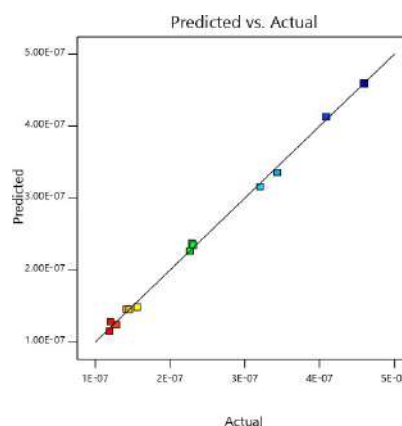


Figure:7.18.1 (b)

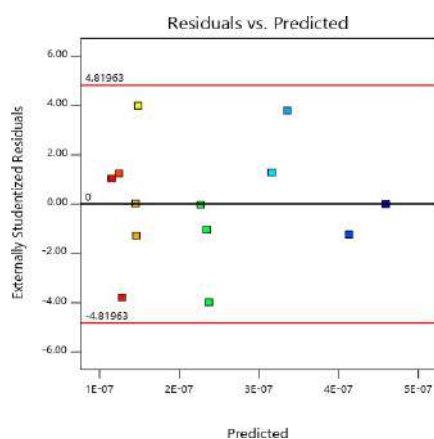


Figure:7.18.1 (c)

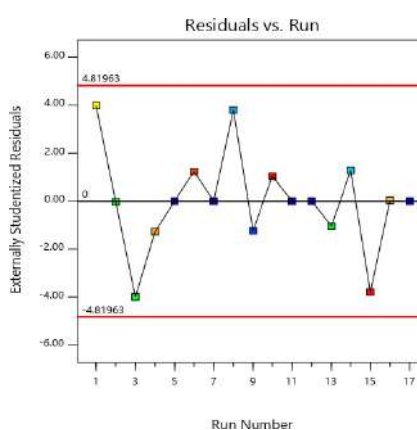


Figure:7.18.1 (d)

Figure 7.18.1(a) to (d) Various predicted, actual, run number, externally studentized residuals and normal % probability plots

ANOVA results for nugget diameter analysis

The experimental values arrived according to the CCRD method is mentioned in Table 7.11. The experimental results will be examined through RSM to get the empirical relationship for good responses. The estimated values show that the relationship in or near the local and central point of the model. The all values within the confidence interval is about 99.5% with the adaption of F-test and design expert software package 9.0.31. The end model has been finalized after finding the coefficients of significance. The final mathematical model has been used to find and calculate the TSFL.

The final TSFL mathematical equation has been arrived and given in Equation (7.3), which has the coded variables A, B and C

Table 7.11 Results of ANOVA for Nugget diameter(AIS5052-AISI1020)

Source	Sum of Squares	df	Mean Square	F-value	p-value	
Model	1.09	9	0.1207	213.26	< 0.0001	significant
A-Power	0.4368	1	0.4368	771.68	< 0.0001	
B-Pressure	0.0131	1	0.0131	23.19	0.0019	
C-Time	0.0044	1	0.0044	7.76	0.0271	
AB	0.0318	1	0.0318	56.24	0.0001	
AC	0.0000	1	0.0000	0.0180	0.8972	
BC	0.0078	1	0.0078	13.87	0.0074	
A ²	0.0918	1	0.0918	162.09	< 0.0001	
B ²	0.1693	1	0.1693	298.98	< 0.0001	
C ²	0.2727	1	0.2727	481.76	< 0.0001	
Residual	0.0040	7	0.0006			
Lack of Fit	0.0040	3	0.0013			
Pure Error	0.0000	4	0.0000			
Cor Total	1.09	16				
			Std. Dev.	0.0238	R²	0.9964
			Mean	3.06	Adjusted R²	0.9917
			C.V. %	0.7788	Predicted R²	0.9419
					Adeq Precision	36.8763

Coded Equation

$$\begin{aligned}
 (\text{Nugget Diameter})^{0.65} = & 3.33869 + 0.233678 * A + 0.040512 * B + \\
 & 0.0234309 * C + 0.0892117 * AB + 0.00159428 * AC + 0.0442989 * BC + - \\
 & 0.147622 * A^2 + -0.200492 * B^2 + -0.254503 * C^2.
 \end{aligned}
 \tag{7.3}$$

From the Table 7.11, the actual coefficient of determination of R^2 obtained from ANOVA table is 0.9964, which is less than the 1%. The adjacent coefficient of determination R^2 of the developed model is 0.9917 which is less than the actual R^2 , which indicates that the developed model is highly significant. Similarly the R^2 value and predicted R^2 value are in good agreement. The optimized ANOVA table for TSFL shows that the ability of the developed model to predict the parameters is about 99% confidence level and the p values are less than 0.001. The experimentally obtained values are in good agreement with predicted values. Based on the R^2 value, it is concluded that Equation 7.3 is able to predict the TSFL more accurately and the results are highly reliable as stated in various literature.

Checking of data and adequacy of the model

The plots externally studentized residual and internally studentized residuals are achieved by design expert software for TSFL as shown in Figure 7.19.1 (a) to (d). In that plots, the residuals are very near to the straight line, which indicates that the errors are normally distributed. Similarly, the plot run number versus internally studentized residuals is shown in Figure 7.19.1 (d). The plot shows that all residuals are falling between -6 to 6, which is also in better agreement with the various literature reviews.

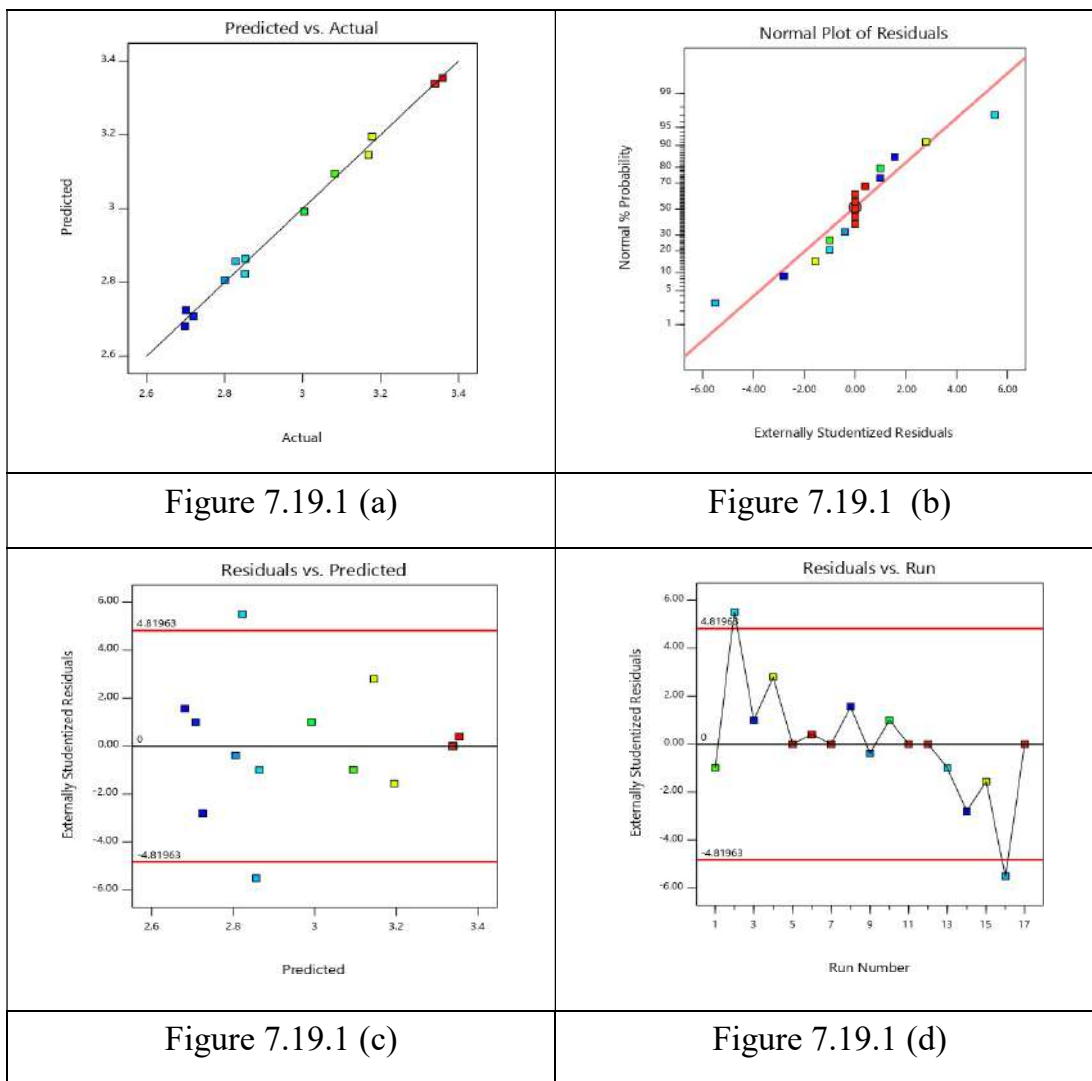


Figure 7.19.1(a) to (d) Various predicted, actual, run number, externally studentized residuals and normal % probability plots

7.3.2 Prediction of Process Parameters ERSW Welded AISI1020-AL Dissimilar Joints using ANOVA

This section illustrates the ANOVA response for TSFL, Microhardness, nugget diameter of ERSW joints welded at various input conditions for AISI1020-AL dissimilar joints.

ANOVA results for TSFL analysis

The experimental values arrived according to the CCRD method is mentioned in Table 7.12. The experimental results will be examined through RSM to get the empirical relationship for good responses. The estimated values show that the relationship in or near the local and central point of the model. The all values within the confidence interval is about 99.5% with the adaption of F-test and design expert software package 9.0.31. The end model has been finalized after finding the coefficients of significance. The final mathematical model has been used to find and calculate the TSFL.

The final TSFL mathematical equation has been arrived and given in Equation 7.4, which has the coded variables A, B, and C.

7.3.2.1.1 Checking of data and adequacy of the model

The plots externally studentized residual and internally studentized residuals are achieved by design expert software for TSFL as shown in Figure 7.21.1 (a) to (d). In that plots, the residuals are very near to the straight line, which indicates that the errors are normally distributed. Similarly, the plot run number versus internally studentized residuals is shown in Figure 7.21.1 (d). The plot shows that all residuals are falling between -30 to 30, which is also in better agreement with the various literature reviews.

Table 7.12 Results of ANOVA for TSFL(AISI1020-AA1008)

Source	Sum of Squares	df	Mean Square	F-value	p-value	
Model	0.0003	9	0.0000	1893.60	< 0.0001	significant
A-Power	0.0002	1	0.0002	10485.91	< 0.0001	
B-Pressure	0.0000	1	0.0000	2089.48	< 0.0001	
C-time	3.283E-06	1	3.283E-06	164.75	< 0.0001	
AB	0.0000	1	0.0000	748.36	< 0.0001	
AC	2.106E-06	1	2.106E-06	105.70	< 0.0001	
BC	1.542E-06	1	1.542E-06	77.39	< 0.0001	
A ²	0.0000	1	0.0000	2425.62	< 0.0001	
B ²	6.580E-06	1	6.580E-06	330.19	< 0.0001	
C ²	7.070E-06	1	7.070E-06	354.76	< 0.0001	
Residual	1.395E-07	7	1.993E-08			
Lack of Fit	1.395E-07	3	4.650E-08			
Pure Error	0.0000	4	0.0000			
Cor Total	0.0003	16				
	Std. Dev.	0.0001		R²	0.9996	
	Mean	1.01		Adjusted R²	0.9991	
	C.V. %	0.0140		Predicted R²	0.9934	
				Adeq Precision	136.5521	

Coded formula

$$\begin{aligned}
 (\text{TSFL})^{0.01} = & 1.00798 + 0.00511094 * A + 0.00228148 * B + 0.000640643 \\
 & * C + -0.00193093 * AB + -0.00072568 * AC + -0.000620951 * BC + \\
 & -0.00338833 * A^2 + -0.00125014 * B^2 + -0.00129582 * C^2 \quad (7.4)
 \end{aligned}$$

From the Table 7.12, the actual coefficient of determination of R^2 obtained from ANOVA table is 0.9991, which is less than the 1%. The adjacent coefficient of determination R^2 of the developed model is 0.9934 which is less than the actual R^2 , which indicates that the developed model is highly significant. Similarly the R^2 value and predicted R^2 value are in good agreement. The optimized ANOVA table for TSFL shows that the ability of

the developed model to predict the parameters is about 99% confidence level and the p values are less than 0.001. The experimentally obtained values are in good agreement with predicted values. Based on the R^2 value, it is concluded that Equation 7.4 is able to predict the TSFL more accurately and the results are highly reliable as stated in various literature.

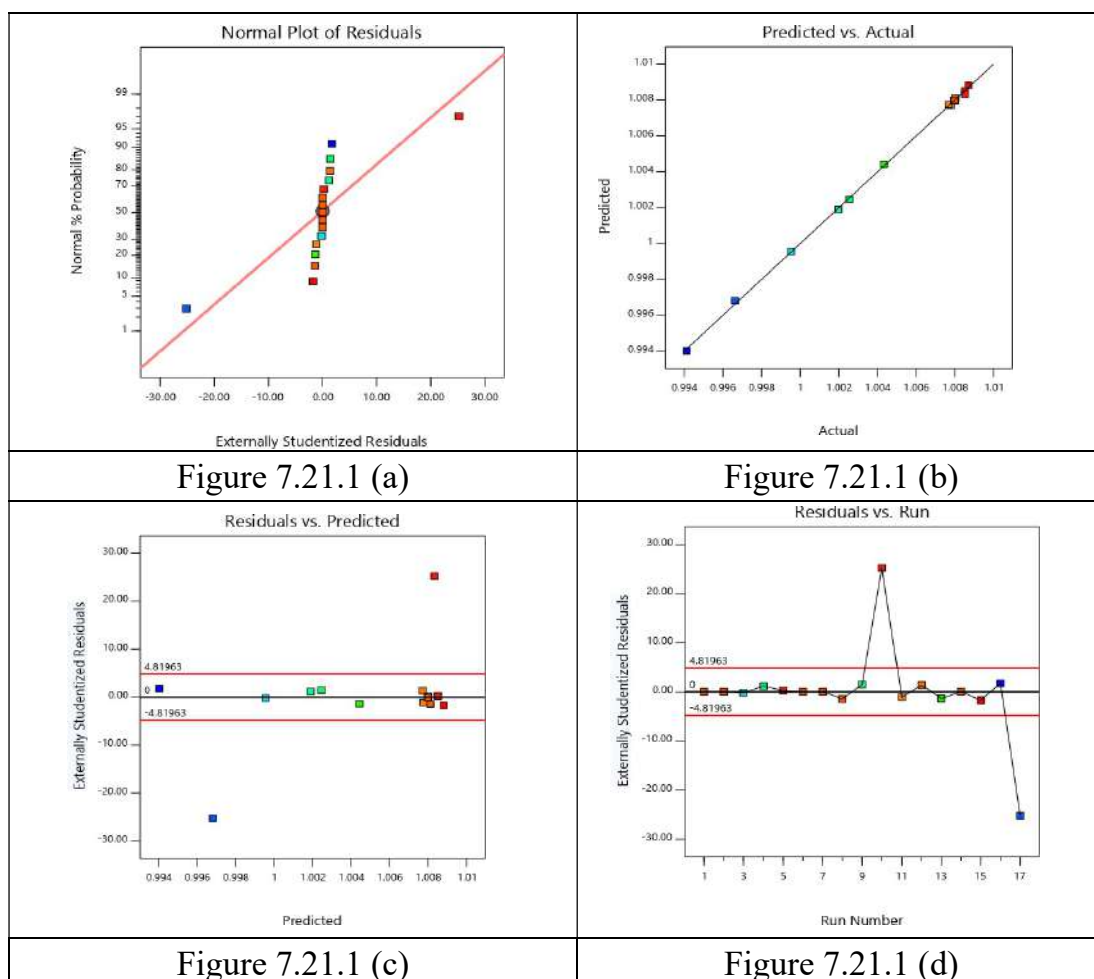


Figure 7.21.1(a) to (d) Various predicted, actual, run number, externally studentized residuals and normal % probability plots

ANOVA results for hardness analysis

The experimental values arrived according to the CCRD method is mentioned in Table 7.13. The experimental results will be examined through

RSM to get the empirical relationship for good responses. The estimated values show that the relationship in or near the local and central point of the model. The all values within the confidence interval is about 99.5% with the adaption of F-test and design expert software package 9.0.31. The end model has been finalized after finding the coefficients of significance. The final mathematical model has been used to find and calculate the TSFL.

The final TSFL mathematical equation has been arrived and given in Equation 7.5, which has the coded variables A, B and C.

Table 7.13 Results of ANOVA for Hardness (AISI1020-AA1008)

Source	Sum of Squares	df	Mean Square	F-value	p-value	
Model	2.193E-12	9	2.436E-13	283.66	< 0.0001	significant
A-Power	3.327E-13	1	3.327E-13	387.35	< 0.0001	
B-Pressure	6.700E-14	1	6.700E-14	78.00	< 0.0001	
C-time	2.537E-14	1	2.537E-14	29.53	0.0010	
AB	2.213E-14	1	2.213E-14	25.77	0.0014	
AC	2.586E-15	1	2.586E-15	3.01	0.1263	
BC	9.499E-15	1	9.499E-15	11.06	0.0127	
A ²	4.230E-13	1	4.230E-13	492.43	< 0.0001	
B ²	5.232E-13	1	5.232E-13	609.07	< 0.0001	
C ²	6.062E-13	1	6.062E-13	705.72	< 0.0001	
Residual	6.013E-15	7	8.589E-16			
Lack of Fit	6.013E-15	3	2.004E-15			
Pure Error	0.0000	4	0.0000			
Cor Total	2.199E-12	16				
	Std. Dev.		2.931E-08	R²		0.9973
	Mean		6.728E-07	Adjusted R²		0.9937
	C.V. %		4.36	Predicted R²		0.9562
				Adeq Precision		43.6892

Coded formula

(Hardness)⁻³

$$= 1.16635e-06 + -2.03933e-07 * A + -9.15155e-08 * B + -5.63106e-08 * C + 7.43864e-08 * AB + -2.5426e-08 * AC + -4.87303e-08 * BC + -3.16947e-07 * A^2 + -3.52492e-07 * B^2 + -3.79431e-07 * C^2 \quad (7.5)$$

From the Table 7.13, the actual coefficient of determination of R^2 obtained from ANOVA table is 0.9973, which is less than the 1%. The adjacent coefficient of determination R^2 of the developed model is 0.9937 which is less than the actual R^2 , which indicates that the developed model is highly significant. Similarly the R^2 value and predicted R^2 value are in good agreement. the optimized ANOVA table for TSFL shows that the ability of the developed model to predict the parameters is about 99% confidence level and the p values are less than 0.001. The experimentally obtained values are in good agreement with predicted values. Based on the R^2 value, it is concluded that Equation 7.5 is able to predict the TSFL more accurately and the results are highly reliable as stated in various literature.

7.3.2.2.1 Checking of data and adequacy of the model

The plots externally studentized residual and internally studentized residuals are achieved by design expert software for TSFL as shown in Figure 7.22.1 (a) to (d). in that plots, the residuals are very near to the straight line, which indicates that the errors are normally distributed. Similarly, the plot run number versus internally studentized residuals is shown in Figure 7.22.1 (d). the plot shows that all residuals are falling between -6 to 6. Which is also has better agreement with the various literature reviews.

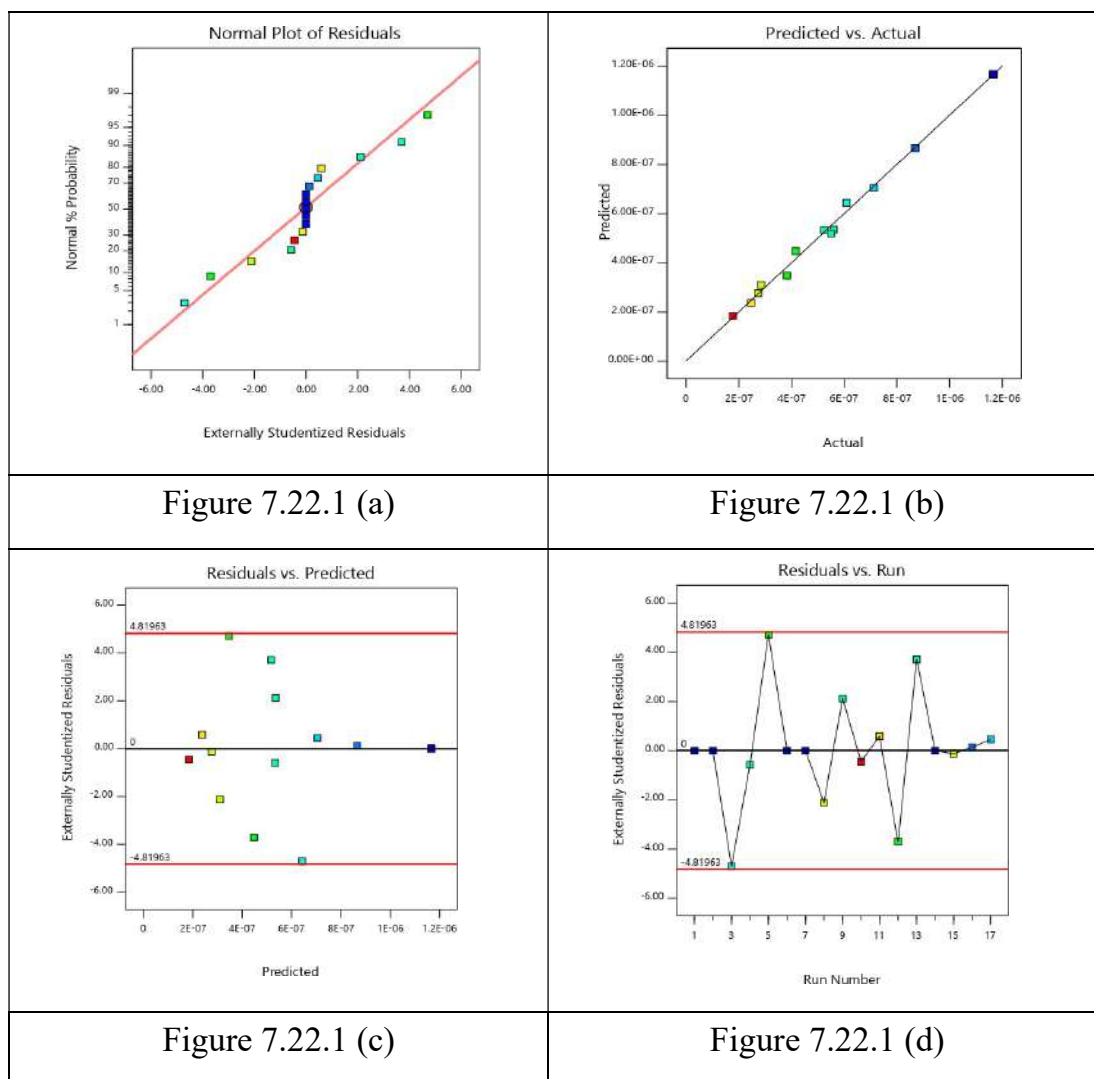


Figure 7.22.1(a) to (d) Various predicted, actual, run number, externally studentized residuals and normal % probability plots

ANOVA results for nugget diameter analysis

The experimental values arrived according to the CCRD method is mentioned in Table 7.14. The experimental results will be examined through RSM to get the empirical relationship for good responses. The estimated values show that the relationship in or near the local and central point of the model. The all values within the confidence interval is about 99.5% with the adaption of F-test and design expert software package 9.0.31. The end model has been finalized after finding the coefficients of significance. The final mathematical model has been used to find and calculate the TSFL.

The final TSFL mathematical equation has been arrived and given in Equation 7.6, which has the coded variables A, B and C

7.3.2.3.1 Checking of data and adequacy of the model

The plots externally studentized residual and internally studentized residuals are achieved by design expert software for TSFL as shown in Figure 7.23.1 (a) to (d). In that plots, the residuals are very near to the straight line, which indicates that the errors are normally distributed. Similarly, the plot run number versus internally studentized residuals is shown in Figure 7.23.1 (d). The plot shows that all residuals are falling between -30 to 30 . which is also has better agreement with the various literature reviews.

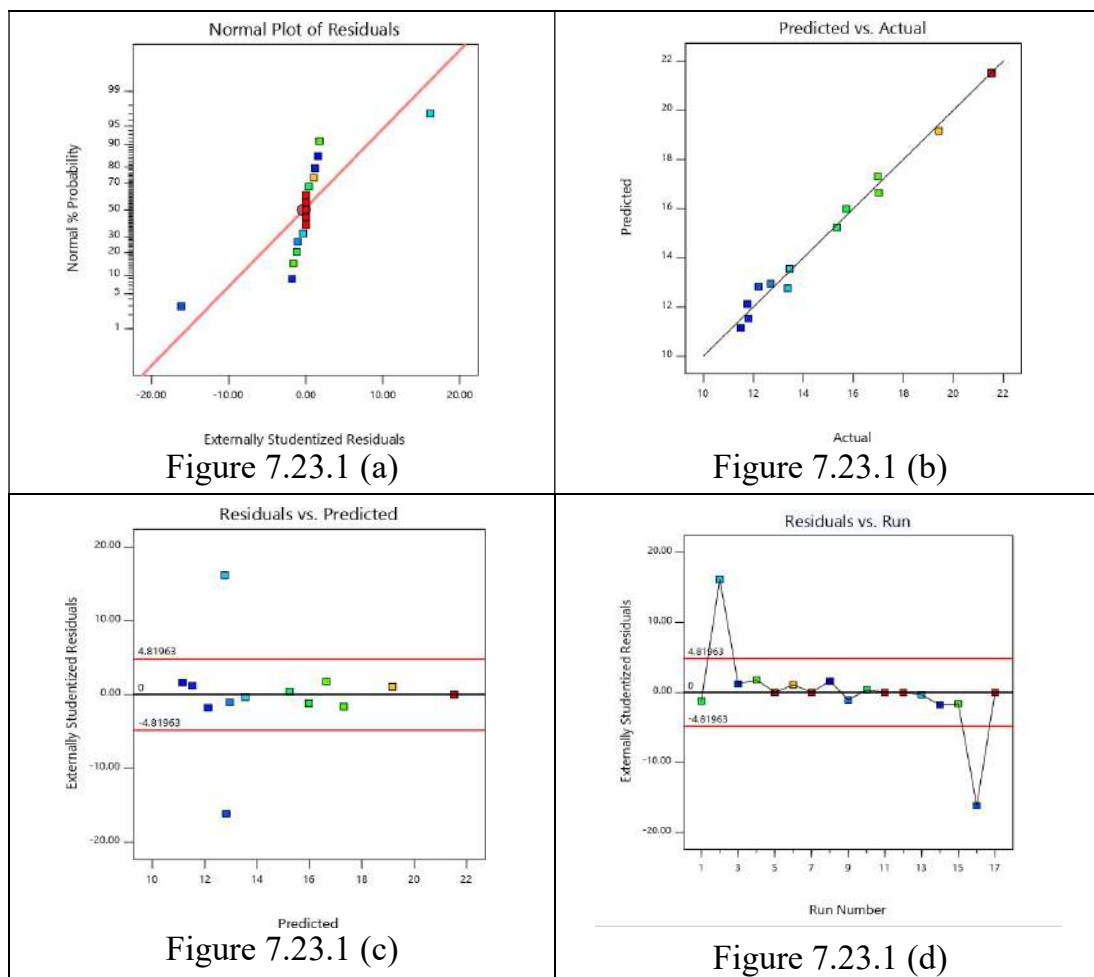


Figure 7.23.1(a) to (d) Various predicted, actual, run number, externally studentized residuals and normal % probability plots

Table 7.14 Results of ANOVA for Nugget diameter(AISI1020-AA1008)

Source	Sum of Squares	df	Mean Square	F-value	p-value	
Model	256.47	9	28.50	128.30	< 0.0001	significant
A-Power	57.04	1	57.04	256.81	< 0.0001	
B-Pressure	1.54	1	1.54	6.94	0.0337	
C-Time	1.34	1	1.34	6.05	0.0435	
AB	5.29	1	5.29	23.84	0.0018	
AC	0.0247	1	0.0247	0.1111	0.7487	
BC	2.58	1	2.58	11.63	0.0113	
A ²	36.48	1	36.48	164.25	< 0.0001	
B ²	56.45	1	56.45	254.14	< 0.0001	
C ²	76.41	1	76.41	344.02	< 0.0001	
Residual	1.55	7	0.2221			
Lack of Fit	1.55	3	0.5183			
Pure Error	0.0000	4	0.0000			
Cor Total	258.03	16				
		Std. Dev.	0.4713	R²		0.9940
		Mean	16.40	Adjusted R²		0.9862
		C.V. %	2.87	Predicted R²		0.9036
				Adeq Precision		28.6676

Coded equation

$$\begin{aligned}
 (\text{Nugget Diameter})^{1.59} = & 21.5114 + 2.67021 * A + 0.439006 * B + 0.409882 \\
 & * C + 1.15047 * AB + -0.0785426 * AC + 0.803548 * BC + -2.94354 * A^2 + \\
 & -3.6614 * B^2 + -4.25994 * C^2
 \end{aligned}
 \tag{7.6}$$

From the Table 7.14, the actual coefficient of determination of R^2 obtained from ANOVA table is 0.9940, which is less than the 1%. The adjacent coefficient of determination R^2 of the developed model is 0.9862 which is less than the actual R^2 , which indicates that the developed model is highly significant. Similarly the R^2 value and predicted R^2 value are in good agreement. The optimized ANOVA table for TSFL shows that the ability of the developed model to predict the parameters is about 99% confidence level and the p values are less than 0.001. The experimentally obtained values are in good agreement with predicted values. Based on the R^2 value, it is concluded that equation 7.6 is able to predict the TSFL more accurately and the results are highly reliable as stated in various literature.

7.3.3 Prediction of Process Parameters ERSW Welded SS-AL Dissimilar Joints Using ANOVA

This section illustrates the ANOVA response for TSFL, Microhardness, nugget diameter of ERSW joints welded at various input conditions for SS-AL dissimilar joints.

ANOVA results for TSFL analysis

The experimental values arrived according to the CCRD method is mentioned in Table 7.15. The experimental results will be examined through RSM to get the empirical relationship for good responses. The estimated values show that the relationship in or near the local and central point of the model. The all values within the confidence interval is about 99.5% with the adaption of F-test and design expert software package 9.0.31. The end model has been finalized after finding the coefficients of significance. The final mathematical model has been used to find and calculate the TSFL.

The final TSFL mathematical equation has been arrived and given in Equation 7.7, which has the coded variables A, B and C

Table 7.15 Results of ANOVA for TSFL(AIS5052-AA1008)

Source	Sum of Squares	df	Mean Square	F-value	p-value	
Model	7.88	9	0.8751	156.09	< 0.0001	significant
A-Power	4.05	1	4.05	721.63	< 0.0001	
B-Pressure	0.2168	1	0.2168	38.67	0.0004	
C-time	1.20	1	1.20	213.44	< 0.0001	
AB	0.0112	1	0.0112	2.00	0.1998	
AC	0.0344	1	0.0344	6.14	0.0424	
BC	0.4837	1	0.4837	86.28	< 0.0001	
A ²	1.32	1	1.32	235.32	< 0.0001	
B ²	0.2390	1	0.2390	42.63	0.0003	
C ²	0.1787	1	0.1787	31.87	0.0008	
Residual	0.0392	7	0.0056			
Lack of Fit	0.0392	3	0.0131			
Pure Error	0.0000	4	0.0000			
Cor Total	7.91	16				
		Std. Dev.	0.0749	R²	0.9950	
		Mean	2.69	Adjusted R²	0.9887	
		C.V. %	2.78	Predicted R²	0.9207	
				Adeq Precision	41.9888	

Coded Equation TSFL

$$3.165 + 0.711125 * A + 0.164625 * B + 0.38675 * C + -0.053 * AB + -0.09275 * AC + 0.34775 * BC + -0.55975 * A^2 + -0.23825 * B^2 + -0.206 * C^2 \quad (7.7)$$

From the table 7.15, the actual coefficient of determination of R^2 obtained from ANOVA table is 0.9950, which is less than the 1%. The adjacent coefficient of determination R^2 of the developed model is 0.9887 which is less than the actual R^2 , which indicates that the developed model is highly significant. Similarly the R^2 value and predicted R^2 value are in good agreement. The optimized ANOVA table for TSFL shows that the ability of the developed model to predict the parameters is about 99% confidence level and the p values are less than 0.001. The experimentally obtained values are in good agreement with predicted values. Based on the R^2 value, it is concluded that Equation 7.7 is able to predict the TSFL more accurately and the results are highly reliable as stated in various literature.

7.3.3.1.1 Checking of data and adequacy of the model

The plots externally studentized residual and internally studentized residuals are achieved by design expert software for TSFL as shown in Figure 7.24.1 (a) to (d). In that plots, the residuals are very near to the straight line, which indicates that the errors are normally distributed. Similarly, the plot run number versus internally studentized residuals is shown in Figure 7.24.1 (d). The plot shows that all residuals are falling between -6 to 6. Which is also has better agreement with the various literature reviews.

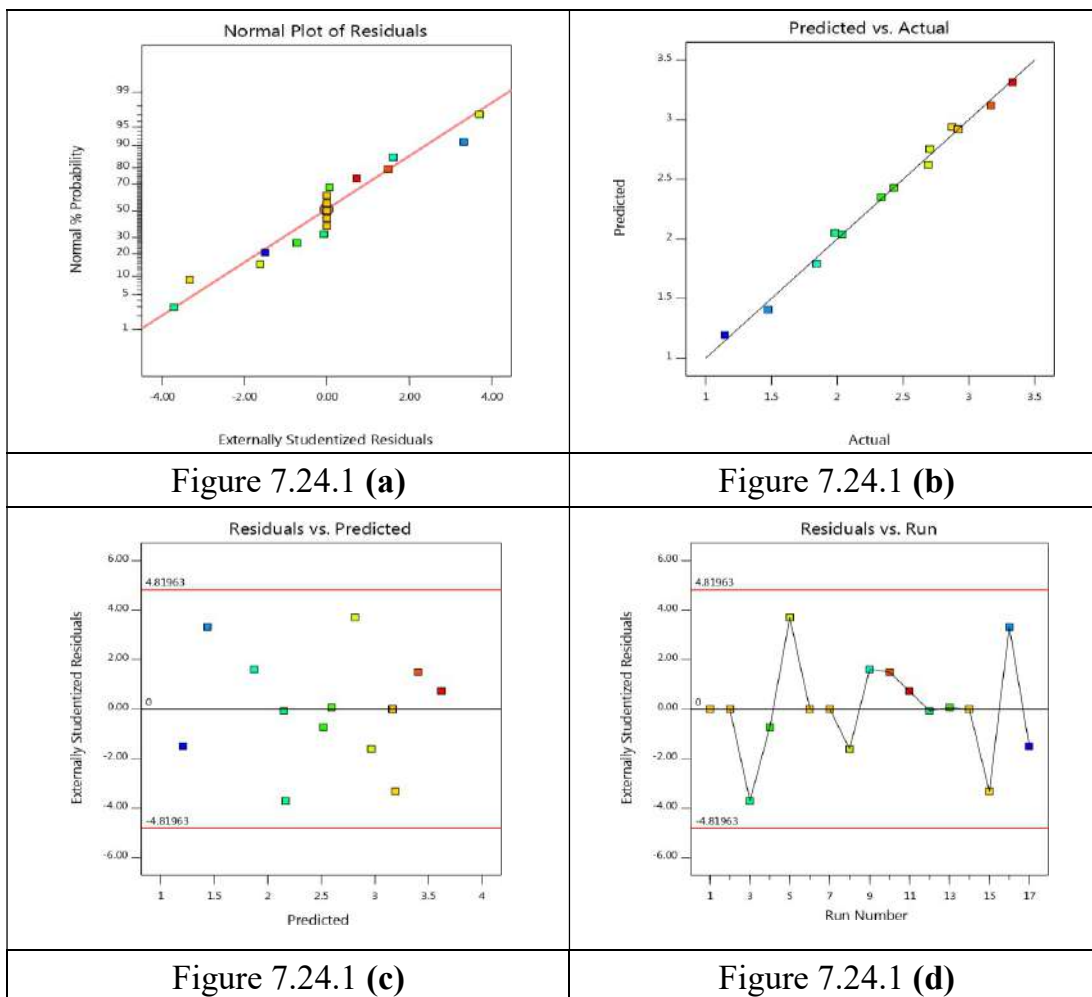


Figure 7.24.1(a) to (d) Various predicted, actual, run number, externally studentized residuals and normal % probability plots

ANOVA results for hardness analysis

The experimental values arrived according to the CCRD method is mentioned in Table 7.16. The experimental results will be examined through RSM to get the empirical relationship for good responses. The estimated values show that the relationship in or near the local and central point of the model. The all values within the confidence interval is about 99.5% with the adaption of F-test and design expert software package 9.0.31. The end model has been finalized after finding the coefficients of significance. The final mathematical model has been used to find and calculate the TSFL.

The final TSFL mathematical equation has been arrived and given in Equation 7.8, which has the coded variables A, B, and C.

7.3.3.2.1 Checking of data and adequacy of the model

The plots externally studentized residual and internally studentized residuals are achieved by design expert software for TSFL as shown in Figure 7.25.1 (a) to (d). In that plots, the residuals are very near to the straight line, which indicates that the errors are normally distributed. Similarly, the plot run number versus internally studentized residuals is shown in Figure 7.25.1 (d). The plot shows that all residuals are falling between -6 to 6. Which is also has better agreement with the various literature reviews.

Table 7.16 Results of ANOVA for Hardness(AIS5052-AA1008)

Source	Sum of Squares	df	Mean Square	F-value	p-value	
Model	2.581E-06	9	2.868E-07	71.18	< 0.0001	significant
A-Power	3.696E-07	1	3.696E-07	91.75	< 0.0001	
B-Pressure	2.207E-07	1	2.207E-07	54.80	0.0001	
C-time	9.098E-08	1	9.098E-08	22.58	0.0021	
AB	1.652E-11	1	1.652E-11	0.0041	0.9507	
AC	3.485E-08	1	3.485E-08	8.65	0.0217	
BC	7.765E-10	1	7.765E-10	0.1927	0.6739	
A ²	2.348E-07	1	2.348E-07	58.28	0.0001	
B ²	5.150E-07	1	5.150E-07	127.83	< 0.0001	
C ²	9.354E-07	1	9.354E-07	232.18	< 0.0001	
Residual	2.820E-08	7	4.029E-09			
Lack of Fit	2.820E-08	3	9.400E-09			
Pure Error	0.0000	4	0.0000			
Cor Total	2.609E-06	16				

Coded formula for hardness =

$$0.00281474 + -0.000214943 * A + -0.000166113 * B + -0.000106642 * C + 2.03217e-06 * AB + -9.3339e-05 * AC + 1.39329e-05 * BC + -0.000236128 * A^2 + -0.000349727 * B^2 + -0.000471328 * C^2 \quad (7.8)$$

From the table7.16, the actual coefficient of determination of R^2 obtained from ANOVA table is 0.9997, which is less than the 1%. The adjacent coefficient of determination R^2 of the developed model is 0.9993 which is less than the actual R^2 , which indicates that the developed model is highly significant. Similarly the R^2 value and predicted R^2 value are in good

agreement. the optimized ANOVA table for TSFL shows that the ability of the developed model to predict the parameters is about 99% confidence level and the p values are less than 0.001. The experimentally obtained values are in good agreement with predicted values. Based on the R^2 value, it is concluded that equation 7.8 is able to predict the TSFL more accurately and the results are highly reliable as stated in various literature.

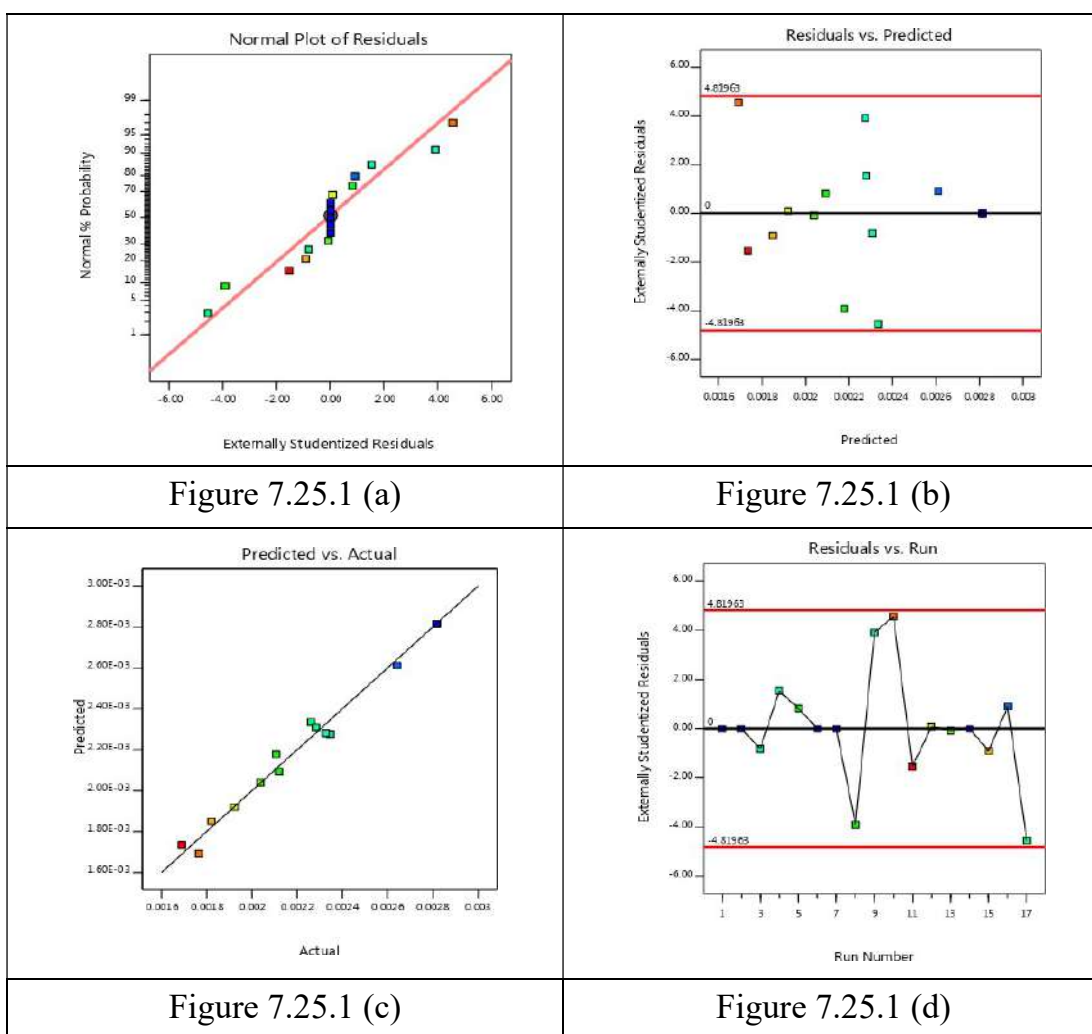


Figure 7.25.1(a) to (d) Various predicted, actual, run number, externally studentized residuals and normal % probability plots

ANOVA results for nugget diameter analysis

The experimental values arrived according to the CCRD method is mentioned in Table 7.17. The experimental results will be examined through RSM to get the empirical relationship for good responses. The estimated values show that the relationship in or near the local and central point of the model. The all values within the confidence interval is about 99.5% with the adaption of F-test and design expert software package 9.0.31. The end model has been finalized after finding the coefficients of significance. The final mathematical model has been used to find and calculate the TSFL

The final TSFL mathematical equation has been arrived and given in equation 7.9, which has the coded variables A, B and C

Table 7.17 Results of ANOVA for Nugget diameter (AIS5052-AA1008)

Model	0.0000	9	4.425E-06	72.75	< 0.0001	significant	
A-Power	9.004E-06	1	9.004E-06	148.03	< 0.0001		
B-Pressure	4.026E-06	1	4.026E-06	66.19	< 0.0001		
C-time	2.571E-06	1	2.571E-06	42.27	0.0003		
AB	2.792E-09	1	2.792E-09	0.0459	0.8365		
AC	1.671E-07	1	1.671E-07	2.75	0.1414		
BC	9.495E-08	1	9.495E-08	1.56	0.2517		
A ²	4.801E-06	1	4.801E-06	78.94	< 0.0001		
B ²	0.0000	1	0.0000	198.84	< 0.0001		
C ²	4.708E-06	1	4.708E-06	77.40	< 0.0001		
Residual	4.258E-07	7	6.082E-08				
Lack of Fit	4.258E-07	3	1.419E-07				
Pure Error	0.0000	4	0.0000				
Cor Total	0.0000	16					
			Std. Dev.	0.0002		R²	0.9894
			Mean	0.0105		Adjusted R²	0.9758
			C.V. %	2.35		Predicted R²	0.8307
						Adeq Precision	24.1041

Coded equation:

$$\begin{aligned} (\text{Nugget Diameter})^{-3} = & -0.706377 + 0.00517207 * \text{Power} + 0.306188 * \\ & \text{Pressure} + 0.0262357 * \text{time} + -2.64187\text{e-}05 * \text{Power} * \text{Pressure} + -8.17463\text{e-} \\ & 05 * \text{Power} * \text{time} + -0.00154066 * \text{Pressure} * \text{time} + -4.27137\text{e-}05 * \\ & \text{Power}^2 + -0.0423706 * \text{Pressure}^2 + -0.00422959 * \text{time}^2. \end{aligned} \quad (7.9)$$

From the Table 7.17, the actual coefficient of determination of R^2 obtained from ANOVA table is 0.9894, which is less than the 1%. The adjacent coefficient of determination R^2 of the developed model is 0.9758 which is less than the actual R^2 , which indicates that the developed model is highly significant. Similarly the R^2 value and predicted R^2 value are in good agreement. the optimized ANOVA table for TSFL shows that the ability of the developed model to predict the parameters is about 99% confidence level and the p values are less than 0.001. The experimentally obtained values are in good agreement with predicted values. Based on the R^2 value, it is concluded that Equation 7.9 is able to predict the TSFL more accurately and the results are highly reliable as stated in various literature.

7.3.3.3.1 Checking of data and adequacy of the model

The plots externally studentized residual and internally studentized residuals are achieved by design expert software for TSFL as shown in Figure 7.26.1 (a) to (d). In that plots, the residuals are very near to the straight line, which indicates that the errors are normally distributed. Similarly, the plot run number versus internally studentized residuals is shown in Figure 7.26.1 (c). The plot shows that all residuals are falling between -6 to 6. Which is also has better agreement with the various literature reviews.

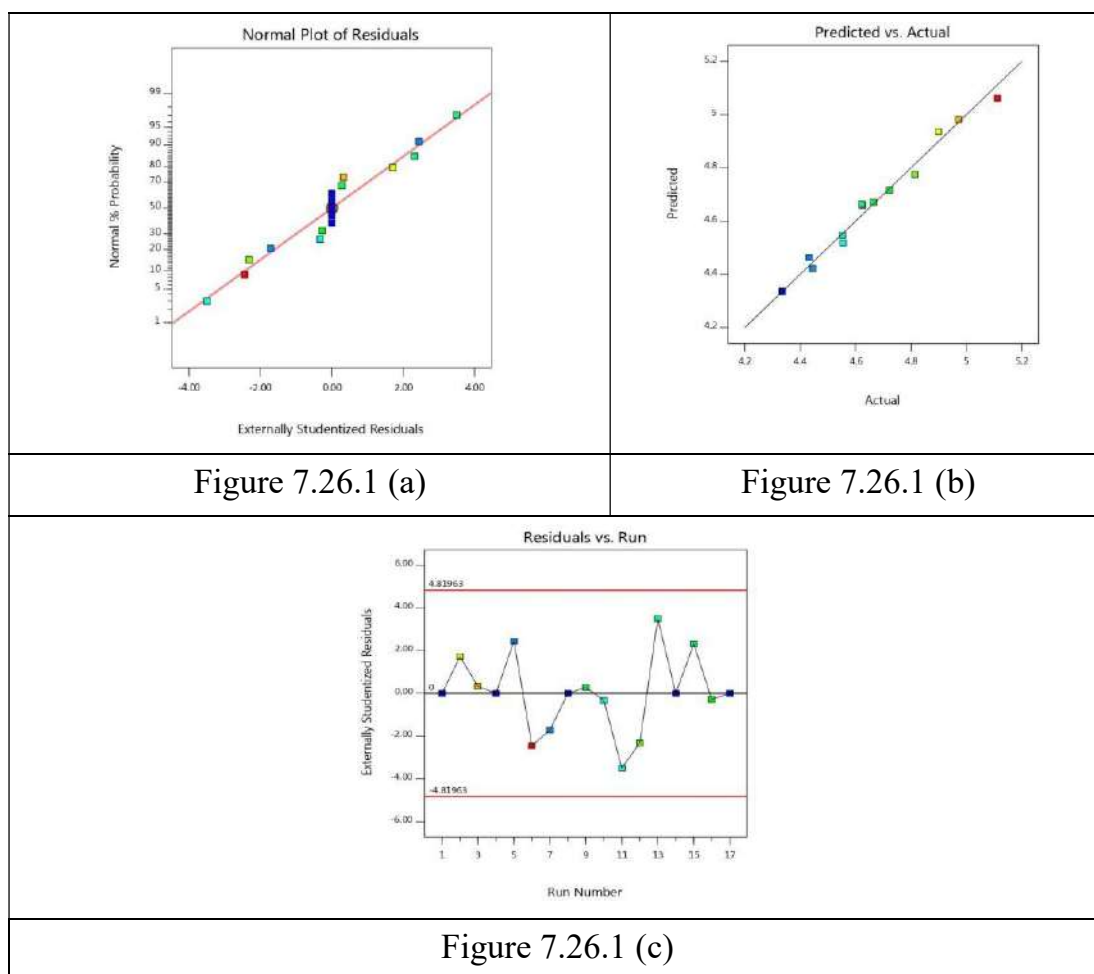


Figure 7.26.1(a) to (c) Various predicted, actual, run number, externally studentized residuals and normal % probability plots

RESULTS OF CORROSION STUDY

In the present world, scenario materials will fail much earlier due to the application in the certain intrinsic operating environment. Among this intrinsic operating environment corrosion failure is the one of the major failures as reported in various literature. Therefore, the testing of the material in corrosion environment is very important among the various corrosion test for evaluation of the corrosion rate, potensio dynamic polarization is the

predominant technique. In this technique, the potential of the electrode will be varied in different ranges by applying suitable current on the electrode. In this work the potentiodynamic polarization test was conducted on the AIS5052-AISI1020, AISI1020-AA1008 and AIS5052-AA1008 dissimilar joints welded using the ERSW process at the optimum parameters. The results obtained from this test are discussed in detail in the below sections.

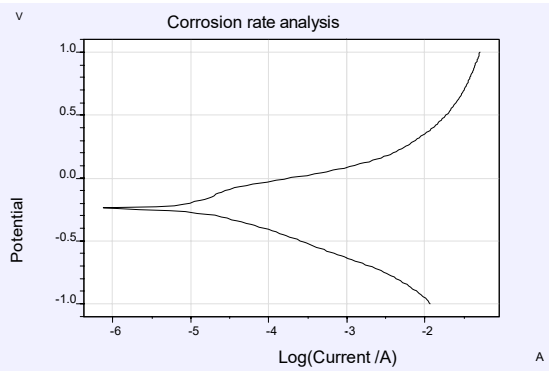
Corrosion Rate Analysis on AIS5052-AISI1020 dissimilar ERSW welded joints at optimum Condition

The potentiodynamic polarization test was carried out on the AIS5052-AISI1020 ERSW joint welded at the optimum condition and the sample used in this study are shown in figure 7.27.



Figure 7.27 Corrosion Tested Sample Image of AIS5052-AISI1020

The TAFEL data plot table 7.18 and TAFEL data model are shown in figure 7.28. From table 7.18 and figure 7.28 shows that the maximum corrosion is found that 2.103mm/y.

Table 7.18 Optimized Corrosion rate analysis		
E. corrV	-0.243	
i cor. A	391E-06	
I Cor. A/cm ²	0.000244	
RpOhm	5819	
baV/dec	0.161	
bcV/dec	0.078	
C. Rate mm/y	2.103	Figure 7.28 Corrosion rate analysis(optimized)

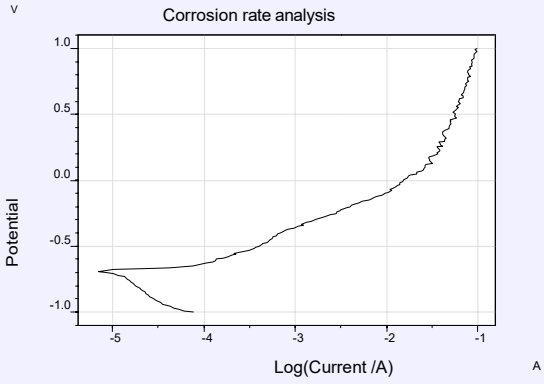
Corrosion Rate Analysis on AISI1020-AA1008 dissimilar ERSW welded joints at optimum Condition

The potentiodynamic polarization test was carried out on the AISI1020-AA1008 ERSW joint welded at the optimum condition and the sample used in this study are shown in figure 7.29.



Figure 7.29 Corrosion Tested Sample Image of AISI1020-AA1008

The TAFEL data plot table 7.19 and TAFEL data model are shown in figure 7.30. From table 7.19 and figure 7.30 shows that the maximum corrosion is found that 5.788mm/y.

Table 7.19 Optimized Corrosion rate analysis		
E. corrV	-0.6988	
i cor. A	1.08E-05	
I Cor. A/cm ²	0.000673	
RpOhm	2202	
baV/dec	0.062	
bcV/dec	0.471	
C. Rate mm/y	5.788	Figure 7.30 Corrosion rate analysis(optimized)

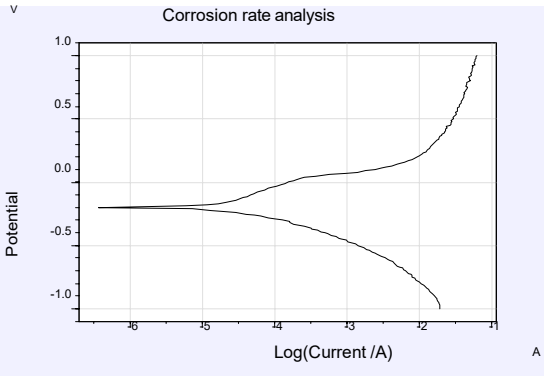
Corrosion Rate Analysis on AIS5052-AA1008 dissimilar ERSW welded joints at optimum Condition

The potentiodynamic polarization test was carried out on the AIS5052-AA1008 ERSW joint welded at the optimum condition and the sample used in this study are shown in figure 7.31.



Figure 7.31 Corrosion Tested Sample Image of AIS5052-AA1008

The TAFEL data plot table 7.20 and TAFEL data model are shown in figure 7.32. From table 7.20 and figure 7.32 shows that the maximum corrosion is found that 7.836mm/y.

Table 7.20 Optimized Corrosion rate analysis		
E. corrV	-0.2035	
i cor. A	1.46E-05	
I Cor. A/cm ²	0.000911	
RpOhm	2040	
baV/dec	0.206	
bcV/dec	0.103	
C. Rate mm/y	7.836	Figure 7.32 Corrosion rate analysis(optimized)

Comparison of corrosion rate of AIS5052-AISI1020, AISI1020-AA1008 and AIS5052-AA1008 joints.

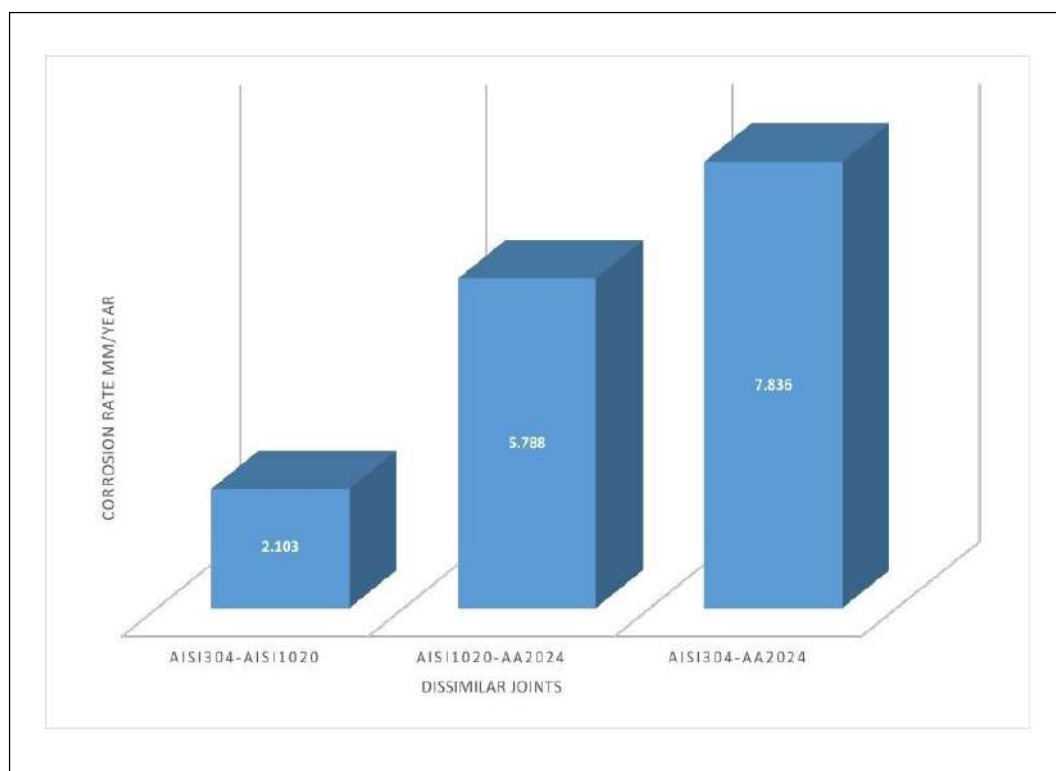


Figure 7.33 Corrosion rate of AIS5052-AISI1020, AISI1020-AA1008 and AIS5052-AA1008 joints

The corrosion rate of all the dissimilar joints welded at optimum process parameters is compared in figure 7.33. From the figure 7.33, it is identified that the maximum corrosion rate of AISI 304-AA2014 was 7.836mm/year. Similarly, the maximum corrosion rate of AISI1020-AA2014 was 5.788 mm/year and maximum corrosion rate of AISI 304-AISI1020 was 2.103mm/year. This results clearly show the lesser corrosion rate occurs on AIS5052-AISI1020 than AISI1020-AA1008 and AIS5052-AA1008.

7.6 SUMMARY

This chapter describes in detail about various test results obtained from a various mechanical tests such as TSFL, microhardness and nugget diameter. The metallurgical studies of SEM, EDAX and Factography test was also discussed. The corrosion test results of dissimilar joints were discussed in detail for optimum condition. The optimization and prediction results obtained for optimizing and predicting the ERSW weld process parameters using RSM and ANOVA was also discussed. The confirmation test results clearly indicate that the developed model is much accurate in predicting and optimizing the ERSW process parameters. The next chapter presents the major conclusion obtained from the detailed experimental and optimization study conducted in this present work.

CHAPTER 8

CONCLUSION AND SCOPE OF FUTURE WORK

From the elaborated experimental works and a computational study conducted based on the research objective and methodology the following important conclusions are drawn:

WELDING OF AISI 304 SIMILAR JOINTS USING ERSW WELDING PROCESS AT DIFFERENT WELD PRESSURE

From the experimental investigation carried out on welding of AISI 304 similar joints using ERSW welding process by varying the weld pressure and keeping the power and time as constant. The summarized results obtained from this study are given below:

1. From the TSFL results is identified that the maximum 1.85kN tensile strength was obtained for the sample weld at pressure 3.7Kgf. All the TSFL samples are failed at the nugget zone.
2. The hardness test results showed that for the ERSW welded samples are having higher hardness value at nugget zone when compared to the base region. When comparing the hardness value of the nugget zone welded at various weld pressures reveals that the maximum hardness value of 220.2 VHN was obtained from the sample weld at the weld pressure of 3.7kgf.

3. The macrostructure, microstructure, SEM image was taken at the nugget zone shows that the high hardness solidification mode. The nugget zone consists of coarse austenitic ferrite mode and similarly, the presence of high chromium content in AISI 304 promotes the formation of ferrite content. The increasing in weld pressure causes the reduction in the size of intermediate phasing which causes an increase in hardness and TSFL strength.
4. The fracture surface SEM images show fine dimples with large crest and trough high appearance. The fracture surface shows more ductile mode failure due to the presence of fine dimples.
5. The chemical characterization and elemental analysis of all the samples welded at various weld pressure are executed by EDAX analysis, which shows that the presence of iron-chromium and cobalt in the spot welded joints.
6. The TAFEL plotted obtained from the potentiodynamic polarization method for the ERSW sample welded at 3.5.kgf and 3.7 kgf weld pressure shows that the sample welded at 3.7kgf weld pressure posses low corrosion rate when compared to the sample weld at 3.5kgf weld pressure

WELDING OF AISI 1020(MS) SIMILAR JOINTS USING ERSW WELDING PROCESS AT DIFFERENT WELD PRESSURE

From the experimental investigation carried out on welding of AISI 1020 similar joints using ERSW welding process by varying the weld

pressure keeping power and time as constant. The summarized results obtained from this study are given below:

1. From the TSFL results is identified that the maximum 0.91kN tensile strength was obtained for the sample weld at pressure 3.5kgf all the TSFL samples are failed at the nugget zone.
2. The hardness test results showed that for the ERSW welded samples are having higher hardness value at nugget zone when compared to the base region. When comparing the hardness value of the nugget zone welded at various weld pressures reveals that the maximum hardness value of 267.5(VHN) was obtained from the sample weld at the weld pressure of 3.7kgf.
3. The macrostructure, microstructure, SEM image was taken at the nugget zone shows that the high hardness solidification mode. The nugget zone consists of coarse austenitic ferrite mode and similarly, the presence of high chromium content in AISI 1020 promotes the formation of ferrite content. The increase in weld pressure causes the reduction in the size of intermediate phasing, which causes an increase in hardness and TSFL strength.
4. The fracture surface SEM images show fine dimples with large crest and trough high appearance. The fracture surface showed more ductile mode failure due to the presence of fine dimples.
5. The chemical characterization and elemental analysis of all the samples welded at various weld pressure are executed by EDAX analysis, which shows that the presence of iron, chromium, and cobalt in the spot welded joints.

6. The TAFEL plotted obtained from the potentiodynamic polarization method for the ERSW sample welded at 3.3kgf and 3.7kgf weld pressure shows that the sample welded at 3.7kgf weld pressure possess low corrosion rate when compared to the sample weld at 3.5kgf weld pressure.

OPTIMIZATION OF WELD INPUT PROCESS PARAMETERS ON MECHANICAL PROPERTIES AND NUGGET DIAMETER OF ERSW AIS5052-AISI1020, AISI1020-AA1008 AND AIS5052-AA1008 DISSIMILAR JOINTS USING RSM TECHNIQUE

For the identification of influencing of ERSW process parameters on dissimilar joints the weld trials are carried out on AIS5052-AISI1020, AISI1020-AA1008 AND AIS5052-AA1008 dissimilar joints and its corresponding mechanical properties and nugget diameter are investigated. In this work, the RSM model was used to optimize the weld input process parameters. The experimental trials were carried out based on the central composite rotatable design (CCRD) model and the following conclusions are drawn:

Optimization using RSM for AIS5052-AISI1020 Joints

In the RSM optimization technique, central composite rotatable design model design was applied to identify the most dominant ERSW weld process parameters that influence the mechanical properties and nugget diameter of AIS5052-AISI1020 joints and the following conclusions are inferred

1. The full factorial CCRD model involves 3 independents at 3 level where applied which addresses the various ranges of power, time and weld pressure.
2. The regression analysis was carried out and a (cubic or quadratic) model was developed. From the regression analysis, the various response surface and contour plots were obtained.
3. For TSFL, hardness and nugget diameter as a function of ERSW weld input process parameter were analyzed. The developed RSM model reveals that the optimal TSFL strength, microhardness and nugget diameter was obtained. For the sample welded at the power of 55W weld time 1.5 seconds and weld pressure 3.5Kgf.
4. This study also reveals that the developed RSM model can accurately find out the optimum ERSW weld input process parameters for welding of AIS5052-AISI1020 joints.
5. Similarly, the confirmation experiments are conducted in order to check the accuracy of the developed model and it is identified that the predicted values for each response variable are much closer to the experimentally obtained value from the confirmation test. The percentage of error obtained between the predicted and experimental values are within the permitted level.
6. Therefore, it clearly implies that the developed mathematical model can efficiently use to predict the TSFL, microhardness and nugget diameter for any combination of current, time and welding pressure within the range of performed experimentation.

7. The RSM technique can able to model the response in terms of significant parameters their interaction and square terms.
8. The results obtained from the RSM model for welding of AIS5052-AISI1020 dissimilar joints using ERSW process reveals that the weld pressure is the most influencing process parameter followed by current and time.

Optimization using RSM for AIS5052-AA1008 Joints

In the RSM optimization technique, central composite rotatable design model design was applied to intensity the most dominant ERSW weld process parameters that influences the mechanical properties and nugget diameter of AIS5052-AA1008 joints and the following conclusions are inferred

1. The full factorial CCRD model involves 3 independents at 3 level where applied which addresses the various ranges of power, time and weld pressure.
2. The regression analysis was carried out and a (cubic or quadratic) model was developed. From the regression analysis, the various response surface and contour plots were obtained.
3. For TSFL, hardness and nugget diameter as a function of ERSW weld input process parameter were analyzed. The developed RSM model reveals that the optimal TSFL strength, microhardness and nugget diameter was obtained. For the sample welded at the current of 55W weld time 1.5seconds and weld pressure 3.5Kgf

4. This study also reveals that the developed RSM model can accurately find out the optimum ERSW weld input process parameters for welding of AISI1020-AL joints.
5. Similarly, the confirmation experiments are conducted in order to check the accuracy of the developed model and it is identified that the predicted values for each response variable are much closer to the experimentally obtained value from the confirmation test. The percentage of error obtained between the predicted and experimental values are within the permitted level.
6. Therefore, it clearly implies that the developed mathematical model can efficiently use to predict the TSFL, microhardness and nugget diameter for any combination of current, time and welding pressure within the range of performed experimentation.
7. The RSM technique can able to model the response in terms of significant parameters their interaction and square terms.
8. The results obtained from the RSM model for welding of AISI1020-AL dissimilar joints using ERSW process reveals that the weld pressure is the most influencing process parameter followed by current and time.

Optimization using RSM for AISI1020-AA1008 Joints

In the RSM optimization technique, central composite rotatable design model design was applied to identify the most dominant ERSW weld process parameters that influence the mechanical properties and nugget diameter of AISI1020-AA1008 joints and the following conclusions are inferred

1. The full factorial CCRD model involves 3 independents at 3 level where applied which addresses the various ranges of power, time and weld pressure.
2. The regression analysis was carried out and a (cubic or quadratic) model was developed. From the regression analysis, the various response surface and contour plots were obtained.
3. For TSFL, hardness and nugget diameter as a function of ERSW weld input process parameter were analyzed. The developed RSM model reveals that the optimal TSFL strength, microhardness and nugget diameter was obtained. For the sample welded at the power of 55 W weld time 1.5 seconds and weld pressure 3.5 Kgf
4. This study also reveals that the developed RSM model can accurately find out the optimum ERSW weld input process parameters for welding of SS-AL joints.
5. Similarly, the confirmation experiments are conducted in order to check the accuracy of the developed model and it is identified that the predicted values for each response variable are much closer to the experimentally obtained value from the confirmation test. The percentage of error obtained between the predicted and experimental values are within the permitted level.
6. Therefore, it clearly implies that the developed mathematical model can efficiently use to predict the TSFL, microhardness and nugget diameter for any combination of current, time and welding pressure within the range of performed experimentation.

7. The RSM technique can able to model the response in terms of significant parameters their interaction and square terms.
8. The results obtained from the RSM model for welding of AISI1020-AA1008 dissimilar joints using ERSW process reveals that the weld pressure is the most influencing process parameter followed by current and time.

PREDICTION OF TSFL, MICROHARDNESS AND NUGGET DIAMETER ON ERSW WELDED AIS5052-AISI1020, AISI1020-AA1008 AND AIS5052-AA1008 DISSIMILAR JOINTS USING ANOVA

ANOVA was used to predict the TSFL, microhardness and nugget diameter of AIS5052-AISI1020, AISI1020-AA1008 AND AIS5052-AA1008 dissimilar joints, The ANOVA model was developed based on the data obtained from the experimental results. The following conclusions drawn from the ANOVA analysis was discussed in this session:

Prediction of TSFL, Micro Hardness and Nugget Diameter on ERSW AIS5052-AISI1020 Dissimilar Joint Using ANOVA

1. In this work, the ANOVA model was developed and the accuracy of the developed model for predicting the output values was tested against the experimentally obtained values. It was identified that the developed ANOVA model can able to produce the best performance.
2. The predictive capacity of the ANOVA model can be checked in terms of various statistical parameters calculated such as coefficient of determination R- square value.

3. The comparison of experimental values and predicted values obtained by ANOVA model reveal that the coefficient of determination for ANOVA is closure to unity.
4. From the ANOVA model for predicting the output parameters for SS-AISI1020 dissimilar joints, it is identified that the maximum TSFL 10.5kN micro hardness 256VHN and nugget diameter 3.8mm was obtained for the input parameter of power (65W), Pressure (3.8kgf) and time(2sec)

Prediction of TSFL, Micro Hardness and Nugget Diameter on ERSW Welded AIS5052-AA1008 Dissimilar Joint Using ANOVA

1. In this work, the ANOVA model was developed and the accuracy of the developed model for predicting the output values was tested against the experimentally obtained values. It was identified that the developed ANOVA model can able to produce the best performance.
2. The predictive capacity of the ANOVA model can be checked in terms of various statistical parameters calculated such as coefficient of determination R- square value.
3. The comparison of experimental values and predicted values obtained by ANOVA model reveal that the coefficient of determination for ANOVA is closure to unity.
4. From the ANOVA model for predicting the output parameters for AIS5052-AA1008 dissimilar joints is identified that the maximum TSFL10.5kN, microhardness 289VHN and nugget diameter .33mm obtained for the input parameter of power (65W), Pressure (3.8kgf) and time(2sec)

Prediction of TSFL, Micro Hardness and Nugget Diameter on ERSW Welded AISI1020-AA1008 Dissimilar Joint Using ANOVA

1. In this work, the ANOVA model was developed and the accuracy of the developed model for predicting the output values was tested against the experimentally obtained values. It was identified that the developed ANOVA model can able to produce the best performance.
2. The predictive capacity of the ANOVA model can be checked in terms of various statistical parameters calculated such as coefficient of determination R- square value.
3. The comparison of experimental values and predicted values obtained by ANOVA model reveal that the coefficient of determination for ANOVA is closure to unity.
4. From the ANOVA model for predicting the output parameters for AISI1020-AA1008 dissimilar joints is identified that the maximum TSFL 10.5kN, microhardness 300VHN and nugget diameter 4.4 mm obtained for the input parameter of power (65W), Pressure (3.8kgf) and time(2sec)

FUTURE WORK

Based on the conclusion drawn in this work the following future work was identified for further investigation:

1. The experimental investigation may also be carried out on the welded joints under fatigue, creep and high-temperature applications.

2. The other optimization techniques such as ANN, Genetic Algorithm, Taguchi method can be applied for optimization and prediction of the weld input process parameters.
3. The various simulation software such as ANSYS, SYSWELD can be applied for simulation of an ERSW process parameter in identifying the temperature distribution and the same can be compared with the experimental results.
4. The comparison study may be conducted by changing the various electrode material in ERSW process.
5. The comparative study may be carried out by conducting welding using various another weld process such as laser welding, electron beam welding, friction stir welding etc on and AIS5052-AISI102 AA1008 compared with the ERSW process.

REFERENCES

1. Ahmet Hasanbasoglu & Ramazan Kaçar 2007, 'Resistance spot weldability of dissimilar materials (AISI 316L–DIN EN 10130-99 steels)' *Materials and Design* vol. 28, pp. 1794–1800.
2. Akkas, N, Ferikb, E, İlhana, E & Aslanlarb, S 2016, 'The Effect of Welding Current on Nugget Sizes in Resistance Spot Welding of SPA-C Steel Sheets Used in Railway Vehicles', 2nd International Conference on Computational and Experimental Science and Engineering (ICCESEN 2016), vol. 130, pp. 142-144.
3. Alenius, M, Pekka Pohjanne, Somervuori, M & Hannu Hänninen 2006, 'Exploring the Mechanical Properties of Spot Welded Dissimilar Joints for Stainless and Galvanized Steels', *Welding Journal*, pp. 305-313.
4. Alizadeh-Sh, M, Marashi, SPH & Pournvari, M 2013, 'Resistance spot welding of AISI 430 ferritic stainless steel: Phase transformations and mechanical properties', *Materials and Design ELSEVIER*, vol. 58, pp. 258-267.
5. Anurag Tewari & Ekta Rawat 2017, 'A Review Paper on Optimization of Process Parameter of Resistance Spot Welding', *International Journal for Research in Applied Science & Engineering Technology (IJRASET)*, vol. 5, pp. 24-27.
6. Aravinthan Arumugam & MohdAmizi Nor 2015, 'Spot Welding Parameter Optimization To Improve Weld Characteristics For Dissimilar Metals', *International Journal Of Scientific & Technology Research*, vol. 4, pp. 75-80.
7. Aslanlar, S 2006, 'The effect of nucleus size on mechanical properties in electrical resistance spot welding of sheets used in automotive industry', *Materials and Design ELSEVIER*, vol.27, pp. 125–131.

8. Baca, N, Ngo, TT, Conner, RD & Garrett, SJ 2013, 'Small-scale resistance spot welding of Cu₄₇Ti₃₄Zr₁₁Ni₈ (Vitreloy 101) bulk metallic glass', *Journal of Materials Processing Technology*, vol. 213, pp. 2042–2048.
9. Boriwal Lokesh, Sarviya, RM & Mahapatra, MM 2015, 'Review On Modeling Of Resistance Spot Welding Process', *American International Journal of Research in Science, Technology, Engineering & Mathematics*, vol. 15, pp. 154-159.
10. Brauser, S, Pepke, LA, Weber, G & Elsevier 2010, 'Deformation behavior of spot-welded high strength steels for automotive applications', *Materials Science and Engineering A*, vol. 527, pp. 7099–7108.
11. Chetan R Patel & Dhaval A Patel 2012, 'Effect Of Process Parameters On The Strength Of Aluminium Alloy A5052 Sheets Joint Welded By Resistance Spot Welding With Cover Plates', *International Journal of Engineering Research and Applications (IJERA)* ISSN: 2248-9622, vol. 2, pp. 1081-1087.
12. CHO, Y & Rhee, S 2003, 'Experimental Study of Nugget Formation in Resistance Spot Welding', *Welding Journal*, pp. 195-201.
13. Choughule, PP, Biradar, AK & Modi, AK 2016, 'Resistance Spot Weldability of Dissimilar Materials in 1 MM Thick Sheet', *Journal of Mechanical Engineering and Technology (JMET)*, vol. 4, issue 1, pp. 15–21, Article ID: JMET_04_01_003.
14. Darwish, SM 2003, 'Weld bonding strengthens and balances the stresses in spot welded dissimilar thickness joints', *Journal of Materials Processing Technology*, vol. 134, pp. 352-362.
15. Dawei Zhao, Yuanxun Wang, Suning Sheng & Zongguo Lin 2013, 'Real time monitoring weld quality of small scale resistance spot welding for titanium alloy', *Measurement ELSEVIER*, vol. 46, pp. 1957-1963.
16. Dickinson, DW, Franklin, JE & Stanya A 1980, 'Characterization of Spot Welding Behavior by Dynamic Electrical Parameter Monitoring', *Welding Research supplements Journal*, pp. 170-176.

17. Dursun O Zyurek 2007, 'An effect of weld current and weld atmosphere on the resistance spot weldability of 304L austenitic stainless steel' *Materials and Design ELSEVIER*, vol. 29, pp. 597-693.
18. Emel Taban, Jerry E Gould, John C Lippold 2010, 'Dissimilar friction welding of 6061-T6 aluminum and AISI 1018 steel: Properties and microstructural characterization', *Materials and Design ELSEVIER*, vol. 31, pp. 2305-2311.
19. Emil Spisak *et al.* 2013, 'Influence of Corrosive Environment on the Surface Quality of Spot Welds', *AMS*, vol. 15, no.4, pp. 00126-11.
20. Farzeen Shahid, Abid Ali Khan & Saqib Hameed, M 2015, 'Mechanical and Microstructural Analysis of Dissimilar Metal Welds', [www.arpapress.com/ Volumes/ Vol25Issue1/ IJRRAS](http://www.arpapress.com/Volumes/Vol25Issue1/IJRRAS)
21. Fatih Hayat 2011, 'The effects of the welding current on heat input, nugget geometry, and the mechanical and fractural properties of resistance spot welding on Mg/Al dissimilar materials' *Materials and Design*, vol. 32, pp. 2476–2484.
22. Feramuz Karcı, Ramazan Kaçar & Süleyman Gündüz 2009, 'The effect of process parameter on the properties of spot welded cold deformed AIS5052 grade austenitic stainless steel' *Journal of Materials Processing Technology*, vol. 209, pp. 4011-4019.
23. Florea, RS, Bammann, DJ, Yeldell, A, Solanki, KN & Hammi, Y 2013, 'Welding parameters influence on fatigue life and microstructure in resistance spot welding of 6061-T6 aluminum alloy', *Materials and Design ELSEVIER*, vol. 45, pp. 456–465.
24. Hamid Eisazadeh, Mohsen Hamedi & Ayob Halvae 2010, 'New parametric study of nugget size in resistance spot welding process using finite element method', *Materials and Design*, vol. 31, pp. 149–157.
25. Hao, M, Osman, KA, Boomer, DR & Newton, CJ 1996, 'Developments in Characterization of Resistance Spot Welding of Aluminum', *Supplement To The Welding Journal by the American Welding Society and the Welding Research Council*, pp. 1-8.

26. Hatsuhiko Oikawa Tatsuya Sakiyama, Tadashi Ishikawa, Gen Murayama & Yasuo Takahashi 2007, 'Resistance Spot Weldability of High Strength Steel (HSS) Sheets for Automobiles', Nippon Steel Technical Report, no. 95.
27. Hayriye Ertek Emre & Ramazan kacar 2016, 'Resistance Spot Weldability of Galvanize Coated and Uncoated TRIP Steels', *Metals* 2016, 6, 299; DOI:10.3390/met6120299 www.mdpi.com/journal/metals.
28. Hessamoddin Moshayedi & Iradj sattari far 2012, 'Numerical and experimental study of nugget size growth in resistance spot welding of austenitic stainless steels', *Journal of Materials Processing Technology*, vol. 212, pp. 347– 354.
29. Jae Hyung Kim, Yongjoon Cho & Yong Hoon Jang 2013, 'Estimation of the weldability of single-sided resistance spot welding', *Journal of Manufacturing Systems*, vol. 32, pp. 505– 512.
30. Jamasri, MN & Ilman R Soekrisno Triyono 2011, 'Corrosion Fatigue Behaviour Of Resistance Spot Welded Dissimilar Metal Welds Between Carbon Steel And Austenitic Stainless Steel With Different Thickness', *Procedia Engineering ELSEVIER ICM 11*, vol. 10, pp. 649-654.
31. Jan Vinas, Lubos Kascak & Milan Abel 2012, 'Analysis of Materials for Resistance Spot Welding Electrodes', *Analysis of Materials for Resistance CODEN STJSAO ISSN 0562-1887*, vol. 54, pp. 393-397.
32. Jeevan A Karande & Inamdar, KH 2017, 'Effect of Process Parameters on Resistance Spot Welding - A Review', *Welding Journal*, pp. 195-201.
33. Khan, MS, Bhole, SD, Chen, DL, Biro, E, Boudreau, G & van Deventer, J 2009, 'Welding behavior, microstructure and mechanical properties of dissimilar resistance spot welds between galvanized HSLA350 and DP600 steels', *Science and Technology of Welding and Joining*, vol. 14, no. 7, pp. 616-625.
34. Kishore, N, Sreenu, S, Ramachandran, N & Allesu, K 2014, 'Parametric Studies and Finite Element Analysis of Welded Steel in Resistance Spot Welding Process' the International & 26th All India Manufacturing Technology, Design and Research Conference (AIMTDR 2014) December 12th–14th, 2014, IIT Guwahati, Assam, India.

35. Ladislav Kolarik, Miroslav Sahul, Marie Kolarikova, Martin Sahul, Milan Turna & Michal Felix 2012, 'Resistance Spot Welding of dissimilar Steels', *Acta Polytechnica*, vol. 52, no. 3/2012, pp. 43-47.
36. Liang, D, Sowards, JW, Frankel, GS, Alexandrov, BT & Lippold, JC 2010, 'Corrosion resistance of welds in type 304L stainless steel made with a nickel-copper-ruthenium welding consumable', *Corrosion Science*, vol. 52, pp. 2439–2451.
37. Makwana Brijesh, V, Shah Jay, D & Bhatt Jayant, A 2017, 'Effect of Process Parameters for Resistance Spot Welding Process using Taguchi Method for 2.0mm Sheet Thickness', *International Journal of Science and Research (IJSR)*, vol. 6, pp. 705-710.
38. Manoj Raut & Vishal Achwal 2014, 'Optimization of Spot Welding Process Parameters For Maximum Tensile Strength', *International Journal of Mechanical Engineering and Robotics Research*, vol. 3, pp. 506-517.
39. Marashi, P, Pouranvari, M, Amirabdollahian, S, Abedi, A & Goodarzi, M 2007, 'Microstructure and failure behavior of dissimilar resistance spot welds between low carbon galvanized and austenitic stainless steels', *Materials Science and Engineering A* 480, pp. 175–180
40. Marashi, P, Pouranvari, M, Sanaee, SMH, Abedi, A, Abootalebi, SH & Goodarzi, M 2008, 'Relationship between failure behavior and weld fusion zone attributes of austenitic stainless steel resistance spot welds', *Materials Science and Technology*, vol. 24, no. 12, pp. 1506-1512.
41. Martín, O, De Tiedra, P, López, M & San-Juan, M 2012, 'Combined Effect of Resistance Spot Welding and Post-Welding Sensitization on the Pitting Corrosion Behavior of AISI 304 Stainless Steel', *NACE International Corrosion Science Section ISSN 0010-9312*, vol. 69, pp. 268-275.
42. Masoud Alizadeh-Sh, Pirooz Marashi & Majid Pouranvari 2014, 'Microstructure-properties relationships in martensitic stainless steel resistance spot welds', *Science and Technology of Welding and Joining*, vol. 19, pp. 595-602.

43. Massoud Goodarzi, Pirooz Marashi & Majid Pouranvari 2009, 'Dependence of overload performance on weld attributes for resistance spot welded galvanized low carbon steel', *Journal of Materials Processing Technology*, vol. 209, pp. 4379–4384.
44. Mathew Vinoth, T & Saravanan, M 2016, 'Parametric Study in Spot Welding for Dissimilar Weld Joints', *International Journal of Innovative Research in Science, Engineering and Technology*, vol. 5, pp. 10704-10711.
45. Mehdi Jafari Vardanjani, Jacek Senkara & Alireza Araee 2016, 'A Review of Shunting Effect in Resistance Spot Welding', *Prezeglad Spawalnictwa ICI Journals*, vol. 88, no. 1/2016, pp. 46-50.
46. Milan Brozek, Alexandra Novakova & Ota Niedermeier 2017, 'Resistance Spot Welding of Steel Sheets of the Same and Different Thickness', *Acta Universitatis Agriculturae Et Silviculturae Mendelianae Brunensis*, vol. 65, pp. 807-814.
47. Min jou 2003, 'Real time monitoring weld quality of resistance spot welding for the fabrication of sheet metal assemblies' *Journal of Materials Processing Technology*, vol. 132, pp. 102–113.
48. Mircea Burca & Loan Lucaciu 2013, 'Research On Weld Nuts Fixed By Resistance Welding', *Annals of the Oradea University Fascicle of Management and Technological Engineering*, vol. 3, pp. 15-20.
49. Mustafa Acarer, Hayrettin Ahlatci & Fatih Hayat 2013, 'Investigation of corrosion properties of uncoated and hot dip galvanized dual phase steel (DP450) welded using spot welding', vol. 8, no. 20, pp. 815-822, DOI 10.5897/SRE11.800 ISSN 1992-2248 © 2013 Academic Journals.
50. NIED, HA 1983, 'The Finite Element Modeling of the Resistance Spot Welding Process', *Welding Research Supplement*, pp.123-132.
51. Nizamettin Kahraman 2007, 'The influence of welding parameters on the joint strength of resistance spot-welded titanium sheets', *Materials and Design Elsevier*, vol. 28, pp. 420-427.
52. Oikawa, H, Ohmiya, S, Yoshimura, T & Saitoh, T 1999, 'Resistance spot welding of steel and aluminium sheet using insert metal sheet', *Science and Technology of Welding and Joining*, vol. 4, pp. 80-88.

53. Oscar Martín, Pilar De Tiedra, Manuel López, Manuel San-Juan, Cristina García, Fernando Martín & Yolanda Blanco 2009, 'Quality prediction of resistance spot welding joints of 304 austenitic stainless steel' *Materials and Design*, vol. 30, pp. 68-77.
54. Panchakshar, AS & Kadam, MS 2013, 'Comparative Study of Responses of Resistance Spot Welding Obtained From Genetic Algorithm, Response Surface and D-Optimal Method', *International Journal of Engineering Science and Innovative Technology (IJESIT)*, vol. 2, pp. 597-601.
55. Pandey, AK, Khan, MI & Moeed, KM 2013, 'Optimization Of Resistance Spot Welding Parameters Using Taguchi Method', *International Journal of Engineering Science and Technology (IJEST)*, vol. 5, pp. 234-241.
56. Pasquale Russo Spena, Stefano Rossi & Rudi Wurzer 2017, 'Effects of Welding Parameters on Strength and Corrosion Behavior of Dissimilar Galvanized Q&P and TRIP Spot Welds', *Metals* 2017, vol. 7, p. 534; doi:10.3390/met7120534 www.mdpi.com/journal/metals.
57. Patel, VK, Bhole, SD & Chen, DL 2011, 'Microstructure and mechanical properties of dissimilar welded Mg-Al joints by ultrasonic spot welding technique', *Science and Technology of Welding and Joining*, vol. 17, no. 3, pp. 202-206.
58. Penner, P, Liu, L, Gerlich, A & Zhou, Y 2014, 'Dissimilar Resistance Spot Welding of Aluminum to Magnesium with Zn Coated Steel Inter layers', June 2014 / *Welding Journal*, pp. 226-231.
59. Pereira, AM, Ferreira, JM, Loureiro, A, Costa, JDM & Bártoolo, PJ 2010, 'Effect of process parameters on the strength of resistance spot welds in 6082-T6 aluminium alloy', *Materials and Design Elsevier*, vol. 31, pp. 2454-2463.
60. Pouranvari, M & Marashi, SPH 2008, 'Failure Mode of Dissimilar Resistance Spot Welds Between Austenitic Stainless and Low Carbon Steels', *Materials Science and Engineering ELSEVIER*, vol. 48, pp. 175-180.

61. Pouranvari, M, Mousavizadeh, SM, Marashi, SPH & Ghorbani, M 2011, 'Influence of fusion zone size and failure mode on mechanical performance of dissimilar resistance spot welds of AISI 1008 low carbon steel and DP600 advanced high strength steel', *Materials and Design*, vol. 32, pp. 1390–1398.
62. Pouranvari, M, Sobhani, S & Goodarzi, F 2018, 'Resistance spot welding of MS1200 martensitic advanced high-strength steel: Microstructure-properties relationship', *Journal of Manufacturing Processes ELSEVIER*, vol. 31, pp. 867-874.
63. Pradeep, M 2014, 'Process Parameter Optimization in Resistance Spot Welding of Dissimilar Thickness Materials', *International Journal of Mechanical and Mechatronics Engineering*, vol. 8 1/2014, pp. 80-83.
64. Prasad S Salke & Kailash C Bhosale 2016, 'Optimization of a Process parameter in Resistance spot welding for unequal thickness sheet using the Grey Relational Analysis', *International Research Journal of Engineering and Technology (IRJET)*, vol. 3 8/2016, pp. 908-912.
65. Quanfeng Song, Wenqi Zhang & Niels Bay 2005, 'An Experimental Study Determines the Electrical Contact Resistance in Resistance Welding', *Welding Journal*, vol. 4, pp. 73-75.
66. Ranfeng Qiu Shinobu Satonaka & ChihiroI wamoto 2010, 'Effect of interfacial reaction layer continuity on the tensile strength of resistance spot welded joints between aluminum alloy and steels', *Materials and Design*, vol. 30, pp. 3686–3689.
67. Ranfeng Qiu, Hongxin Shi, Keke Zhang, Yimin Tu, ChihiroI Wamoto & Shinobu Satonaka 2008, 'Interfacial characterization of joint between mild steel and aluminum alloy welded by resistance spot welding', *Materials Characterization*, vol. 61, pp. 684-688.
68. Rogeon, P, Carre, P, Costa, J, Sibilia, G & Saindrenan, G 2008, 'Characterization of electrical contact conditions in spot welding assemblies', *Journal Of Materials Processing Technology*, vol. 1, pp. 117–124.
69. Shah, LH, Akhtar, Z & Ishak, M 2013, 'Dissimilar metal joining of aluminum alloy to galvanized steel with Al–Si, Al–Cu, Al–Si–Cu and Zn–Al filler wires', *Journal of Materials Processing Technology*, vol. 212, pp. 458– 464.

70. Shashi Dwivedi & Satpal Sharma 2016, 'Optimization of Resistance Spot Welding Process Parameters on Shear Tensile Strength of SAE 1010 steel sheets Joint using Box-Behnken Design', *Jordan Journal of Mechanical and Industrial Engineering*, vol. 10 2/2016, pp. 115-122.
71. Shende, HA & Kadam, NA 2017, 'Optimization of Resistance Spot Welding Process Parameters of AISI 3041 and AISI 1020 Welded Joints', *International Research Journal of Engineering and Technology (IRJET)*, vol. 4 2/2017, pp.1059-1062.
72. Shih-Fu Ling, Li-XueWan, Yoke-Rung Wong, Dong-Neng Li 2010, 'Input electrical impedance as quality monitoring signature for characterizing resistance spot welding' *NDT&E International*, vol. 43, pp. 200-205.
73. Shinji Fukumoto, Kana Fujiwara, Shin Toji & Atsushi Yamamoto 2008, 'Small-scale resistance spot welding of austenitic stainless steels', *Materials Science and Engineering A*, vol. 492, pp. 243–249.
74. Somervuori, ME, Johansson, LS, Heinonen, MH, van Hoecke, DHD, Akdut, N & Hänninen, HE 2004, 'Characterisation and corrosion of spot welds of austenitic stainless steels', *Materials and Corrosion* 2004, vol. 55, no. 6, DOI: 10.1002/maco.200303753.
75. Subramanian, A & Jabaraj, DB 2013, 'Research on Resistance Spot Welding of Stainless Steel - An Overview', *International Journal of Scientific & Engineering Research*, vol. 4, issue 12, ISSN 2229-5518, pp. 1741-1750.
76. Sumit Chaudhary, Vipin Kumar Sharma & Kulvinder Rana 2014, 'Taguchi Analysis of the tensile strength of Resistance Spot Welding weld', *International Journal of Enhanced Research in Science Technology & Engineering*, ISSN: 2319-7463, vol. 3, issue 10, pp. 217-221.
77. Sun, X & Dong, P 2000, 'Analysis of Aluminum Resistance Spot Welding Processes Using Coupled Finite Element Procedures', *Welding Research Supplement*, pp. 215-221.

78. Sun, X 2004, 'Resistance Spot Welding of Aluminum Alloy to Steel with Transition Material Part II: Finite Element Analyses of Nugget Growth', *Welding Journal*, pp. 197-202.
79. Sun, X & Khaleel, MA 2004, 'Resistance Spot Welding of Aluminum Alloy to Steel with Transition Material from Process to Performance Part I: Experimental Study', *Welding Research*, pp.188-195.
80. Tao Jian-Feng Liang Gong, Cheng-Liang LIU & Yang ZHAO 2012, 'Multi-field dynamic modeling and numerical simulation of aluminum alloy resistance spot welding' *Trans. Nonferrous Met. Soc. China*, vol. 22, pp. 3066–3072.
81. Tsai, CL, Jammal, OA, Papritan, JC & Dickinson, DW 1990, 'Modeling of Resistance Spot Weld Nugget Growth', *Welding Research Supplement*, pp. 47-53.
82. Valera, J, Miguel, V, Martínez, A & Naranjo, J 2017, 'Optimization of electrical parameters in Resistance Spot Welding of dissimilar joints of micro-alloyed steels TRIP sheets', *Procedia Manufacturing*, vol. 13, pp. 291-298.
83. Verma, AB, Ghunage, SU & Ahuja, BB 2014, 'Resistance Welding of Austenitic Stainless Steels (AISI 304 with AISI 316)', 5th International & 26th All India Manufacturing Technology, Design and Research Conference (AIMTDR 2014) December 12th -14th, 2014, IIT Guwahati, Assam, India.
84. Vural, M, Akkus, A & Eryürek, B 2006, 'Effect of welding nugget diameter on the fatigue strength of the resistance spot welded joints of different steel sheets', *Journal of Materials Processing Technology*, vol. 176, pp. 127–132.
85. Wei, PS & Wu, TH 2012, 'Electrical contact resistance effect on resistance spot welding', *International Journal of Heat and Mass Transfer*, vol. 55, pp. 3316-3324.
86. Weihua Zhang, Daqian Sun, Lijun Han, Wenqiang Gao & Xiaoming Qiu 2011, 'Characterization of Intermetallic Compounds in Dissimilar Material Resistance Spot Welded Joint of High Strength Steel and Aluminum Alloy', *ISIJ International*, vol. 51, no. 11, pp. 1870–1877.

87. Weihua Zhang, Daqian Sun, Lijun Han & Dongyang Liu 2014, 'Interfacial microstructure and mechanical property of resistance spot welded joint of high strength steel and aluminium alloy with 4047 AlSi12 interlayers' *Materials and Design*, vol. 57, pp. 186–194.
88. Xu, W, Chen, DL, Liu, L, Mori, H & Zhou, Y 2012, 'Microstructure and mechanical properties of weld-bonded and resistance spot welded magnesium-to-steel dissimilar joints' *Materials Science and Engineering A*, vol. 537, pp. 11– 24.
89. Yi Luo, Jinhe Liu, Huibin Xu, Chengzhi Xiong & Lin Liu 2009, 'Regression modeling and process analysis of resistance spot welding on galvanized steel sheet' *Materials and Design*, vol. 30, pp. 2547–2555.
90. Yi Luo & Jinglong Li 2014, 'Analysis of Nugget Formation During Resistance Spot Welding on Dissimilar Metal Sheets of Aluminum and Magnesium Alloys', *The Minerals, Metals & Materials Society and ASM International*, vol. 45A, pp.5107-5113.
91. Zhigang Hou *et al.* 2007, 'Finite element analysis for the mechanical features of resistance spot welding process', *Journal of Materials Processing Technology*, vol. 185, pp. 160–165.
92. Zoha Nasir & Khan, MI 2016, 'Resistance spot welding and optimization techniques used to optimize its process parameters', *International Research Journal of Engineering and Technology (IRJET)*, vol. 3, pp. 887-893.